Analysis and Applications of Optical Diffraction by Gratings

THOMAS K. GAYLORD, FELLOW, IEEE, AND M. G. MOHARAM, SENIOR MEMBER, IEEE

Diffraction characteristics of general dielectric planar (slab) gratings and surface-relief (corrugated) gratings are reviewed. Applications to laser-beam deflection, guidance, modulation, coupling, filtering, wavefront reconstruction, and distributed feedback in the fields of acoustooptics, integrated optics, holography, and spectral analysis are discussed. An exact formulation of the grating diffraction problem without approximations (rigorous coupled-wave theory developed by the authors) is presented. The method of solution is in terms of state variables and this is presented in detail. Then, using a series of fundamental assumptions, this rigorous theory is shown to reduce to the various existing approximate theories in the appropriate limits. The effects of these fundamental assumptions in the approximate theories are quantified and discussed.

I. Introduction

Diffraction of optical electromagnetic radiation by periodic structures is of increasing importance in an expanding variety of engineering applications. Grating diffraction is central in the fields of acoustooptics, integrated optics, holography, optical data processing, and spectral analysis. Applications are broad and varied and extend well beyond these basic fields. Grating applications include: acoustic wave generation, ambiguity processing, analog-to-digital conversion, antennas, associative storage, beam coding, beam coupling, beam deflection, beam expansion, beam sampling, beam shaping, beam splitting, coherent light generation, convolution processing, correlation processing, data processing and optical logic, data storage, diagnostic measurements, displays, distributed feedback, filtering, head-up displays, holographic optical elements, image amplification, image processing, incoherent-to-coherent converter, instrumentation, interferometry, lenses, mode conversion, modulation, monochromator, multiport storage, multiple beam generation, multiplexing, demultiplexing, optical testing, pattern recognition, phase conjugation, pulse shaping and compression, Q-switching, mode locking, resonator mirror, signal processing, solar concentration, spatial light modulators, spectral analysis, and switching. These applications are discussed in this paper.

Manuscript received September 28, 1984. This work was supported in part by the National Science Foundation and the Joint Services Electronics Program. The submission of this paper was encouraged after review of an advance proposal.

The authors are with the School of Electrical Engineering, Georgia Institute of Technology, Atlanta, GA 30332, USA.

Optical gratings may be planar (slab) gratings. The periodic modulation may be in the permittivity (or equivalently index of refraction) or in the conductivity (or equivalently absorption) or a combination of these. Also gratings may be of the surface-relief (corrugated) type with periodic variations in the surface of a dielectric or conducting material. All of these cases are of practical importance.

The analysis of diffraction by gratings has a long and interesting history. Since 1930, there have been over 400 scientific papers on the subject of grating diffraction. Diffraction of electromagnetic waves by spatially periodic media may be analyzed by numerous methods and with a wide variety of possible assumptions. The most common methods of analyzing grating diffraction are the coupled-wave approach [1]–[9] and the modal approach [10]–[19]. The modal approach is sometimes referred to as the Floquet, Floquet–Bloch, eigenmode, characteristic-mode, or coupled-mode approach. The coupled-wave approach is confusingly also sometimes called coupled-mode approach. The basics of coupled-wave and modal theories have been treated in several reviews [20]–[22]. Both of these approaches can produce exact formulations without approximations. In their full rigorous forms these formulations are completely equivalent [23]. They represent merely alternative methods of representing the electromagnetic fields inside the grating. Starting from the wave equation, both rigorous forms of analysis will be developed as two aspects of a common derivation.

Starting with rigorous theory and using a series of fundamental assumptions, these general theories are shown to reduce to the various approximate theories (two-wave modal theory, two-wave second-order coupled-wave theory, multiwave coupled-wave theory, two-wave first-order coupled-wave theory (Kogelnik theory), optical path method Raman–Nath theory, and amplitude transmittance theory) in the appropriate limits. This is shown in this paper.

II. Analysis of Fields Inside Grating

A. Field Representation

A plane dielectric grating as depicted in Fig. 1 has a relative permittivity (dielectric constant) in the region from $z = 0$ to $z = d$ given by

0018-9219/85/0500-0894$01.00

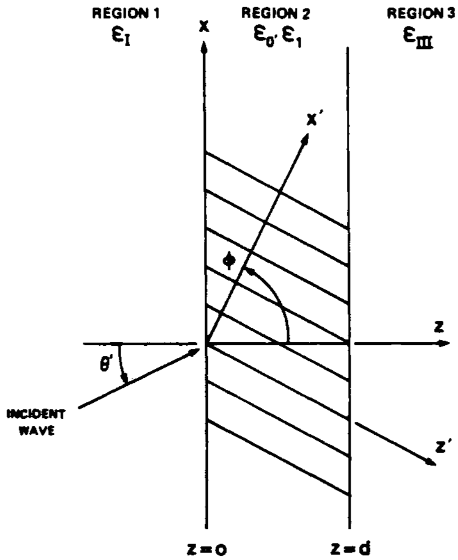

Fig. 1. Planar slanted-fringe dielectric grating geometry.

$$\varepsilon(x') = \varepsilon_0 + \varepsilon_1 \cos Kx' \tag{1}$$

where ε_0 is the average relative permittivity in the grating region, ε_1 is the amplitude of the sinusoidal relative permittivity, ϕ is the grating slant angle, and $K = 2\pi/\Lambda$, where Λ is the grating period. The cosinusoidal form used in (1) is common in the volume holographic grating literature. In the acoustooptics literature, a sinusoidal form for (1) is more common. Using the sinusoidal form would alter the resulting equations in the following sections as well as their amplitude solutions. However, the diffracted intensities are identical in either case. For an incident plane wave with TE polarization (electric field perpendicular to the plane of incidence) the wave equation is

$$\nabla^2 \hat{E}_y(x', z') + k^2 \varepsilon(x') \hat{E}_y(x', z') = 0 \tag{2}$$

where $k = 2\pi/\lambda$ and $\hat{E}_y(x', z')$ is the total electric field inside the grating. The fields and the grating are unchanging in the y direction. The field in the grating region may be expressed in terms of "modes," each of which individually satisfies Maxwell's equations. Thus the total field may be written as

$$\hat{E}_y(x', z') = \sum_{\nu=-\infty}^{+\infty} \hat{E}_{y\nu}(x', z'). \tag{3}$$

The field corresponding to a particular mode ν, $\hat{E}_{y\nu}(x', z')$, may be assumed to be expressable as a product so that $\hat{E}_{y\nu}(x', z') = A_\nu X_\nu(x') Z_\nu(z')$. Upon substitution of this assumed solution into the wave equation and dividing by $\hat{E}_{y\nu}(x', z')$, separation of variables in the wave equation is achieved. Thus the x' part and the z' part must be equal to a constant. Letting the constant be $-\xi_\nu^2$, the z' equation becomes

$$\frac{d^2 Z_\nu(z')}{dz'^2} + \xi_\nu^2 Z_\nu(z') = 0. \tag{4}$$

The solution for $Z_\nu(z')$ may be written

$$Z_\nu(z') = B_\nu \exp(-j\xi_\nu z'). \tag{5}$$

The x' equation resulting from separation of variables is

$$\frac{d^2 X_\nu(x')}{dx'^2} + \left[k^2 \varepsilon(x') - \xi_\nu^2\right] X_\nu(x') = 0 \tag{6}$$

or

$$\frac{d^2 X_\nu(x')}{dx'^2} + \left(a_1 + a_2 \cos Kx'\right) X_\nu(x') = 0 \tag{7}$$

where $a_1 = k^2\varepsilon_0 - \xi_\nu^2$ and $a_2 = k^2\varepsilon_1$. This is the Mathieu differential equation [24]. The general solution of this equation was found by Floquet to be

$$X_\nu(x') = \Phi_\nu(x') \exp(-j\beta_\nu x') \tag{8}$$

where β_ν is a phase factor and $\Phi_\nu(x')$ is periodic in x' with period Λ. That is,

$$\Phi_\nu(x') = \Phi_\nu(x' + \Lambda) \tag{9}$$

for any x'. Since $\Phi_\nu(x')$ is periodic, it may be expanded in a Fourier series as

$$\Phi_\nu(x') = \sum_{i=-\infty}^{+\infty} C_{\nu i} \exp(jiKx') \tag{10}$$

and so $X_\nu(x')$ may be written as

$$X_\nu(x') = \sum_{i=-\infty}^{+\infty} C_{\nu i} \exp(-j\beta_{\nu i} x') \tag{11}$$

where

$$\beta_{\nu i} = \beta_\nu - iK. \tag{12}$$

Equation (12) is often referred to as the "Floquet condition." Each modal field, $\hat{E}_{y\nu}(x', z') = A_\nu X_\nu(x') Z_\nu(z')$, may thus be expressed as

$$\hat{E}_{y\nu}(x', z') = D_\nu \exp(-j\xi_\nu z') \sum_{i=-\infty}^{+\infty} C_{\nu i} \exp(-j\beta_{\nu i} x') \tag{13}$$

where $D_\nu = A_\nu B_\nu$. Rotating from the coordinate system of the grating (x', z') to the coordinate system of the boundary (x, z) using

$$x' = x \sin\phi + z \cos\phi$$
$$z' = -x \cos\phi + z \sin\phi \tag{14}$$

the field $\hat{E}_{y\nu}(x', z')$ becomes $E_{y\nu}(x, z)$ given by

$$E_{y\nu}(x, z) = D_\nu \sum_{i=-\infty}^{+\infty} C_{\nu i} \exp\{-j[(\beta_\nu - iK)\sin\phi - \xi_\nu \cos\phi]x\} \cdot \exp\{-j[\xi_\nu \sin\phi + (\beta_\nu - iK)\cos\phi]z\}. \tag{15}$$

The normalized field of the incident plane wave is given by

$$E_{\text{inc}} = \exp(-j\bar{k}_1 \cdot \bar{r}) = \exp[-j(k_{1x}x + k_{1z}z)] \tag{16}$$

where $k_{1x} = k\varepsilon_1^{1/2}\sin\theta'$, and $k_{1z} = k\varepsilon_1^{1/2}\cos\theta'$. In the limit of zero grating modulation ($\varepsilon_1 \to 0$), the $i = 0$ undiffracted field of each mode is phased matched to the incident field at the $z = 0$ boundary. That is,

$$k_{1x} = k_{2x} \tag{17}$$

where $k_{2x} = k\varepsilon_0^{1/2}\sin\theta$ and θ is the angle of refraction of the incident wave in the second region. From (15), the phase-matching condition $k_{1x} = k_{2x}$ is thus

$$k\varepsilon_1^{1/2}\sin\theta' = \beta_\nu \sin\phi - \xi_\nu \cos\phi. \tag{18}$$

The total field inside the grating is represented by the sum of all of the individual modal fields as

$$E_y(x,z) = \sum_{\nu=-\infty}^{+\infty} E_{y\nu}(x,z)$$

and so the total field is

$$E_y(x,z) = \sum_{\nu=-\infty}^{+\infty} D_\nu \sum_{i=-\infty}^{+\infty} C_{\nu i} \exp[-j(k_{2x} - iK\sin\phi)x] \cdot \exp\{-j[\xi_\nu \sin\phi + (\beta_\nu - iK)\cos\phi]z\}. \quad (19)$$

This is a general form for the field $E_y(x,z)$. Both modal and coupled-wave field expansions can be obtained from it.

B. Modal Expansion and Resulting Equation

Recognizing, in (19), the Fourier series

$$\sum_{i=-\infty}^{+\infty} C_{\nu i} \exp[jiK(x\sin\phi + z\cos\phi)] = \sum_{i=-\infty}^{+\infty} C_{\nu i} \exp(ji\bar{K}\cdot\bar{r}) \quad (20)$$

and its equivalence to the function $\Phi_\nu(\bar{r})$, where $\Phi_\nu(\bar{r}) = \Phi_\nu(\bar{r} + \bar{\Lambda})$, allows the field to be written in the modal expansion form as

$$E_y(x,z) = \sum_{\nu=-\infty}^{+\infty} D_\nu \Phi_\nu(\bar{r}) \cdot \exp[-j(k_{2x}x + \xi_\nu z\sin\phi + \beta_\nu z\cos\phi)]. \quad (21)$$

This expansion expresses the field inside the grating as a sum of "modes," each of which satisfies Maxwell's equations. Therefore, these individual modes are similar to the modes used to describe the fields in waveguiding structures (such as hollow metallic waveguides and dielectric waveguides) in the sense that the modes are independent of each other within the region. The "modal equation" can be obtained by substituting (11) into (7) and performing the indicated differentiations. The result is

$$(k^2\varepsilon_0 - \beta_{\nu i}^2 - \xi_\nu^2) C_{\nu i} + \frac{k^2\varepsilon_1}{2}(C_{\nu,i+1} + C_{\nu,i-1}) = 0 \quad (22)$$

and this provides a second relationship between $\beta_{\nu i}$ and ξ_ν [in addition to (18)]. Solutions of the modal equation are frequently presented as $\beta_{\nu i}$ versus ξ_ν "dispersion diagrams." See, for example, [19]. These diagrams can provide considerable physical insight into the diffraction process. This approach, however, can be computationally difficult and is not treated further in this paper.

C. Coupled-Wave Expansions and Resulting Equations

1) Fundamental Expansion (Wavevector Along Boundary): Interchanging the order of the summations in (19), the total field inside the grating may be rewritten

$$E_y(x,z) = \sum_{i=-\infty}^{+\infty} \exp[-j(k_{2x} - iK\sin\phi)x] \cdot \sum_{\nu=-\infty}^{+\infty} D_\nu C_{\nu i} \exp\{-j[\xi_\nu \sin\phi + (\beta_\nu - iK)\cos\phi]z\}. \quad (23)$$

Performing the summation over the modes ν, the quantity $\hat{S}_i(z)$ may be defined as

$$\hat{S}_i(z) \equiv \sum_{\nu=-\infty}^{+\infty} D_\nu C_{\nu i} \exp\{-j[\xi_\nu \sin\phi + (\beta_\nu - iK)\cos\phi]z\} \quad (24)$$

and this is a function of z *only*. The total field is therefore

$$E_y(x,z) = \sum_{i=-\infty}^{+\infty} \hat{S}_i(z) \exp[-j(k_{2x} - iK\sin\phi)x] \quad (25)$$

and this represents the fundamental coupled-wave expansion of the total field in the grating region. The quantity z is perpendicular to the grating boundary. The field as expressed by (25) has the appearance of a sum of inhomogeneous plane waves traveling in the x direction (along the boundary). These inhomogeneous plane waves have wavevectors given by

$$\bar{\sigma}_i = (k_{2x} - iK\sin\phi)\hat{x} \quad (26)$$

where $\hat{x}$ is the unit vector in the x direction. This is shown as case ① in Fig. 2. The amplitudes, $\hat{S}_i(z)$, of these waves

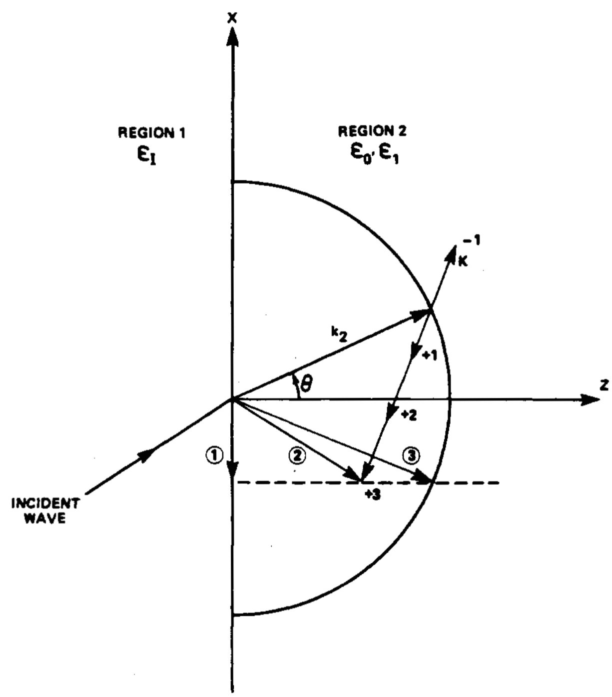

Fig. 2. Wavevector diagram showing three possible choices for wavevector inside grating for coupled-wave expansion of the total field: ① fundamental expansion (wavevector along boundary), ② wavevector from vector Floquet condition, and ③ wavevector of magnitude equal to undiffracted wavevector.

vary in the z direction and thus the waves are inhomogeneous. Alternatively, the $\hat{S}_i(z)$ values are the amplitudes of the space-harmonic components of the total field $E_y(x,z)$ that result when the field is expanded in a Fourier series in the periodic direction (along the boundary or x direction). For an arbitrary slant angle ϕ, the grating as bounded by region 1 (at $z = 0$) and region 3 (at $z = d$) is periodic *only* in the x direction since only in the boundary direction (x) is the relative permittivity periodic. That is, $\varepsilon(x) = \varepsilon(x + \Lambda')$ for *all* x where Λ' is the grating period along the boundary given by $\Lambda' = \Lambda/\sin\phi$. This periodicity is of key importance in the expansion of the total field in terms of space-harmonic components $\hat{S}_i(z)$.

Substituting the fundamental coupled-wave expansion (25) and the permittivity (1) into the wave equation (2) and using $k_{2x} = k\epsilon_0^{1/2}\sin\theta$ and $k = 2\pi/\lambda$ and performing the indicated differentiations gives

$$\sum_{i=-\infty}^{+\infty}\Bigg\{\frac{\partial^2 \hat{S}_i(z)}{\partial z^2} - \left(k\epsilon_0^{1/2}\sin\theta - iK\sin\phi\right)^2 \times \hat{S}_i(z) + k^2\epsilon_0\hat{S}_i(z) + \frac{k^2\epsilon_1}{2}\hat{S}_{i-1}(z)\exp(+jKz\cos\phi) + \frac{k^2\epsilon_1}{2} \times \hat{S}_{i+1}(z)\exp(-jKz\cos\phi)\Bigg\} \times \exp\left\{-j\left[\left(k\epsilon_0^{1/2}\sin\theta - iK\sin\phi\right)x\right]\right\} = 0. \quad (27)$$

This represents an infinite series, the sum of which is zero. Each term in the series is a coefficient multiplied by an exponential. The coefficients are functions of z only. The x dependence is entirely in the exponential factor of each term. Since the exponentials are linearly independent, the coefficient of each exponential must individually be equal to zero. Using this fact together with the definitions of k and K, (27) reduces to the set of coupled-wave equations

$$\frac{1}{2\pi^2}\frac{d^2\hat{S}_i(z)}{dz^2} - 2\left\{\left[\frac{(\epsilon_0)^{1/2}\sin\theta}{\lambda} - \frac{i\sin\phi}{\Lambda}\right]^2 - \frac{\epsilon_0}{\lambda^2}\right\}\hat{S}_i(z) + \frac{\epsilon_1}{\lambda^2}\exp\left(+j2\pi z\frac{\cos\phi}{\Lambda}\right)\hat{S}_{i-1}(z) + \frac{\epsilon_1}{\lambda^2}\exp\left(-j2\pi z\frac{\cos\phi}{\Lambda}\right)\hat{S}_{i+1}(z) = 0. \quad (28)$$

This is an infinite set of second-order coupled difference-differential equations. By inspection, it is seen that the wave corresponding to each value of i (space harmonic inside the grating or diffracted order outside of the grating) is coupled to its adjacent ($i+1$ and $i-1$) space harmonics. There is no direct coupling between nonadjacent orders. This set of coupled-wave equations has no first derivative terms in contrast to the coupled-wave equations to be derived in the next two sections. It is a nonconstant-coefficient differential equation due to the presence of z in the coefficients of the $\hat{S}_{i-1}(z)$ and $\hat{S}_{i+1}(z)$ terms. The equations in the form of (28) represent a linear, *shift-variant* system and direct solution would be difficult. As will be seen in the next section, a constant-coefficient set of coupled-wave equations can be developed by a different selection of the wavevectors of the inhomogeneous plane waves in the coupled-wave expansion. For the special case of an unslanted grating ($\phi = \pi/2$, fringes perpendicular to the surface), expressions (28) become constant-coefficient differential equations. For this limiting case, the equations become identical to the second-order coupled-wave equations of Kong [6, eqs. (6a) and (6b)] if only two waves are retained (the $i = 0$ undiffracted wave and the $i = +1$ fundamental diffracted wave).

2) Expansion with Wavevector from Vector Floquet Condition: A new function of $S_i(z)$ may be defined as

$$S_i(z) \equiv \hat{S}_i(z)\exp[+j(k_{2z} - iK\cos\phi)z] \quad (29)$$

so that $E_y(x,z)$ may be expressed as

$$E_y(x,z) = \sum_{i=-\infty}^{+\infty} S_i(z)\exp\{-j[(k_{2x} - iK\sin\phi)x + (k_{2z} - iK\cos\phi)z]\} \quad (30)$$

or in vector notation

$$E_y(x,z) = \sum_{i=-\infty}^{+\infty} S_i(z)\exp[-j(\bar{k}_2 - i\bar{K})\cdot\bar{r}] \quad (31)$$

where $\bar{k}_2$ would be the wavevector of the refracted incident wave in the absence of grating modulation. This form of the total field in the grating region is more useful than (25) since this form leads to constant-coefficient coupled-wave differential equations for general slanted gratings. This form of the coupled-wave expansion (31) expresses the total field as the sum of inhomogeneous plane waves having wavevectors given by the vector Floquet condition

$$\bar{\sigma}_i = \bar{k}_2 - i\bar{K}. \quad (32)$$

This choice of wavevectors is shown as case ② in Fig. 2. The x component of $\bar{\sigma}_i$ is equal to $k_{2x} - iK\sin\phi$ as is required by phase matching. The expansion (31) has great intuitive appeal. The incident homogeneous plane wave may be visualized as being divided into many diffracted inhomogeneous plane waves that have directions given by (32), the vector Floquet condition for an unbounded periodic medium. The phase fronts of the inhomogeneous plane waves $i = -1$ to $i = +2$ are depicted in Fig. 3 together with the corresponding vector Floquet condition. The $i = 0$ inhomogeneous plane wave corresponds to the

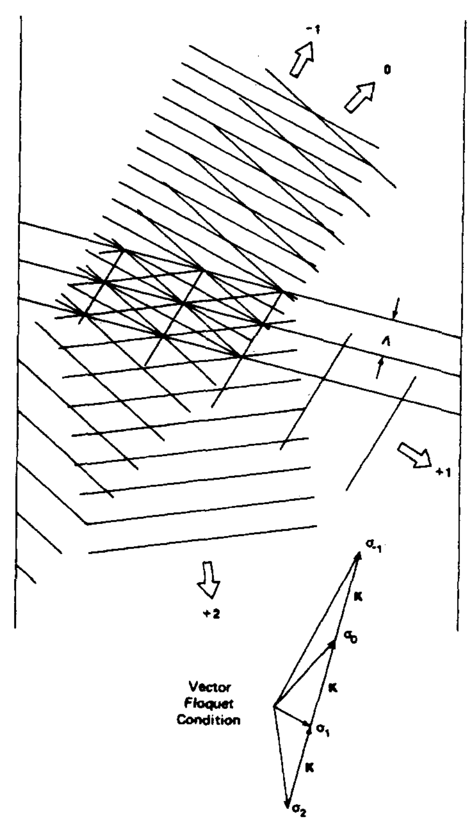

Fig. 3. Visualization of inhomogeneous plane waves (space-harmonic components) inside the grating according to the vector Floquet condition (shown in inset).

refracted incident wave. In this and the other expansions, the diffracted inhomogeneous plane waves form an interference pattern with the incident wave that has a periodicity Λ and slant angle ϕ that are the same as the grating producing the diffraction. However, (31) is only another one of many possible valid expansions for the field inside the grating. Other expansions can be equally valid. Following the procedure of the previous section and substituting the coupled-wave expansion (30) and the permittivity into the wave equation, performing the indicated differentiations, and setting the coefficient of each exponential equal to zero gives the set of coupled-wave equations

$$\frac{1}{2\pi^2}\frac{d^2 S_i(z)}{dz^2} - j\frac{2}{\pi}\left[\frac{(\varepsilon_0)^{1/2}\cos\theta}{\lambda} - \frac{i\cos\phi}{\Lambda}\right]\frac{dS_i(z)}{dz} + \frac{2i(m-i)}{\Lambda^2}S_i(z) + \frac{\varepsilon_1}{\lambda^2}\left[S_{i-1}(z) + S_{i+1}(z)\right] = 0 \quad (33)$$

where the quantity m has been defined as

$$m = \frac{2\Lambda(\varepsilon_0)^{1/2}}{\lambda}\cos(\theta - \phi). \quad (34)$$

These rigorous coupled-wave equations are constant-coefficient differential equations representing a linear, *shift-invariant* system. Using state variable methods from linear systems analysis [25], a solution may be obtained in terms of the eigenvalues and eigenvectors of the coefficient matrix of the set of differential equations. The quantity m may have any value in general. For the case when m is an integer, (34) represents the mth Bragg condition. However, the analysis presented in this paper in no way depends on the Bragg condition being satisfied. It applies to an arbitrary angle of incidence and an arbitrary wavelength. Only if the angle of incidence and wavelength are such that m is an integer does Bragg incidence occur.

3) Expansion with Wavevector of Magnitude Equal to Undiffracted Wavevector: Still another amplitude function $\hat{\hat{S}}_i(z)$ may be defined as

$$\hat{\hat{S}}_i(z) \equiv \hat{S}_i(z)\exp\left\{+j\left[k_2^2 - (k_{2x} - iK_x)^2\right]^{1/2} z\right\} \quad (35)$$

so that $E_y(x,z)$ may be expressed as

$$E_y(x,z) = \sum_{i=-\infty}^{+\infty} \hat{\hat{S}}_i(z)\exp\left\{-j[(k_{2x} - iK\sin\phi)x + \left[k_2^2 - (k_{2x} - iK\cos\phi)^2\right]^{1/2} z\right\}. \quad (36)$$

This form of the coupled-wave equations also expresses the total field as a sum of inhomogeneous plane waves. In this case, the wavevectors are given by

$$\bar{\sigma}_i = (k_{2x} - iK\sin\phi)\hat{x} + \left[k_2^2 - (k_{2x} - iK\cos\phi)^2\right]^{1/2}\hat{z} \quad (37)$$

where $\hat{z}$ is the unit vector in the z direction. This is shown as case 3 in Fig. 2. The x component of $\bar{\sigma}_i$ is obviously equal to $k_{2x} - iK\sin\phi$ as required by phase matching. The choice of (37) forces the wavevector magnitudes to be equal to k_2 where $k_2 = k\varepsilon_0^{1/2}$ is the magnitude of the refracted wavevector in region 2 in the absence of grating modulation. This choice has been used in approximate treatments together with neglecting higher order waves [26] and neglecting second derivatives of the amplitudes [27]. Following the procedure of the previous sections and substituting the coupled-wave expansion (36) into the wave equation leads to the set of coupled-wave equations

$$\frac{1}{2\pi^2}\frac{d^2\hat{\hat{S}}_i(z)}{dz^2} - j\frac{2}{\pi}\left[\frac{\varepsilon_0}{\lambda^2} - \left(\frac{(\varepsilon_0)^{1/2}\sin\theta}{\lambda} - \frac{i\sin\phi}{\Lambda}\right)^2\right]^{1/2}\frac{d\hat{\hat{S}}_i(z)}{dz} + \frac{\varepsilon_1}{\lambda^2}\exp\left\{j2\pi z\left\{\frac{\cos\phi}{\Lambda} + \left[\frac{\varepsilon_0}{\lambda^2} - \left(\frac{(\varepsilon_0)^{1/2}\sin\theta}{\lambda} - \frac{i\sin\phi}{\Lambda}\right)^2\right]^{1/2} - \left[\frac{\varepsilon_0}{\lambda^2} - \left(\frac{(\varepsilon_0)^{1/2}\sin\theta}{\lambda} - \frac{(i-1)\sin\phi}{\Lambda}\right)^2\right]^{1/2}\right\}\right\}\hat{\hat{S}}_{i-1}(z) + \frac{\varepsilon_1}{\lambda^2}\exp\left\{-j2\pi z\left\{\frac{\cos\phi}{\Lambda} + \left[\frac{\varepsilon_0}{\lambda^2} - \left(\frac{(\varepsilon_0)^{1/2}\sin\theta}{\lambda} - \frac{(i+1)\sin\phi}{\Lambda}\right)^2\right]^{1/2} - \left[\frac{\varepsilon_0}{\lambda^2} - \left(\frac{(\varepsilon_0)^{1/2}\sin\theta}{\lambda} - \frac{i\sin\phi}{\Lambda}\right)^2\right]^{1/2}\right\}\right\}\hat{\hat{S}}_{i+1}(z) = 0. \quad (38)$$

These coupled-wave equations are nonconstant-coefficient differential equations. Unlike the coupled-wave equations (33), these are not straightforwardly solvable in this form.

D. Rigorous Nature and Equivalence of Expansions

The total field $E_y(x,z)$ inside the grating produced by a TE-polarized incident plane wave is given by (19). This equation has been rigorously derived (without approximations). The total field has been rewritten as a sum over the modes ν (modal expansion) as (21) and as sums over the space-harmonic components i (coupled-wave expansions) as (25), (30), and (36). *All four of these expansions are completely rigorous.* Since they are all developed without any approximations from the same equation, these expansions are completely equivalent. They represent merely alternative mathematical representations of the total field inside the grating. Associated with each expansion is a different physical perspective of the total field inside the grating. However, these different physical views are also equivalent and each is just an alternative representation of the *same* total field. One is no more or no less correct than the others.

In the modal representation (21), the fields inside the grating are expanded in terms of the allowable modes of the periodic medium. The fields are visualized as waveguide modes in the grating region. In the modal approach, the total electric field is expressed as a weighted summation over all possible modes. The summation includes both forward- and backward-propagating modes. The backward-propagating modes are due to diffraction in the grating volume (when the grating fringes are slanted) and due to reflections at the $z = d$ boundary. Each individual νth mode satisfies the wave equation (and thus Maxwell's equations) and may be either evanescent or propagating. These modes in the grating are similar to modes in a waveguide. Each mode satisfies the wave equation by itself and it may be either cutoff or propagating. Each mode (ν) consists of an infinite number of space harmonics (i) and each mode propagates through the medium without change. The space harmonics may be viewed as arising from the Fourier expansion of the periodic function $\Phi_\nu(\bar{r})$.

In the coupled-wave representation [(25), (30), (36)], the field inside the modulated medium is expanded in terms of

Table 1 Three Possible Electric Field Expansions and the Resulting Coupled-Wave Equations for TE Polarization and Sinusoidal Permittivity

Field Expansion	Resulting Coupled-Wave Equations
$E(x,z)=\sum_{i=-\infty}^{+\infty} S_i(z)\exp[-j(k_{2x}-iK_x)x]$	$\frac{1}{2\pi^2}\frac{d^2S_i}{dz^2}-2\left\{\left[\frac{(\varepsilon_0)^{1/2}\sin\theta}{\lambda}-\frac{i\sin\phi}{\Lambda}\right]^2-\frac{\varepsilon_0}{\lambda^2}\right\}S_i+\frac{\varepsilon_1}{\lambda^2}\exp\left(j2\pi z\frac{\cos\phi}{\Lambda}\right)S_{i-1}+\frac{\varepsilon_1}{\lambda^2}\exp\left(-j2\pi z\frac{\cos\phi}{\Lambda}\right)S_{i+1}=0$
$E(x,z)=\sum_{i=-\infty}^{+\infty} S_i(z)\exp[-j(k_{2x}-iK_x)x]\cdot\exp[-j(k_{2z}-iK_z)z]$	$\frac{1}{2\pi^2}\frac{d^2S_i}{dz^2}-j\frac{2}{\pi}\left[\frac{(\varepsilon_0)^{1/2}\cos\theta}{\lambda}-\frac{i\cos\phi}{\Lambda}\right]\frac{dS_i}{dz}+\frac{2i(m-i)}{\Lambda^2}S_i+\frac{\varepsilon_1}{\lambda^2}(S_{i-1}+S_{i+1})=0$
$E(x,z)=\sum_{i=-\infty}^{+\infty} S_i(z)\exp[-j(k_{2x}-iK_x)x]\cdot\exp\left\{-j\left[k_2^2-(k_{2x}-iK_x)^2\right]^{1/2}z\right\}$	$\frac{1}{2\pi^2}\frac{d^2S_i}{dz^2}-j\frac{2}{\pi}\left[\frac{\varepsilon_0}{\lambda^2}-\left(\frac{(\varepsilon_0)^{1/2}\sin\theta}{\lambda}-\frac{i\sin\phi}{\Lambda}\right)^2\right]^{1/2}\frac{dS_i}{dz}+\frac{\varepsilon_1}{\lambda^2}\exp\left\{j2\pi z\left\{\frac{\cos\phi}{\Lambda}+\left[\frac{\varepsilon_0}{\lambda^2}-\left(\frac{(\varepsilon_0)^{1/2}\sin\theta}{\lambda}-\frac{i\sin\phi}{\Lambda}\right)^2\right]^{1/2}-\left[\frac{\varepsilon_0}{\lambda^2}-\left(\frac{(\varepsilon_0)^{1/2}\sin\theta}{\lambda}-\frac{(i-1)\sin\phi}{\Lambda}\right)^2\right]^{1/2}\right\}\right\}S_{i-1}+\frac{\varepsilon_1}{\lambda^2}\exp\left\{-j2\pi z\left\{\frac{\cos\phi}{\Lambda}+\left[\frac{\varepsilon_0}{\lambda^2}-\left(\frac{(\varepsilon_0)^{1/2}\sin\theta}{\lambda}-\frac{(i+1)\sin\phi}{\Lambda}\right)^2\right]^{1/2}-\left[\frac{\varepsilon_0}{\lambda^2}-\left(\frac{(\varepsilon_0)^{1/2}\sin\theta}{\lambda}-\frac{i\sin\phi}{\Lambda}\right)^2\right]^{1/2}\right\}\right\}S_{i+1}=0$

the space harmonic components (i) of the field in the periodic structure. These space harmonics inside the grating are phase matched to diffracted orders (either propagating or evanescent) outside of the grating. Unlike the individual modal fields (ν), the individual space-harmonic fields (i) do not satisfy the wave equation. The sum of all the space harmonic fields, of course, does satisfy the wave equation. However, the space-harmonic fields cannot exist alone. The partial space-harmonic fields may be visualized as inhomogeneous plane waves (plane waves with a varying amplitude along the planar phase front). These inhomogeneous plane waves are not independent and they couple energy back and forth between each other in the modulated medium. The coupled-wave expansions together with the resulting sets of coupled-wave equations are summarized in Table 1.

In an overly simplified manner, the diffraction process is sometimes interpreted as 1) the incident wave is refracted into the grating medium at $z=0$, 2) the refracted plane wave in the grating is diffracted into an infinite set (i) of plane waves (or "coupled waves") propagating toward the $z=d$ boundary, and 3) the waves inside the grating are phase matched into propagating (and evanescent) waves in the third region. This picture somewhat agrees with simple physical intuition about the process of diffraction by a volume grating. However, this sequential interpretation is misleading in many ways. For example, the backward-diffracted waves in region 1 are not predicted in this interpretation. Obviously, the *total* electromagnetic problem of the diffraction by the grating must be solved, as is done in this paper. Even though it is tempting to think of the space-harmonic fields as simple waves in the grating, this is a very incomplete view.

The coupled-wave or space-harmonic expansion of the total field, however, is quite natural since the inhomogeneous plane waves (i) that result are phased matched to the forward-diffracted and backward-diffracted plane waves that are so obvious experimentally. The modal fields (ν), on the other hand, all partially contribute to each observed diffracted order and thus their individual significance is not obvious. Beyond the appeal of the coupled-wave approach based on practical device operation, the more persuasive argument for its use is the ease with which solutions may be obtained. It is shown in Section IV that the constant-coefficient form of the coupled-wave equations can be solved in a straightforward manner in terms of the eigenvalues and eigenvectors of the differential equation coefficient matrix. This is accomplished *without* numerical instabilities using readily available standard eigenvalue/eigenvector programs.

E. Other Grating Cases

To clarify the mathematical and physical concepts involved, the analysis presented in this paper is being restricted to 1) lossless dielectric phase gratings, 2) sinusoidal permittivity profile, 3) TE-incident polarization, 4) the grating vector $\vec{K}$ lying in the plane of incidence, and 5) slanted gratings ($0<\phi\leqslant\pi/2$). With the exception of the last restriction, these are not essential assumptions for the analysis. Relaxing these restrictions produces a more complicated formulation, but the basic physical principles are the same.

Gratings with a periodic modulation in their conductivity (producing optical absorption) have been analyzed using rigorous coupled-wave theory [28]. The presence of TM polarization in the incident wave results in a vector wave-equation description of the field inside the grating rather than a scalar wave-equation description (2). The coupled-wave expansion in this case produces a more complicated set of coupled-wave equations. However, these equations can also be solved using the state-variables method described in Section IV. The rigorous coupled-wave equations for this case and their solution are described in [29]. If the grating vector does not lie in the plane of incidence, the TE and TM polarizations become coupled and can no longer be treated separately and independently. Since the diffracted wavevectors lie on the surface of a cone (rather than in a plane), this case is sometimes referred to as conical diffraction. Due to the coupling between the TE and TM polarizations, this situation requires a three-dimensional vector treatment. Rigorous coupled-wave equations for this three-dimensional vector case have been developed and solved using the state-variables approach [9]. Rather than constructing and solving two relatively complicated vector-wave equations, it is more convenient and straightforward in this case to solve Maxwell's equations directly. This approach produces four sets of first-order coupled-wave equations. However, even though more complicated, these equations are in a form that can be solved directly by the methods of Section IV.

Because the rigorous coupled-wave approach is based on the Fourier expansion [of $\Phi_v(\bar{r})$] into space-harmonic components of the total field, a truly periodic grating (an infinite number of periods) is required. The coupled-wave approach may be applied in the angular limit as the slanted fringes of a general grating approach being parallel to the surface (ϕ approaches zero) [30]. However, for exact parallelism with the surface ($\phi = 0$), the grating is no longer strictly periodic and a continuum of solutions is possible depending on the number of periods, the starting conditions, and the ending conditions of the grating. This pure reflection grating case can be analyzed without approximation using a rigorous chain-matrix method of analysis. This is discussed in [31]. Alternatively, the pure reflection grating case ($\phi = 0$) can be analyzed using the modal formulation [19].

III. Diffracted Orders Outside of Grating

A. Phase Matching and Grating Equations

Obtaining an accurate representation of the total field inside the grating is an essential first step in describing the diffraction by the grating. However, possibly the most obvious feature of grating diffraction is the multiple backward- and forward-propagating diffracted orders that typically exist outside of the grating as shown in Fig. 4. The total electric field in region 1 is the sum of the incident and the backward-traveling waves. The normalized total electric field in region 1 may be expressed as

$$E_1 = \exp(-j\bar{k}_1 \cdot \bar{r}) + \sum_{i=-\infty}^{\infty} R_i \exp(-j\bar{k}_{1i} \cdot \bar{r}) \quad (39)$$

where R_i is the normalized amplitude of the ith reflected wave in region 1 with wavevector $\bar{k}_{1i}$. Likewise, the normalized total electric field in region 3 is

$$E_3 = \sum_{i=-\infty}^{\infty} T_i \exp[-j\bar{k}_{3i}(\bar{r} - d\hat{z})] \quad (40)$$

where T_i is the normalized amplitude of the ith transmitted wave in region 3 with wavevector $\bar{k}_{3i}$. Each ith field in region 1 and 3 must be phase matched to the ith space harmonic field (inhomogeneous plane wave) inside the grating. Thus the x components of the wavevectors of the ith wave (regions 1 and 3) and the x component of the wavevector of the ith space harmonic field (region 2) must be the same. That is,

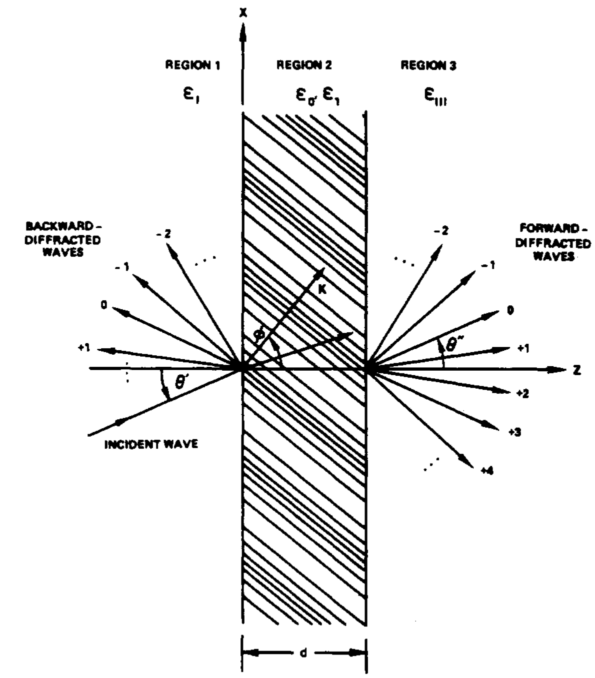

Fig. 4. Planar grating diffraction geometry showing backward-diffracted and forward-diffracted propagating waves.

$$\bar{k}_{1i} \cdot \hat{x} = \bar{\sigma}_i \cdot \hat{x} = \bar{k}_{3i} \cdot \hat{x} \quad (41)$$

where $k_{1i} = k(\varepsilon_I)^{1/2}$ and $k_{3i} = k(\varepsilon_{III})^{1/2}$. Evaluating this expression gives the "grating equation" for the backward-diffracted waves

$$n_1 \sin\theta_i' = n_1 \sin\theta' - i(\lambda/\Lambda)\sin\phi \quad (42)$$

and the forward-diffracted waves

$$n_3 \sin\theta_i'' = n_1 \sin\theta' - i(\lambda/\Lambda)\sin\phi \quad (43)$$

where n_1 and n_3 are the indices of refraction of regions 1 and 3, respectively, and are given by $n_1 = (\varepsilon_I)^{1/2}$ and $n_3 = (\varepsilon_{III})^{1/2}$. The angles of diffraction of the propagating diffracted orders are given by these relationships. Each ith space-harmonic field inside the grating produces a corresponding ith field in regions 1 and 3.

B. Propagating and Evanescent Waves

In the homogeneous regions (1 and 3) the backward- and forward-diffracted waves have wavevectors and magnitudes

$$|\bar{k}_{1i}| = |\bar{k}_1| \quad \text{and} \quad |\bar{k}_{3i}| = |\bar{k}_3|. \quad (44)$$

Knowing the total amplitudes and the x components of the diffracted wavevectors from phase-matching requirements, the z components are then determined to be

$$\begin{aligned}\bar{k}_{1i} \cdot \hat{z} &= \left[|\bar{k}_1|^2 - (\bar{k}_{1i} \cdot \hat{x})^2\right]^{1/2} \\ &= \left[k_1^2 - (k_2 \sin\theta - iK\sin\phi)^2\right]^{1/2} \quad (45)\end{aligned}$$

and

$$\bar{k}_{3i} \cdot \hat{z} = \left[|\bar{k}_3|^2 - (\bar{k}_{3i} \cdot \hat{x})^2 \right]^{1/2}$$
$$= \left[k_3^2 - (k_2 \sin\theta - iK \sin\phi)^2 \right]^{1/2}. \qquad (46)$$

These quantities are either positive real (propagating wave) or negative imaginary (evanescent wave) in region 3, or negative real (propagating wave) or positive imaginary (evanescent wave) in region 1. Whether the ith field in region 1 or 3 is propagating or cut off may be visualized as shown in Fig. 5. The wavevectors in regions 1 and 3 have

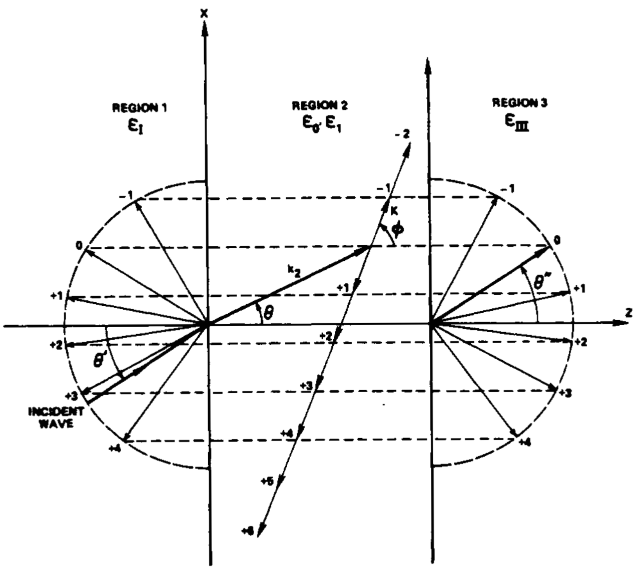

Fig. 5. Wavevector diagram showing phase matching of space-harmonic components of total field inside the grating with propagating backward-diffracted orders (region 1) and forward-diffracted orders (region 3). For $-1 \leqslant i \leqslant +4$, propagating diffracted orders exist, whereas for $i \leqslant -2$ and $i \geqslant +5$, the waves are evanescent (cut off) outside the grating.

magnitudes k_1 and k_3, respectively. Semicircles with these radii are shown in the figure. The allowed wavevectors in these regions must be phased matched to the boundary components of the space-harmonic component fields inside the grating. This is shown by the horizontal dashed lines in the figure. For the incident wave of wavevector $\bar{k}_1$ and the slanted grating with grating vector $\bar{K}$, the $i = -1$ to $+4$ waves exist as propagating diffracted orders in regions 1 and 3. For $i \leqslant -2$ and $i \geqslant +5$, the waves are evanescent (cutoff).

C. Bragg Condition

The mth Bragg condition occurs if the wavelength and angle of the incident wave satisfy the relationship $m = 2\Lambda(\epsilon_0)^{1/2}\cos(\theta - \phi)$ where m is an integer. For this case, the diffraction efficiency is generally (but not always) maximized for the ith diffracted order, where $i = m$. For the case shown in Fig. 3, the incidence is near the second Bragg angle. Therefore, $m = 2$. In this situation, it is expected that the $i = +2$ diffracted order will be maximized compared to other possible angles of the incident wave. The $m = 2$ Bragg condition may be visualized in terms of the vector Floquet conditions as the magnitude of the $i = +2$ wavevector being equal to the magnitude of the $i = 0$ (undiffracted) wavevector, $|\sigma_2| = |\sigma_0|$. Thus $\bar{\sigma}_2$ and $\bar{\sigma}_0$ form an isosceles triangle. Alternatively, the $i = +2$ inhomogeneous plane wave constructed with the vector Floquet condition has its "wavelength" equal to $\lambda/(\epsilon_0)^{1/2}$, the wavelength of the incident wave in region 2 in the absence of grating modulation. This view of the Bragg condition is intuitively appealing. Further illustration of this view is given in Fig. 6. Fig. 6(a) shows first Bragg incidence ($m = 1$) for an incident short wavelength. Fig. 6(b) illustrates the same case for a longer wavelength and the corresponding larger Bragg angle. Fig. 6(c) depicts second Bragg incidence ($m = 2$) for the same grating.

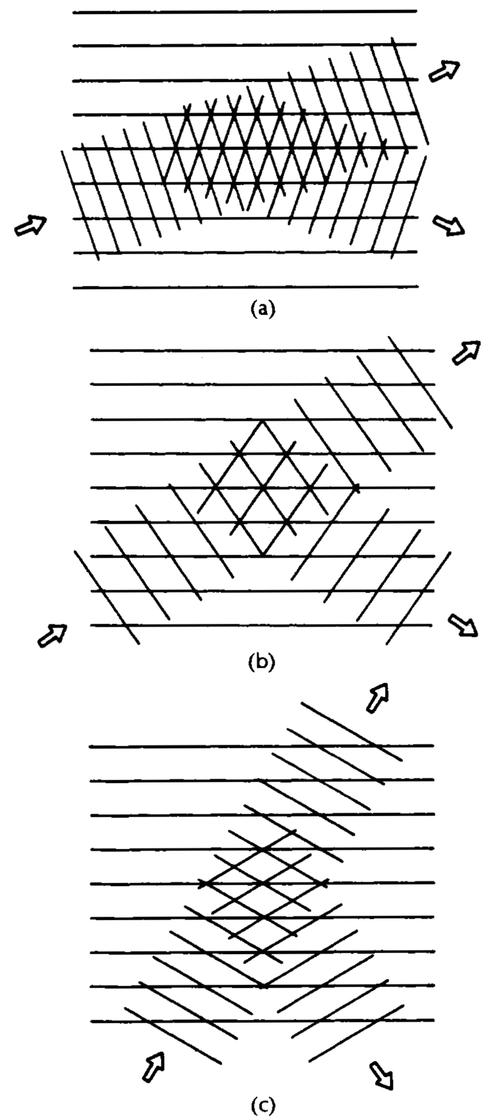

Fig. 6. Visualization of diffraction at the Bragg condition. (a) Incidence at first ($m = 1$) Bragg angle (short wavelength). (b) Incidence at first Bragg angle (long wavelength). (c) Incidence at second ($m = 2$) Bragg angle.

IV. Analysis of Amplitudes of Diffracted Orders

A. State-Space Representation of Coupled-Wave Equations

The rigorous coupled-wave equations as given by (33) represent a set of second-order linear differential equations with constant coefficients. Using the methods of linear systems analysis [25] this differential equation description of this continuous system may be transformed into a state-space description and a solution obtained directly. By defining the state variables as

$$S_{1,i}(z) = S_i(z) \tag{47}$$

$$S_{2,i}(z) = \frac{dS_i(z)}{dz} \tag{48}$$

the infinite set of second-order differential equations (33) are transformed into two infinite sets of first-order differential equations

$$\frac{dS_{1,i}(z)}{dz} = S_{2,i}(z) \tag{49}$$

$$\begin{aligned}\frac{dS_{2,i}(z)}{dz} = &-\frac{2\pi^2\epsilon_1}{\lambda^2}S_{1,i-1}(z) + \frac{4\pi^2(i-m)}{\Lambda^2}S_{1,i}(z)\\ &-\frac{2\pi^2\epsilon_1}{\lambda^2}S_{1,i+1}(z)\\ &+j4\pi\left(\frac{(\epsilon_0)^{1/2}\cos\theta}{\lambda} - \frac{i\cos\phi}{\Lambda}\right)S_{2,i}(z).\end{aligned} \tag{50}$$

Equations (49) and (50) are the state equations corresponding to the rigorous coupled-wave equations (33). These constituent state equations may be written in matrix form as

$$\begin{bmatrix} \vdots \\ \dot{S}_{1,-2} \\ \dot{S}_{1,-1} \\ \dot{S}_{1,0} \\ \dot{S}_{1,1} \\ \dot{S}_{1,2} \\ \vdots \\ \dot{S}_{2,-2} \\ \dot{S}_{2,-1} \\ \dot{S}_{2,0} \\ \dot{S}_{2,1} \\ \dot{S}_{2,2} \\ \vdots \end{bmatrix} = \begin{bmatrix} & & & \vdots & & & & & & \vdots & & & \\ & 0 & 0 & 0 & 0 & 0 & & 1 & 0 & 0 & 0 & 0 & \\ & 0 & 0 & 0 & 0 & 0 & & 0 & 1 & 0 & 0 & 0 & \\ \cdots & 0 & 0 & 0 & 0 & 0 & \cdots & 0 & 0 & 1 & 0 & 0 & \cdots \\ & 0 & 0 & 0 & 0 & 0 & & 0 & 0 & 0 & 1 & 0 & \\ & 0 & 0 & 0 & 0 & 0 & & 0 & 0 & 0 & 0 & 1 & \\ & & & \vdots & & & & & & \vdots & & & \\ & b_{-2} & a & 0 & 0 & 0 & & c_{-2} & 0 & 0 & 0 & 0 & \\ & a & b_{-1} & a & 0 & 0 & & 0 & c_{-1} & 0 & 0 & 0 & \\ \cdots & 0 & a & b_0 & a & 0 & \cdots & 0 & 0 & c_0 & 0 & 0 & \cdots \\ & 0 & 0 & a & b_1 & a & & 0 & 0 & 0 & c_1 & 0 & \\ & 0 & 0 & 0 & a & b_2 & & 0 & 0 & 0 & 0 & c_2 & \\ & & & \vdots & & & & & & \vdots & & & \end{bmatrix} \begin{bmatrix} \vdots \\ S_{1,-2} \\ S_{1,-1} \\ S_{1,0} \\ S_{1,1} \\ S_{1,2} \\ \vdots \\ S_{2,-2} \\ S_{2,-1} \\ S_{2,0} \\ S_{2,1} \\ S_{2,2} \\ \cdots \end{bmatrix} \tag{51}$$

where $a = -2\pi^2\epsilon_1/\lambda^2$, $b_i = 4\pi^2 i(i-m)/\Lambda^2$, and $c_i = j4\pi[(\epsilon_0)^{1/2}\cos\theta/\lambda - i\cos\phi/\Lambda]$. This equation may be represented concisely as $\dot{\boldsymbol{S}} = \boldsymbol{AS}$ where $\dot{\boldsymbol{S}}$ and $\boldsymbol{S}$ are the column vectors in (51) and $\boldsymbol{A}$ is the coefficient matrix.

B. Solution for Space-Harmonic Components

Since the constituent state equations (49) and (50) are homogeneous equations, they correspond to unforced state equations. State equations that are linear differential equations with constant coefficients such as these, may be solved for closed-form expressions for the state variables. In this case, only the homogeneous solution is necessary as there are no driving terms in these equations. The homogeneous solutions are

$$S_{\ell,i}(z) = \sum_{m=-\infty}^{+\infty} C_m w_{\ell,im} \exp(\lambda_m z) \tag{52}$$

for $\ell = 1, 2$. The coefficients C_m are unknown constants to be determined from the boundary conditions. The solution for the wave amplitudes (the "output equation" in linear systems terminology) is $S_i(z) = S_{1,i}(z)$. The quantity $w_{\ell,im}$ is an element of an eigenvector and λ_m is an eigenvalue. These needed eigenvalues and eigenvectors are determined from the coefficient matrix $\boldsymbol{A}$. Although $\boldsymbol{A}$ is an infinite matrix, results may be obtained in practice to an arbitrary level of accuracy with a truncated matrix. Each of the four submatrices is truncated to $n \times n$. As the integer n increases, the calculated results rapidly converge to the exact results. The quantity n corresponds to the total number of space harmonics retained in the analysis. This in turn means that the analysis includes n diffracted waves in region 1 and n diffracted waves in region 3. To put the four submatrices into standard form, the integers i and m are replaced with the new integers p and q that run from 1 to n. For example, if an odd number of waves are retained symmetrically about $i = 0$ (the undiffracted wave) in the analysis, then $p = i + (n+1)/2$ and $q = m + (n+1)/2$. The $2n$ solutions may then be expressed

$$s_{\ell,p}(z) = \sum_{r=1}^{2}\sum_{q=1}^{n} C_{r,q} w_{\ell,p;r,q} \exp(\lambda_{r,q} z) \tag{53}$$

for $\ell = 1$, 2 and $p = 1$ to n. The eigenvalues $\lambda_{r,q}$ are determined by solving the determinantal equation

$$|\boldsymbol{A} - \lambda_{r,q}\boldsymbol{I}| = 0 \tag{54}$$

where $\boldsymbol{I}$ is the unit matrix. The eigenvector corresponding to a particular eigenvalue $\lambda_{r,q}$ is determined by substituting $2n$ expressions ($\ell = 1$, 2, and $p = 1$ to n) for $S_{\ell,p}$ of the form $S_{\ell,p} = B_{\ell,p;r,q}\exp(\lambda_{r,q})$ into the state equation (51), performing the indicated differentiations, and then solving for each element of the eigenvector as $w_{\ell,p;r,q} = B_{\ell,p;r,q}/B_{1,1;r,q}$ using Cramer's rule and thus expressing each element as a ratio of determinants. The eigenvalues and eigenvectors for a matrix are typically calculated numerically using a computer library program [32].

C. Boundary Conditions

The amplitudes of the fields in regions 1 and 3 must be such that the electromagnetic boundary conditions from Maxwell's equations are satisfied at the two grating boundaries ($z = 0$ and $z = d$). The fields (39) and (40) in regions 1 and 3 are phased matched to the field in the grating (31). Using the phase-matching conditions (41) and the requirements on the wavevectors in regions 1 and 3 as given by (45) and (46), the total fields in regions 1 and 3, (39) and (40) may be rewritten

$$E_1 = \exp\{-j[k_1(\sin\theta' x + \cos\theta' z)]\} + \sum_{i=-\infty}^{\infty} R_i \exp\Big[-j\Big\{(k_2\sin\theta - iK\sin\phi)x - \big[k_1^2 - (k_2\sin\theta - iK\sin\phi)^2\big]^{1/2} z\Big\}\Big] \tag{55}$$

and

$$E_3 = \sum_{i=-\infty}^{\infty} T_i \exp\Big\{-j\Big\{(k_2\sin\theta - iK\sin\phi)x + \big[k_3^2 - (k_2\sin\theta - iK\sin\phi)^2\big]^{1/2}(z-d)\Big\}\Big\}. \tag{56}$$

Electromagnetic boundary conditions require that the tangential electric and tangential magnetic fields be continuous across the two boundaries ($z = 0$ and $z = d$). For the TE polarization treated here, the electric field only has a component in the y direction and so it is the tangential electric field directly. The magnetic field intensity, however, must be obtained through the Maxwell equation $\nabla \times \bar{E} = -\partial \bar{B}/\partial t$. The tangential component of H is in the x direction and is given by $H_x = (-j/\omega\mu)\partial E_y/\partial z$. For each value of i, the four quantities to be matched and the resulting boundary conditions are as follows:

1) Tangential E at $z = 0$:

$$\delta_{i0} + R_i = S_i(0). \tag{57}$$

2) Tangential H at $z = 0$:

$$j\big[k_1^2 - (k_2\sin\theta - iK\sin\phi)^2\big]^{1/2}(R_i - \delta_{i0}) = \frac{dS_i(0)}{dz} - j(k_2\cos\theta - iK\cos\phi)S_i(0). \tag{58}$$

3) Tangential E at $z = d$:

$$T_i = S_i(d)\exp[-j(k_2\cos\theta - iK\cos\phi)d]. \tag{59}$$

4) Tangential H at $z = d$:

$$-j\big[k_3^2 - (k_2\sin\theta - iK\sin\phi)^2\big]^{1/2} T_i = \left[\frac{dS_i(d)}{dz} - j(k_2\cos\theta - iK\cos\phi)S_i(d)\right] \cdot \exp[-j(k_2\cos\theta - iK\cos\phi)d] \tag{60}$$

where δ_{i0} is the Kronecker delta function.

D. Solution for Diffracted Amplitudes

If n values of i are retained in the analysis, then there will be n forward-diffracted waves (n values of T_i) and n backward-diffracted waves (n values of R_i). Correspondingly, there will be $2n$ unknown values of C_m. This is because the coefficient matrix in (51) is a $2n \times 2n$ matrix and therefore has $2n$ eigenvalues and thus there are $2n$ unknown values of C_m. Also this may be viewed as being due to the n coupled-wave equations, each being a second-order differential equation, and thus there are $2n$ roots or eigenvalues and $2n$ unknown constants C_m to be determined from the boundary conditions. Therefore, the total number of unknowns is $4n$. Substituting $S_i(z)$, as given by (45) and (50), into the equations for the boundary conditions (57)–(60) produces $4n$ linear equations containing the $4n$ unknowns. An efficient procedure to solve these equations is to eliminate R_i and T_i from these equations and to solve the resulting $2n$ equations for the $2n$ values of C_m using a technique such as Gauss elimination with the maximum pivot strategy [33]. Then the n values of R_i and n values of T_i may be determined from (57) and (59), respectively. If k_{1i} and k_{3i} are real, then R_i and T_i are the amplitudes of propagating diffracted waves. If k_{1i} and k_{3i} are imaginary, then R_i and T_i are the boundary amplitudes of evanescent waves.

E. Diffraction Efficiency

Having calculated the field amplitudes R_i and T_i, the diffraction problem is essentially solved. However, the quantity commonly measured in grating diffraction experiments is the diffraction efficiency. For any given propagating diffracted order i, the diffraction efficiency is the diffracted power divided by the incident power. Experimentally, the diffraction efficiency is clearly defined due to the finite extent of the light beams involved. Analytically, the incident and diffracted waves have all been treated as infinite plane waves. However, due to the extremely large widths of these beams in comparison to a wavelength of the light, the plane wave model is very accurate. Nevertheless, in making power measurements, the beams are clearly not infinite. Diffracted power is measured in the laboratory on the diffracted beams after they have propagated away from the grating and have become spatially separated. If all of the diffracted waves were infinite plane waves, they would all be present at each point in space and interference effects would occur, complicating the interpretation of diffraction efficiency. Therefore, the diffraction efficiency here is defined corresponding to the experimental case of spatially separated beams and thus interference effects are neglected. This corresponds to using the spatially averaged Poynting vector. The neglect of interference effects and the use of the spatially averaged Poynting vector have been discussed in detail by Russell [34].

The diffraction efficiency for the experimental case is defined as diffracted power of a particular order divided by the input power. In the above formulation, the incident plane wave amplitude was normalized to unity. Thus the diffraction efficiencies in regions 1 and 3 are

$$DE_{1i} = \mathrm{Re}\{(\bar{k}_{1i}\cdot\hat{z})/(\bar{k}_{10}\cdot\hat{z})\} R_i R_i^* = \mathrm{Re}\Big\{\Big\{1 - \big[\sin\theta' - i\lambda\sin\phi/(\varepsilon_1)^{1/2}\Lambda\big]^2\Big\}^{1/2} \Big/ \cos\theta'\Big\} R_i R_i^* \tag{61}$$

and

$$DE_{3i} = \mathrm{Re}\{(\bar{k}_{3i}\cdot\hat{z})/(\bar{k}_{10}\cdot\hat{z})\} T_i T_i^* = \mathrm{Re}\Big\{\Big\{(\varepsilon_{III}/\varepsilon_I) - \big[\sin\theta' - i\lambda\sin\phi/(\varepsilon_I)^{1/2}\Lambda\big]^2\Big\}^{1/2} \Big/ \cos\theta'\Big\} T_i T_i^*. \tag{62}$$

The real part of the ratio of the propagation constants occurs when the time-average power-flow density is obtained by taking the real part of the complex Poynting vector. For an unslanted grating ($\phi = \pi/2$) with the same medium on both sides ($\varepsilon_I = \varepsilon_{III}$), the real part of the ratio of the propagation constants is just the usual ratio of the cosine of the diffraction angle for the ith diffracted wave to the cosine of the incidence angle.

Using the spatially averaged Poynting vector definitions of diffraction efficiency [(61) and (62)], power is conserved among the propagating diffracted orders. This is true regardless of the number of orders (i) retained and the inaccuracies in the diffracted amplitudes that result from the truncation. Thus for a phase grating the sum of all of the efficiencies for the propagating waves is unity. That is,

$$\sum_i (DE_{1i} + DE_{3i}) = 1. \tag{63}$$

F. Example Results

Using the approach described in the preceding sections, it is possible to calculate rigorously the fundamental and higher order forward- and backward-diffracted wave amplitudes and diffraction efficiencies. Example diffraction efficiency results for incidence at the first Bragg angle ($m = 1$) are shown in Fig. 7 for a "transmission" grating (fundamental diffracted order that satisfies the Bragg condition is forward diffracted) and in Fig. 8 for a "reflection" grating (fundamental diffracted order that satisfies the Bragg condition is backward diffracted). A more detailed discussion of the terminology "transmission" and "reflection" gratings is given in Section V-I. Diffraction efficiencies for both TE and TM polarization are presented. For simplicity, the average permittivity is the same in all 3 regions ($\varepsilon_I = \varepsilon_0 = \varepsilon_{III} = 2.25$).

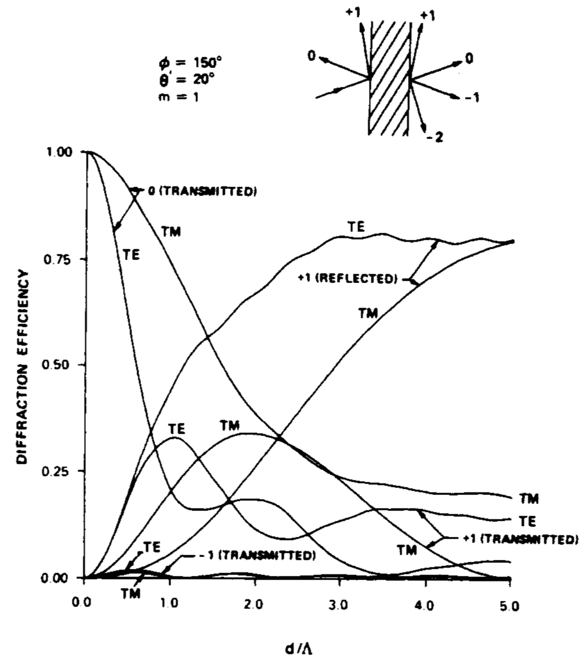

Fig. 8. Rigorously calculated diffraction efficiencies of forward- and backward-diffracted waves for a "reflection" dielectric $\phi = 150°$ slanted grating for both TE and TM polarizations. The average permittivity inside and outside the grating is the same ($\varepsilon_I = \varepsilon_0 = \varepsilon_{III} = 2.25$). The grating modulation is 0.330 and the angle of incidence $\theta' = 20°$ is at the first Bragg angle ($m = 1$). The diffraction efficiencies for all diffracted waves not shown are less than 1 percent.

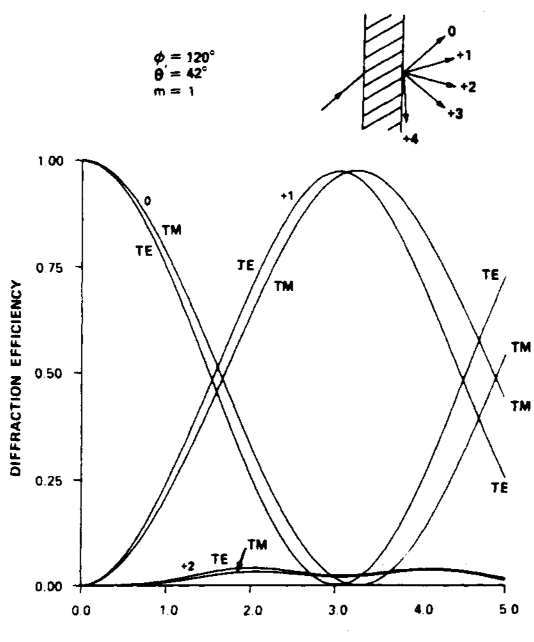

Fig. 7. Rigorously calculated diffraction efficiencies of forward-diffracted waves for a "transmission" dielectric $\phi = 120°$ slanted grating for both TE and TM polarizations. The average permittivity inside and outside the grating is the same ($\varepsilon_I = \varepsilon_0 = \varepsilon_{III} = 2.25$). The grating modulation is $\varepsilon_1/\varepsilon_0 = 0.120$ and the angle of incidence $\theta' = 42°$ is at the first Bragg angle ($m = 1$). The diffraction efficiencies for all diffracted waves not shown are less than 1 percent.

For the "transmission" grating shown in Fig. 7, the grating slant angle is $\phi = 120°$ (angle from z axis to grating vector). The angle of incidence is $\theta' = 42°$ and this is the first Bragg angle ($m = 1$). The corresponding $i = +1$ diffracted order is in region 3 and thus is a forward-diffracted order ("transmission" grating). The grating modulation is $\varepsilon_1/\varepsilon_0 = 0.120$. In Fig. 7, the powers in the $i = 0$, $+1$, and $+2$ forward-diffracted orders are shown. The $i \leqslant -1$ and $i \geqslant +5$ fields in both regions 1 and 3 are evanescent (cut off). The $i = +3$ and $+4$ forward-diffracted waves and all of the backward-diffracted waves have efficiencies of less than 1 percent and are not shown on the graph. In the rigorous coupled-wave analysis performed, the space-harmonic fields from $i = -4$ to $i = +5$ were retained to achieve convergence in the normalized field amplitudes to one part in 10^6. Conservation of power among the beams (63) was accurate to one part in 10^{12} independently of the number of orders retained in the analysis. As the thickness d of the grating is increased, the power in the TM-polarized $i = +1$ and $+2$ diffracted waves is initially less than that for the TE-polarized diffracted waves because of the reduced coupling for the TM compared to the TE polarization. For the appropriate thickness, the $i = +1$ diffraction efficiency approaches 100 percent for both polarizations.

For the "reflection" grating shown in Fig. 8, the grating slant angle is $\phi = 150°$ and the angle of incidence is $\theta' = 20°$. The incident wave is thus at the first Bragg angle ($m = 1$). The corresponding $i = +1$ diffracted order that satisfies the Bragg condition is in region 1 and thus is a backward-diffracted order ("reflection" grating). The grating modulation is $\varepsilon_1/\varepsilon_0 = 0.330$. In Fig. 8, the powers in the $i = -1$, 0, and $+1$ forward-diffracted orders and the $i = +1$ backward-diffracted orders are shown. The $i \leqslant -3$ and $i \geqslant +2$ fields in both regions 1 and 3 are evanescent (cut off). The $i = +2$ forward-diffracted wave and the $i = -2$, -1, and 0 backward-diffracted waves have efficiencies of less than 1 percent and are not shown on the graph. Again the $i = -4$ through $i = +5$ fields were retained in the rigorous coupled-wave analysis and the same level of accuracy was obtained as before. With increasing grating thickness the diffraction efficiency for TM polarization again lags that for the TE polarization due to the reduced coupling in the TM case. The $i = +1$ backward (reflected) diffraction efficiencies increase approximately monotonically to about 85 percent. The $i = +1$ forward- (transmitted) diffracted orders (that do not satisfy the Bragg condition) are observed to be over 30 percent for some thicknesses. The amplitudes of the $i = +1$ forward- and backward-diffracted waves cannot both be calculated if a first-order theory (neglecting second derivatives of the field amplitudes) is used. In these theories, the $i = +1$ forward-diffracted amplitudes would erroneously be set equal to zero. The various approximate theories and their implications are discussed in the next section.

V. Approximate Diffraction Theories

A. *Introduction*

The vast majority of the papers on grating diffraction theory have dealt with approximate theories. There are a large number of possible approximations and assumptions that can be made. These generally lead to enormous simplification in the analyses. In some cases, these simplifications allow analytic solutions to be obtained. A number of famous analytic expressions occur for special limiting cases.

In this section, a large number of planar grating diffraction theories are classified in terms of the fundamental assumptions: 1) neglect of higher order waves, 2) neglect of second derivatives of the field amplitudes, 3) neglect of boundary effects, 4) neglect of dephasing from the Bragg condition, 5) the small grating modulation approximation, and 6) the short-wavelength approximation. In addition to these assumptions, a number of other approximations such as normal incidence and unslanted gratings may also be made. However, in this section, only the fundamental assumptions enumerated above are treated. Thus all of the approximate theories are presented in their general form allowing for arbitrary angle of incidence (θ'), arbitrary grating slant angle (ϕ), and arbitrary grating period (Λ). The various further reductions can then be easily formulated, if desired, from these general forms of the approximate theories.

In region 1 of Fig. 4, backward-traveling waves exist. In general, these waves are produced both by diffraction from within the grating volume and by boundary effects (diffraction and reflection from the periodic boundaries at $z = 0$ and $z = d$). These physical processes produce a spectrum of plane waves traveling back into region 1 ($z < 0$). For the general planar grating of Fig. 4, neglecting the second derivatives of the field amplitudes in the wave equation reduces the number of waves in the analysis from $2n$ to n. The bulk diffracted orders are retained and the boundary-produced waves are eliminated. Thus for a planar grating, the neglect of second derivatives and the neglect of boundary effects are absolutely linked together. When these assumptions are made, the resulting first-order coupled-wave analyses have the amplitude of the diffracted waves calculated *inside* the modulated region. Then the amplitudes T_i of the forward-diffracted output waves are obtained (approximately) by arguing that they are equal to $S_i(d)$, the space harmonic field amplitude at a distance d from the input surface $z = 0$. Likewise, for those values of i that represent backward-diffracted waves, the amplitudes R_i are estimated to be $S_i(0)$. However, in the physical problem being analyzed, there are no boundaries at $z = 0$ and $z = d$. These planes just represent reference locations. There are no reflected or diffracted waves resulting from these planes and thus there are no physical boundaries at these locations! Thus the assumptions of neglecting the second derivatives of field amplitudes and neglecting boundary effects have transformed the problem into a filled-space problem (a grating filling all space) with imaginary boundaries at $z = 0$ and $z = d$ that are used only to obtain an approximate mathematical formulation of the problem. The first-order theory approaches are not capable of solving the problem of general planar slab grating bounded by two media different from the grating medium. These two linked assumptions, therefore, unmistakably imply the filled-space problem. *After* the filled-space problem is solved, *then* it is assumed that the grating terminates at $z = 0$ and $z = d$ and, as a result, that $T_i \approx S_i(d)$ for the forward-diffracted waves and $R_i \approx S_i(0)$ for the backward-diffracted waves. This is obviously only an approximation to the actual situation.

Another consequence of neglecting second derivatives is the exclusion of some propagating waves. In first-order theory, only half of the waves can be retained in the analysis. That is, only one set of i values (as opposed to two sets) is included. For a general slanted grating, some of these waves may be forward-diffracted and some of them may be backward-diffracted. From (30), if $k_{2z} - iK\cos\phi$ is positive, the wave is forward-diffracted and if negative, it is backward-diffracted. For forward-diffracted waves, the boundary condition used must be $S_i(0) = 0$. For backward-diffracted waves, the appropriate boundary condition is $S_i(d) = 0$. The second set of waves (set of i values) is phase matched to these waves. This second set of waves is, of course, neglected in any first-order analysis. For the example depicted in Fig. 5, the backward-diffracted waves for $-1 \leqslant i \leqslant +4$ would all be neglected in first-order theory. The diffraction efficiencies of these backward-diffracted waves are arbitrarily set equal to zero. For the case of a slanted-fringe grating, the power in the neglected phase-matched waves has been shown to be very significant in some cases [8]. Thus the errors introduced by using first-order theory can be particularly significant for slant angles away from $\phi = 0$ and $\phi = \pi/2$.

Still another consequence of neglecting second derivatives is the exclusion of evanescent waves from the analysis. In first-order theory, the filled-space nature of the grating being analyzed, causes one complete set of diffracted orders (i) to exist inside the grating, since all of the $S_i(z)$'s exist there. These calculated values of $S_i(z)$ may have wavevectors with components either in the $+z$ or $-z$ directions. However, many of the wavevectors of the $S_i(z)$'s cannot be phased matched to plane waves outside of the grating

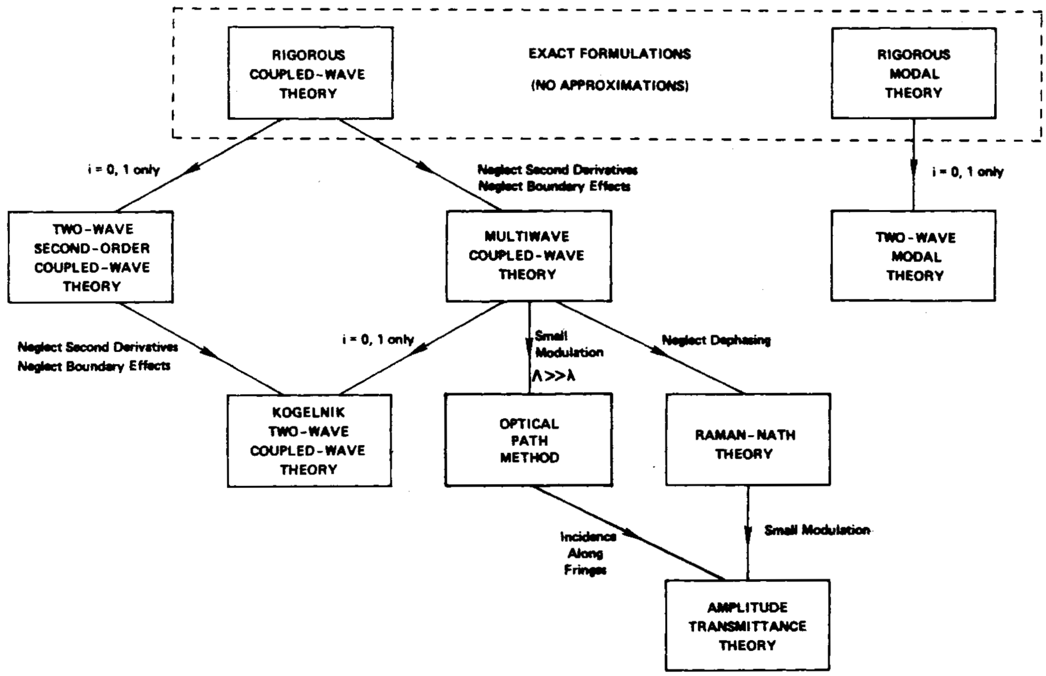

Fig. 9. Interrelationships between various planar grating diffraction theories in terms of fundamental approximations.

(regions 1 and 3). This may be seen from Fig. 5. For this example, the values $-1 \leqslant i \leqslant +4$ correspond to propagating plane waves in regions 1 and 3. The values $i \leqslant -2$ and $i \geqslant +5$ correspond to evanescent waves in region 1 and 3. However, in first-order analysis (without second derivatives) all values of i are treated as representing propagating waves. This is obviously not true. Nevertheless, diffraction efficiencies can be calculated for these evanescent waves as though they were propagating. These predicted efficiencies are clearly incorrect since they should be zero. If the grating period is much larger than a wavelength ($\Lambda \gg \lambda$), then there will be a large number of propagating waves and the effect of excluding evanescent waves would be reduced.

Therefore, it is concluded that all first-order theories inherently contain: 1) the approximate method for calculating diffracted amplitudes described above, 2) neglect of phase-matched diffracted waves, and 3) neglect of evanescent waves.

A depiction of various planar grating diffraction theories and their interrelationships in terms of fundamental assumptions is shown in Fig. 9. Most of the literature on planar grating diffraction theory can be connected with a particular block in this diagram.

B. Two-Wave Modal Theory

If only the zero- and first-order waves ($i = 0, 1$) are retained and all higher order waves are neglected, a two-wave regime is being assumed. There are actually a total of four waves in this analysis since there are two more phases matched to these. Modal theory solutions in the two-wave regime were first obtained by Bergstein and Kermisch [14] with more recent results being contributed by Lederer and Langbein [35] and Russell [21]. In this approach, the standard modal expansion (21) is used to represent the fields in the grating. However, in the two-wave case only the first two Fourier components ($i = 0, 1$) of the periodic function $\Phi_m(\bar{r})$ are retained in the analysis (20). Comparison of two-wave modal theory with exact rigorous theory [8] has shown that this can be valid near Bragg incidence in reflection gratings (backward-diffracted waves dominate). Comparison data are shown in [8, fig. 9].

C. Two-Wave Second-Order Coupled-Wave Theory

Two-wave second-order coupled-wave theory and two-wave modal theory represent exactly the same approximation. Both representations include second derivatives of field amplitudes and boundary effects. Both theories retain only the transmitted wave ($i = 0$) and the fundamental diffracted wave ($i = 1$) and their phased matched waves and neglect higher order waves. This approximate theory has been used by Kong [6]. Additional approximations in this theory have been made by Kessler and Kowarschik [36]–[38] and by Jaaskelainen *et al.* [39]. The two governing equations may be obtained directly from the rigorous coupled-wave equations (33) by keeping only terms in S_0 and S_1 and neglecting all other field amplitudes. The resulting two equations from (33) are

$$\frac{1}{2\pi^2}\frac{d^2S_0(z)}{dz^2} - j\frac{2(\epsilon_0)^{1/2}\cos\theta}{\pi\lambda}\frac{dS_0(z)}{dz} + \frac{\epsilon_1}{\lambda^2}S_1(z) = 0 \tag{64}$$

$$\frac{1}{2\pi^2}\frac{d^2S_1(z)}{dz^2} - j\frac{2}{\pi}\left[\frac{(\epsilon_0)^{1/2}\cos\theta}{\lambda} - \frac{\cos\phi}{\Lambda}\right] \cdot \frac{dS_1(z)}{dz} + \frac{2(m-1)}{\Lambda^2}S_1(z) + \frac{\epsilon_1}{\lambda^2}S_0(z) = 0. \tag{65}$$

Kong [6] has presented analytical solutions for the two-wave second-order coupled-wave theory expressed in the form of two transmission and two reflection coefficients for the unslanted-fringe planar slab grating.

D. Multiwave Coupled-Wave Theory

Multiwave first-order coupled-wave theory may also be developed directly from the rigorous coupled-wave equations (33). In this approach, higher order waves are retained (hence "multiwave"). The second derivatives of the field amplitudes (and thus boundary effects) are neglected. The resulting multiwave coupled-wave equations from (33) are

$$-j\frac{2}{\pi}\left[\frac{(\varepsilon_0)^{1/2}\cos\theta}{\lambda}-\frac{i\cos\phi}{\Lambda}\right]\frac{dS_i(z)}{dz}+\frac{2i(m-i)}{\Lambda^2}S_i(z)+\frac{\varepsilon_1}{\lambda^2}[S_{i+1}(z)+S_{i-1}(z)]=0. \tag{66}$$

For the case of the unslanted transmission grating ($\phi=\pi/2$) and normal incidence ($\theta=0, m=0$), the multiwave coupled-wave equations first appeared in a 1936 paper by Raman and Nath [40] for a sinusoidal (rather than cosinusoidal) grating. This paper [40] was the fourth in a series of five papers by Raman and Nath [40]–[44] on the diffraction of light by sound waves. The first three papers [41]–[43] form the basis of the "Raman–Nath theory" described below. This simplified multiwave coupled-wave equation was referred to by Nath [45] as being due to Nath [46]. In this 1936 paper, Nath [46] obtained a very slowly converging series solution for the multiwave coupled-wave difference-differential equations. An alternative series solution was later presented by Berry [47]. This series solution is in terms of Bessel functions and is also very slowly converging. Numerical solutions of the multiwave coupled-wave equations (also for acoustooptic interaction studies) have been obtained by Klein and Cook [3].

The multiwave coupled-wave equations have been generalized to include loss and gratings of arbitrary nonsinusoidal profile by Magnusson and Gaylord [7]. In that paper, numerical solutions were obtained for unslanted transmission gratings using a Runge–Kutta algorithm to solve the first-order system of coupled-wave equations. Diffraction efficiency results for sinusoidal, square-wave, and sawtooth phase gratings at first, second, and third Bragg incidence are presented there.

Comparison of diffraction efficiency results from multiwave first-order coupled-wave theory with exact rigorous theory has shown that this theory without second derivatives gives good results in transmission gratings (forward-diffraction waves dominate) when the grating modulation is small. Comparison data are shown in [8, figs. 7 and 8].

E. Two-Wave First-Order Coupled-Wave Theory

If higher order waves ($i\neq 0,1$) and second derivatives of field amplitudes (and thus boundary effects) are *both* neglected, the rigorous coupled-wave equations (33) reduce to two-wave first-order coupled-wave theory. For general slanted gratings at arbitrary incidence the two governing equations are

$$\cos\theta\frac{dS_0(z)}{dz}+j\frac{\pi\varepsilon_1}{2(\varepsilon_0)^{1/2}\lambda}S_1(z)=0 \tag{67}$$

$$\left[\cos\theta-\frac{\lambda}{\Lambda(\varepsilon_0)^{1/2}}\right]\frac{dS_1(z)}{dz}+j\frac{\pi\lambda(m-1)}{\Lambda^2(\varepsilon_0)^{1/2}}S_1(z)+j\frac{\pi\varepsilon_1}{2(\varepsilon_0)^{1/2}\lambda}S_0(z)=0. \tag{68}$$

Two-wave first-order coupled-wave theory was applied to acoustooptics by Phariseau [2]. It was first applied to holography by Kogelnik [4]. His thorough 1969 paper [4] is now very widely referenced. As a result, this theory is commonly called "Kogelnik theory" and this is noted in Fig. 9. The substantial recognition received by Kogelnik's paper [4] is due in part to the comprehensive coverage of 1) phase, absorption, and mixed gratings; 2) on-Bragg and off-Bragg incidence; 3) pure transmission ($\phi=\pi/2$), pure reflection ($\phi=0$), and general slanted fringe gratings; and 4) both TE-mode and TM-mode polarization.

From (30), if $k_2\cos\theta-K\cos\phi$ is positive, the single diffracted wave in this analysis is forward-diffracted and the grating is called a transmission grating. If $k_2\cos\theta-K\cos\phi$ is negative, the single diffracted wave is backward-diffracted and the grating is called a reflection grating. For the forward-diffracted case, the boundary condition used is $S_1(0)=0$. In the backward-diffracted case, the boundary condition used is $S_1(d)=0$. Due to the first-order nature of this theory, some phase-matched waves will be neglected. In the transmission grating case, for example, the two backward-traveling waves (that are phase matched to the zero-order transmitted wave and the fundamental diffracted wave) are neglected.

For the special case of a phase grating with unslanted fringes ($\phi=\pi/2$) and incidence at the first Bragg angle ($m=1$), the first-order diffracted amplitude from (67) and (68) is given by [2], [4]

$$S_1(z)=-j\sin\left[\frac{\pi\varepsilon_1 z}{2(\varepsilon_0)^{1/2}\lambda\cos\theta}\right] \tag{69}$$

where z is the distance into the grating at which the amplitude is determined. This well-known expression predicts a diffraction efficiency ($DE=S_i(d)S_i^*(d)$ for this case) that is sinusoidal in modulation and has a maximum value of 100 percent. Although the two-wave first-order coupled-wave theory neglects higher order diffracted waves and second derivations of field amplitudes (and thus also boundary effects), it nevertheless contains many of the basic features of the diffraction process in an extended grating. This theory has been successfully extended to numerous other cases including finite beams [48], [49], finite and nonplanar gratings [50]–[52], and attenuated gratings [38], [53]–[55]. When grating diffraction is described by the two-wave result, (69), it is often referred to as "Bragg regime" diffraction. Incidence at the Bragg angle is essential in "Bragg regime" diffraction whereas in "Raman–Nath regime" diffraction described below it is not. Criteria for "Bragg regime" behavior are given in [56] and [57].

F. Optical Path Method

The optical path length method was first applied to grating diffraction by Raman and Nath [41], [42]. Later it was used by Klein and Cook [3] and Syms and Solymar [58] to treat slanted and unslanted lossless gratings for a general angle of incidence. In this approach, the permittivity modulation ε_1 (and thus the refractive index modulation) is assumed to be small. As a consequence, it is postulated that the small variation of refractive index in the grating does not alter the straight-line directions of the rays but that it does alter the phase of the light. Thus the optical path length (index of refraction multiplied by the propagation distance) varies for different directions through the grating. In addition, it is assumed that the wavelength of the light is very small compared to a period of the grating ($\lambda \ll \Lambda$). This is equivalent to assuming that the waves inside the grating are homogeneous plane waves on a local basis. Using $\lambda/\Lambda \ll 1$, the multiwave coupled-wave equations (66) reduce to

$$-j\frac{2(\varepsilon_0)^{1/2}\cos\theta}{\pi}\frac{dS_i(z)}{dz}+\frac{4i(\varepsilon_0)^{1/2}\cos(\theta-\phi)}{\Lambda}S_i(z)+\frac{\varepsilon_1}{\lambda}[S_{i+1}(z)+S_{i-1}(z)]=0. \quad (70)$$

These optical path method differential equations allow for a general angle of incidence and grating slant angle. However, the grating modulation must be small.

These equations have been generalized for a variety of grating profiles by Syms and Solymar [58]. For a sinusoidal grating with unslanted fringes, (70) may be solved to yield

$$S_i(z)=(-j)^i\exp(ji\pi z\tan\theta/\Lambda)J_i\left[\frac{\Lambda\varepsilon_1\sin(\pi z\tan\theta/\Lambda)}{\lambda(\varepsilon_0)^{1/2}\sin\theta}\right] \quad (71)$$

subject to the boundary conditions $S_0(0)=1$ and $S_i(0)=0$ ($i\neq 0$) where J_i is an integer-order Bessel function of the first kind. It predicts maximum values of $DE_{\pm 1}=33.8$ percent, $DE_{\pm 2}=23.6$ percent, $DE_{\pm 3}=18.8$ percent, and so forth.

G. Raman–Nath Theory

The theory of Raman and Nath [41]–[44] may also be obtained directly from the rigorous coupled-wave equations. If second derivatives of the field amplitudes and dephasing from the Bragg condition are both neglected, the rigorous coupled-wave equations (33) reduce to the Raman–Nath diffraction equations

$$-j\frac{2}{\pi}\left[\frac{(\varepsilon_0)^{1/2}\cos\theta}{\lambda}-\frac{i\cos\phi}{\Lambda}\right]\cdot\frac{dS_i(z)}{dz}+\frac{\varepsilon_1}{\lambda^2}[S_{i+1}(z)+S_{i-1}(z)]=0 \quad (72)$$

where a general angle of incidence and grating slant angle have been retained. The S_i term in (33) has been neglected. For the ith diffracted order, this term is zero for the mth Bragg incidence (34) where $i=m$. For an arbitrary angle of incidence, each diffracted order will be dephased by varying amounts from their corresponding Bragg conditions. This, in turn, reduces the synchronism between the input wave and that diffracted order. The result is less coupling from the input to that order. The Raman–Nath theory therefore, treats all diffracted orders as though the Bragg conditions for all of them were simultaneously satisfied.

For the important case of an unslanted fringe transmission grating ($\phi=\pi/2$), (72) takes the form of a recurrence relation satisfied by Bessel functions. The solution is

$$S_i(z)=(-j)^iJ_i\left[\frac{\pi\varepsilon_1 z}{(\varepsilon_0)^{1/2}\lambda\cos\theta}\right] \quad (73)$$

for boundary conditions $S_0(0)=1$ and $S_i(0)=0$ ($i\neq 0$). Equation (73) is the famous Bessel function expression of Raman and Nath. When grating diffracting behavior may be approximated by (73), it is referred to as "Raman–Nath regime" diffraction. This result, (73), has been extensively used to predict the light intensities diffracted by sound waves [47], [59]. Criteria for "Raman–Nath regime" diffraction are given in [57] and [60]. Raman–Nath theory has been extended to describe nonsinusoidal phase gratings [61]–[63].

H. Amplitude Transmittance Theory

For gratings, the amplitude transmittance approach is closely related to Raman–Nath diffraction theory. The amplitude transmittance approach is widely used in optics [64], [65] and may be applied to slabs, lenses, apertures, and general two-dimensional objects as well as gratings. The amplitude transmittance is defined as the ratio of the field amplitude over the output plane to the field amplitude incident on the input plane. The amplitude transmittance function in general is complex. It may be applied to gratings with unslanted fringes. Both amplitude gratings [64]–[68] and phase gratings [62]–[67] have been treated in the literature using the amplitude transmittance approach.

For a phase grating with periodicity in the x direction, the amplitude transmittance function is

$$\tau(x,z)=\exp\left[-j\frac{2\pi n(x)z}{\lambda\cos\theta}\right] \quad (74)$$

where z is the grating thickness and $n(x)=[\varepsilon(x)]^{1/2}$ is the periodic refractive index. Since the transmittance function is also periodic in x, it may be expanded in a complex Fourier series. Further, because the exponentials in this series are in the form of an expansion of the diffracted plane waves, then the Fourier coefficients are the diffracted wave amplitudes. The Fourier series expansion may thus be written

$$\tau(x,z)=\sum_i S_i(z)\exp(jiKx) \quad (75)$$

where S_i represents the amplitude of the ith diffracted order. By definition, the coefficients of the Fourier series may be calculated from

$$S_i(z)=\frac{1}{\Lambda}\int_0^{\Lambda}\exp\left[-j\frac{2\pi[\varepsilon(x)]^{1/2}z}{\lambda\cos\theta}\right]\exp(-jiKx)\,dx. \quad (76)$$

Thus the diffracted amplitudes may be determined directly, knowing $\varepsilon(x)$, by integrating (76). Results for sinusoidal, square-wave, sawtooth, triangular, and rectangular refractive-index profiles are given in [62].

For the unslanted-fringe (co)sinusoidal-permittivity transmission grating, the corresponding index of refraction is

$$n(x)\equiv[\varepsilon(x)]^{1/2}=(\varepsilon_0+\varepsilon_1\cos Kx)^{1/2} \quad (77)$$

which may be expanded in a Fourier cosine series as

$$[\varepsilon(x)]^{1/2}=[\varepsilon(x)]_0^{1/2}+\sum_{h=1}^{\infty}[\varepsilon(x)]_h^{1/2}\cos(hKx) \quad (78)$$

with Fourier harmonic amplitudes given by

$$[\varepsilon(x)]_h^{1/2} = \frac{2}{\Lambda}\int_0^{\Lambda}(\varepsilon_0 + \varepsilon_1 \cos Kx)^{1/2}\cos(hKx)\,dx. \quad (79)$$

The average value of the refractive index may be expressed concisely as

$$n_0(x) \equiv [\varepsilon(x)]_0^{1/2} = (2/\pi)(\varepsilon_0 + \varepsilon_1)^{1/2} E(\zeta, \pi/2) \quad (80)$$

where $E(\zeta, \pi/2)$ is the complete elliptic integral of the second kind and $\zeta \equiv 2\varepsilon_1/(\varepsilon_0 + \varepsilon_1)$. Clearly, the case of a sinusoidal permittivity (or dielectric constant) being treated throughout this paper is not the same as a sinusoidal refractive-index grating. The index of reflection corresponding to sinusoidal permittivity has higher spatial frequency harmonics ($h > 1$) in addition to a fundamental sinusoidal component ($h = 1$) as represented by (78). However, for the case of sufficiently small modulation, a sinusoidal permittivity produces nearly a sinusoidal index of refraction. In the limit of small modulation (ε_1 approaches zero), (79) and (80) yield

$$[\varepsilon(x)]_0^{1/2} \simeq \varepsilon_0 \quad (81)$$

$$[\varepsilon(x)]_1^{1/2} \simeq \varepsilon_1/2(\varepsilon_0)^{1/2} \quad (82)$$

$$[\varepsilon(x)]_2^{1/2}, [\varepsilon(x)]_3^{1/2}, \cdots \simeq 0. \quad (83)$$

This analysis is important in that it now allows the Raman–Nath theory and amplitude transmittance theory to be interrelated. The result is that although (76) was obtained using the amplitude transmittance approach, it is *also* a solution of the Raman–Nath difference-differential equation (72) for unslanted gratings in the limit of small modulation. This may be shown by direct substitution of S_i as given by (76) into the Raman–Nath diffraction equation (72). Thus for a cosinusoidal refractive-index profile, the integral (76) when evaluated gives the Bessel function result (73). This may be accomplished using the identity

$$\exp(-jb\cos\alpha) \equiv \sum_{i=-\infty}^{+\infty} (-j)^i J_i(b)\exp(ji\alpha) \quad (84)$$

and the orthogonality relationship

$$\frac{1}{\Lambda}\int_0^{\Lambda} \exp(j\ell Kx)\exp(-jiKx)\,dx = \delta_{\ell i} \quad (85)$$

where $\delta_{\ell i}$ is the Kronecker delta. Therefore, as depicted in Fig. 9, it has been shown that Raman–Nath theory and amplitude transmittance theory are equivalent in the limit of small grating modulation. This is true in general for unslanted gratings regardless of the grating profile (square-wave, sawtooth, etc.). Likewise, the optical path method reduces to the amplitude transmittance theory for angles of incidence that are small with respect to the grating fringes.

I. Validity of Approximate Theories

In general, both backward-diffracted orders and forward-diffracted orders are produced when a wave is incident upon a grating. This tends to make the terminology "reflection" grating and "transmission" grating seem imprecise, since the grating both "reflects" and "transmits" diffracted orders. However, the distinction between reflection and transmission gratings can be quantified. The diffracted order (i) that satisfies (or most nearly satisfies) the Bragg condition (34) is used to determine whether the grating is acting as a reflection grating or a transmission grating. The Bragg condition represents, on a local basis, the condition for constructive interference of the individual contributions to a diffracted wavefront. When the Bragg condition is satisfied, the diffracted wave may be visualized as having equal angles of incidence and diffraction (or "reflection") with respect to the grating fringes. If the diffracted order whose integer value of i is equal to (or most nearly equal to) the value of m calculated from the Bragg condition is in region 1, the grating is exhibiting reflection grating behavior. Similarly, if the wave that satisfies (or most nearly satisfies) the Bragg condition is in region 3, the grating is exhibiting transmission grating behavior. Obviously, a single grating might act as reflection grating for one angle of incidence and as a transmission grating for another angle of incidence.

For the basic planar grating case, a comparison of diffraction efficiency results from exact rigorous theory and from approximate theories has been made in [8] for incident TE polarization and in [29] for incident TM polarization. This has been done for a series of angles of incidence and slant angles so that both reflection and transmission behavior were produced. For TE polarization, if the grating behaves as a transmission grating, higher order waves need to be included in the analysis to obtain accurate results. However, second derivatives and boundary effects may be neglected. Conversely, for TE polarization, if the grating behaves as a reflection grating, second derivatives and boundary effects need to be included for accurate results and higher order waves may be neglected. For an incident plane wave of TM polarization, the situation is more complicated. Unlike the case for TE polarization where there is direct coupling only between adjacent orders [i is coupled to $i-1$ and $i+1$ as shown by (28), (33), or (38)], for TM polarization there is direct coupling between all orders (as shown by [29, eq. (13)]). This makes the inclusion of higher order waves necessary for reflection as well as for transmission gratings when the incident wave is TM polarized. As in the case of TE polarization, second derivatives and boundary effects are needed for accurate results when the primary diffracted order is a backward-diffracted order (reflection grating). For a transmission grating and TM polarization, second derivatives and boundary effects can generally be neglected. However, *if* a major low-order wave is at or just above or just below cutoff, the diffraction analysis requires *both* higher order waves and second derivatives together with boundary effects to give accurate results for both TE and TM polarizations and for both reflection and transmission gratings (e.g., see [29, fig. 1]). The complicated diffraction behavior near a cutoff condition is generally referred to as a Wood's anomaly [69]. These cases can, of course, be treated without any approximation using the rigorous coupled-wave theory described in this paper.

For an unslanted fringe transmission grating, Raman–Nath regime diffraction occurs when the diffraction efficiency [from (73)] is given by

$$DE_i = J_i^2(2\gamma) \quad (86)$$

where γ is the grating strength parameter given by $\gamma = \pi\varepsilon_1 d/2\lambda(\varepsilon_0)^{1/2}\cos\theta$ for TE polarization and by $\gamma = \pi\varepsilon_1 d\cos 2\theta/2\lambda(\varepsilon_0)^{1/2}\cos\theta$ for TM polarization. The occurrence (or lack of occurrence) of Raman–Nath regime diffraction as given by (86) may be determined using a number of different criteria [60] depending on the application of the grating. The practical criteria and their interpretations are: 1) *Zero-Order Beam Criterion*—the undiffracted (zero-order) diffraction efficiency is predicted by (86) to within some specified limit; 2) *First-Order Beam Criterion*—the fundamental (first-order) diffraction efficiency is predicted by (86) to within some specified limit; and 3) *Composite Criterion*—all diffracted orders simultaneously have diffraction efficiencies predicted by (86) to within some limit. Each of these criteria is evaluated in [60]. It is shown there that each of these criteria is met to within 1-percent diffraction efficiency when the condition

$$Q'\gamma \leqslant 1 \tag{87}$$

is satisfied. Q' is a grating parameter given by $Q' = Q\cos\theta = 2\pi\lambda d(\varepsilon_0)^{1/2}\Lambda^2\cos\theta$. This condition was originally used by Extermann and Wannier [70] and later in the form $Q'\gamma \leqslant \pi^2/8$ by Willard [71].

For a transmission grating, the Bragg regime (or two-wave regime) occurs when the diffraction efficiency [from (69)] is given by

$$DE_1 = \sin^2\gamma \tag{88}$$

for the single fundamental diffracted order. Correspondingly, the transmitted (zero-order) wave has a diffraction efficiency given by $\cos^2\gamma$. The occurrence (or lack of occurrence) of Bragg regime diffraction as given by (88) may be determined by using a number of different criteria [56] depending on the application. The practical criteria include the *Zero-Order Beam Criterion* and *First-Order Beam Criterion* defined as before except that the deviation is with respect to (88). The other criteria and their interpretations are: *Two-Wave Criterion*—the sum of the diffraction efficiencies associated with all higher order waves is less than some specified limit; and *Composite Criteria*—all three criteria are met to within some specified limit. Each of these criteria is evaluated in [56]. Those evaluations showed that each of these criteria is met to within 1-percent diffraction efficiency when the condition

$$\rho \equiv Q'/2\gamma \geqslant 10 \tag{89}$$

is satisfied. For TE polarization $\rho = 2\lambda^2/\Lambda^2\varepsilon_1$, and TM polarization $\rho = 2\lambda^2/\Lambda^2\varepsilon_1\cos 2\theta$. The regime parameter ρ was first used by Nath [45]. It is now clear that this parameter determines the Bragg diffraction regime boundary.

J. "Thin" and "Thick" Gratings [57]

The terminology "thin" and "thick" gratings is widely used in the literature. The meanings of these phrases may be distinguished either in terms of the diffraction regime *or* in terms of the angular/wavelength selectivity. Both types of definitions are implied in the literature. They are frequently used on an interchangeable basis even though they are based on different physical concepts and give rise to different mathematical definitions.

A "thin" grating may be described as a grating that produces Raman–Nath regime diffraction. In this case, the multiple forward-diffracted orders ideally have efficiencies DE_i given by (86). As described in the previous section, this occurs when $Q'\gamma \leqslant 1$. From this condition, it is apparent that Raman–Nath regime diffraction behavior will be observed for any value of γ (proportional to grating modulation ε_1) if Q' is sufficiently small. This has led to the incomplete popular condition of $Q' < 1$ for describing "thin" gratings [3].

A "thin" grating may alternatively be described as a grating exhibiting relatively little angular and wavelength selectivity. As the incident wave is dephased (either in angle of incidence or in wavelength) from the Bragg condition, the diffraction efficiency generally decreases. The angular range or wavelength range for which the diffraction efficiency decreases to half of its on-Bragg angle value is determined by the thickness of the grating (d) expressed as a number of grating periods. For a "thin" grating this number may be reasonably chosen to be

$$d/\Lambda < 10. \tag{90}$$

Gratings having angular and wavelength selectivities with full widths at half maxima wider than that for $d/\Lambda = 10$ may be considered to be "thin" gratings. This definition does not accurately predict the diffraction regime. It has the desirable feature that the governing parameter (d/Λ) is directly proportional to the grating thickness and thus "thin" and "thick" have direct physical interpretations.

A "thick" grating may be described as a grating that produces Bragg regime diffraction. This is described by the two-wave coupled-wave theory of Kogelnik [4]. In this regime, the single fundamental forward-diffracted order ideally has a diffraction efficiency given by (88). Bragg regime diffraction occurs when $\rho > 10$ as described in the previous section. It is particularly interesting to note that this diffraction-regime-based definition of a "thick" grating is independent of grating thickness! From (89) it is apparent that Bragg regime diffraction behavior will occur for any value of γ (or ε_1) if Q' is sufficiently large. Thus the incomplete condition $Q' > 1$ is often used to define a "thick" grating [3], [4]. However, if the criterion $DE_1 > DE_{-1}$ is added to the criteria for Bragg regime behavior listed in the previous section, then the condition $Q' > 1$ is needed [2], [72] in addition to (89).

A "thick" grating may alternatively be described as a grating exhibiting strong angular and wavelength selectivity. A relatively small change in the angle of incidence from the Bragg angle or a relatively small change in the wavelength at the Bragg angle produces significant dephasing and the diffraction efficiency decreases correspondingly. "Thick" grating behavior may be considered to occur when

$$d/\Lambda > 10. \tag{91}$$

This is the angular-and-wavelength-selectivity-based definition of a "thick" grating.

The definitions of "thin" and "thick" gratings may be concisely summarized as follows:

1) If "thin" grating is intended to mean Raman–Nath regime diffraction, then the required condition is $Q'\gamma \leqslant 1$.

2) If "thin" grating is intended to mean broad angular and wavelength selectivity, then the required condition is $d/\Lambda < 10$.

3) If "thick" grating is intended to mean Bragg regime diffraction, then the required condition is $\rho \geqslant 10$. (If $DE_1 > DE_{-1}$ is also included in the definition of Bragg regime, $Q' > 1$ is required in addition.)

4) If "thick" grating is intended to mean narrow angular and wavelength selectivity, then the required condition is $d/\Lambda > 10$.

A. Overview

Only planar gratings (having planar parallel boundaries) have been treated so far in this review. However, dielectric surface-relief (corrugated) gratings are also of great technological importance. In semiconductor distributed-feedback and distributed-Bragg-reflector lasers, for example, the gratings are invariably a periodic variation in the boundary. These surface-relief structures, like planar gratings, are also capable of very high diffraction efficiencies (approaching 100 percent). Corrugated gratings can be rigorously analyzed using coupled-wave analysis [73]. This is done by dividing the surface-relief grating into a large number of thin (planar) layers. Each thin layer is then analyzed using the state variables method of solution of the rigorous coupled-wave equations for that grating. By formulating the problem in a particular manner, it is shown that the grating layers may be treated one-at-a-time in sequence thus reducing the numerical calculations to an easily manageable size. There are no approximations in the analysis and results again are obtainable to any arbitrary level of accuracy. The diffraction efficiencies of all orders of both the transmitted and reflected waves are determined in the process.

B. Problem Formulation

As before, region 1 (the input region) is a homogeneous dielectric with a relative permittivity (dielectric constant) of ε_{I}. Likewise, region 3 is homogeneous with a relative permittivity of ε_{III}. Region 2 (the grating region) consists of a periodic distribution of both types of dielectrics. The boundary between the ε_{I} dielectric and the ε_{III} dielectric in region 2 is given by

$$z = F(x) = F(x + \Lambda) \tag{92}$$

where Λ is the grating period. The function $F(x)$ thus represents the grating surface profile. Unlike most methods for analyzing surface-relief gratings, there are no restrictions on the form of $F(x)$ in this analysis. Curved lines, straight lines, shadow regions, hidden regions, etc., are all allowed. The total electric field in region 1 is the sum of the incident and the backward-traveling waves in exactly the same manner as it was for the planar grating. The normalized total electric field in region 1 may thus be represented by (53). Likewise, the normalized total electric field in region 3 is given by (54) where d is now the groove depth.

In the present analysis, the grating region (region 2) is divided into N thin planar grating slabs perpendicular to the z axis as shown in Fig. 10. Then the rigorous coupled-wave analysis that has been developed for planar grating is applied to each slab grating. If the individual planar gratings are sufficiently thin, any grating profile can be analyzed to an arbitrary level of accuracy. The nth slab within region 2 as shown in Fig. 10 will consist of a periodic distribution of ε_{I} and ε_{III} dielectrics. The relative permittivity for the nth slab grating is periodic, $\varepsilon_n(x, z_n) = \varepsilon_n(x + \Lambda, z_n)$, and may be expanded in a Fourier series as

$$\varepsilon_n(x, z_n) = \varepsilon_{\text{I}} + (\varepsilon_{\text{III}} - \varepsilon_{\text{I}}) \sum_{h=-\infty}^{+\infty} \tilde{\varepsilon}_{h,n} \exp(jhKx) \tag{93}$$

where z_n is the z coordinate of the nth slab, h is the harmonic index, K is the magnitude of the grating vector

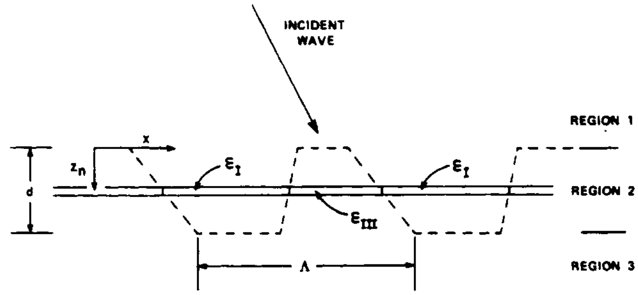

Fig. 10. The nth planar grating resulting from the decomposition of a surface-relief grating into N thin planar gratings.

($K = 2\pi/\Lambda$), and $\tilde{\varepsilon}_{h,n}$ are the normalized complex harmonic amplitude coefficients given by

$$\tilde{\varepsilon}_{h,n} = (1/\Lambda) \int_0^{\Lambda} f(x, z_n) \exp(-jhKx)\, dx \tag{94}$$

where the function $f(x, z_n)$ is equal to either zero or unity depending whether, for a particular value of x, the grating relative permittivity is ε_{I} or ε_{III}, respectively.

Using the coupled-wave equation, (31), the total electric field in the nth slab may be expressed as

$$E_{2,n}(x, z) = \sum_{i=-\infty}^{+\infty} S_{i,n}(z) \exp[(\bar{k}_{2,n} - i\bar{K}) \cdot \bar{r}] \tag{95}$$

where $\bar{K} = K\hat{x}$ and $\bar{k}_{2,n}$ is the wavevector of the zero-order ($i = 0$) refracted wave having a magnitude of $k_{2,n} = 2\pi(\varepsilon_{0,n})^{1/2}/\lambda$, and $\varepsilon_{0,n}$ is the average relative permittivity for the nth slab grating.

Substituting $E_{2,n}(x, z)$ and $\varepsilon_n(x, z_n)$ into the wave equation [cf. (2)], performing the indicated differentiations, and setting the coefficient of each exponential term equal to zero for nontrivial solutions yields the rigorous coupled-wave equations for the nth slab grating

$$\begin{aligned} &\frac{d^2 S_{i,n}(z)}{dz^2} - j2\left(k_{2,n}^2 - k_1^2 \sin^2\theta'\right)^{1/2} \frac{dS_{i,n}(z)}{dz} \\ &+ K^2 i(m - i) S_{i,n}(z) + k^2(\varepsilon_{\text{III}} - \varepsilon_{\text{I}}) \\ &\cdot \sum_{h=1}^{\infty} \left[\tilde{\varepsilon}_{h,n} S_{i-h,n}(z) + \tilde{\varepsilon}_{h,n}^{*} S_{i+h,n}(z)\right] = 0. \end{aligned} \tag{96}$$

These coupled-wave equations are analogous to (33).

C. Calculational Procedure

The dielectric surface-relief grating diffraction problem as formulated in the previous section will be solved in a sequence of steps. First, the rigorous coupled-wave equations will be solved for the nth slab grating using a state-variables method of solution. Second, electromagnetic boundary conditions (continuity of tangential E and tangential H) will be applied between region 1 and the first slab grating, then between the first and second slab gratings, and so forth and finally between the Nth slab grating and region 3. Third, the resulting array of boundary condition equations are solved for the reflected and transmitted diffracted amplitudes, R_i and T_i. From these amplitudes, the diffracted efficiencies are determined directly.

Defining state variables [cf. (47), (48)] for the nth slab grating transforms the infinite set of second-order differential equations (96) into two infinite sets of first-order state equations

$$\frac{dS_{1,i,n}(z)}{dz} = S_{2,i,n}(z) \tag{97}$$

$$\begin{aligned}\frac{dS_{2,i,n}(z)}{dz} = & -k^2(\varepsilon_{\text{III}} - \varepsilon_1)\sum_{h=1}^{\infty} \tilde{\varepsilon}_{h,n} S_{1,i-h,n}(z) \\ & - K^2 i(m-i) S_{1,i,n}(z) - k^2(\varepsilon_{\text{III}} - \varepsilon_1) \\ & \cdot \sum_{h=1}^{\infty} \tilde{\varepsilon}^{*}_{h,n} S_{1,i+h,n}(z) \\ & + j2\left(k_{2,n}^2 - k_1^2 \sin^2\theta'\right) S_{2,i,n}(z).\end{aligned} \tag{98}$$

In matrix form, the state equation for the nth slab grating may be written as:

$$\begin{bmatrix} \vdots \\ \dot{\tilde{S}}_{1,p,n} \\ \vdots \\ \dot{\tilde{S}}_{2,p,n} \\ \vdots \end{bmatrix} = \left[\begin{array}{c|c} a_{p,q,n} & b_{p,q,n} \\ \hline c_{p,q,n} & d_{p,q,n} \end{array}\right] \begin{bmatrix} \vdots \\ \tilde{S}_{1,q,n} \\ \vdots \\ \tilde{S}_{2,q,n} \\ \vdots \end{bmatrix} \tag{99}$$

where $\tilde{S}_{\ell,p,n} \equiv S_{\ell,i,n}$ (for $\ell = 1,2$), $\dot{S} = dS/dz$, and the elements of the four submatrices ($p = 1$ to s and $q = 1$ to s) are specified by (97) and (98) for the nth slab grating. The integers p and q are the row and column indices of the four submatrices. The maximum value of these indicies, s, is equal to the number of diffracted orders retained in the analysis. The value $p = 1$ corresponds to the most negative order (value of i) retained in the analysis and $p = s$ corresponds to the most positive order retained. For example, if an odd number of waves are retained symmetrically about $i = 0$ (the undiffracted wave) in the analysis, then $p = i + (s+1)/2$. Equation (99) corresponds to an unforced state equation $\dot{\boldsymbol{S}} = \boldsymbol{AS}$. As before, the solutions of (99) are

$$\tilde{S}_{p',n}(z) = \sum_{q'=1}^{2s} C_{q',n} w_{p',q',n} \exp(\lambda_{q',n} z) \tag{100}$$

where $\tilde{S}_{\ell,p,n}$ (for $\ell = 1,2$) has been rewritten as $\tilde{S}_{p',n}$ with $p' = p + (\ell - 1)s$. The quantities $\lambda_{q',n}$ and $w_{p',q',n}$ are the eigenvalues and eigenvectors of the matrix A. The integers p' and q' are the row and column indices of the eigenvector matrix $[w]$ and $p' = 1$ to $2s$ and $q' = 1$ to $2s$. The quantities $C_{q',n}$ are unknown constants to be determined by the boundary conditions. The desired diffracted wave amplitudes for the nth grating layer are given by $S_{i,n}(z) = \tilde{S}_{p',n}(z)$ where p' is chosen to correspond to the ith diffracted wave.

Electromagnetic boundary conditions require that the tangential electric and tangential magnetic fields be continuous across the boundaries between the slabs. For the TE-mode polarization described in this paper, the electric field only has a tangential component (y direction). The tangential component of H is in the x direction and from Maxwell's equations it is given by $H_x = (-j/\omega\mu)\partial E_y/\partial z$. Therefore, for the boundary ($z = 0$) between region 1 (the input region) and the first slab grating, the boundary condition for tangential E is

$$\delta_{i0} + R_i = \sum_{q'=1}^{2s} C_{q',1} w_{p',q',1} \tag{101}$$

and for tangential H is

$$j(\bar{k}_{1i} \cdot \hat{z})(R_i - \delta_{i0}) = \sum_{q'=1}^{2s} C_{q',1} w_{p',q',1}\left[\lambda_{q',1} - j(\bar{\sigma}_{i,1} \cdot \hat{z})\right] \tag{102}$$

where the value of p' is chosen to correspond to the ith wave. For the boundary between the nth and $n+1$th slab gratings ($z = nd/N$), the boundary condition for tangential E is

$$\begin{aligned}\sum_{q'=1}^{2s} & C_{q',n} w_{p',q',n} \exp\left\{\left[\lambda_{q',n} - j(\bar{\sigma}_{i,n} \cdot \hat{z})\right] nd/N\right\} \\ & = \sum_{q'=1}^{2s} C_{q',n+1} w_{p',q',n+1} \\ & \quad \cdot \exp\left\{\left[\lambda_{q',n+1} - j(\bar{\sigma}_{i,n+1} \cdot \hat{z})\right] \cdot nd/N\right\}\end{aligned} \tag{103}$$

and for tangential H is

$$\begin{aligned}\sum_{q'=1}^{2s} & C_{q',n} w_{p',q',n}\left[\lambda_{q',n} - j(\bar{\sigma}_{i,n} \cdot \hat{z})\right] \\ & \cdot \exp\left\{\left[\lambda_{q',n} - j(\bar{\sigma}_{i,n} \cdot \hat{z})\right] nd/N\right\} \\ & = \sum_{q'=1}^{2s} C_{q',n+1} w_{p',q',n+1}\left[\lambda_{q',n+1} - j(\bar{\sigma}_{i,n+1} \cdot \hat{z})\right] \\ & \quad \cdot \exp\left\{\left[\lambda_{q',n+1} - j(\bar{\sigma}_{i,n+1} \cdot \hat{z})\right] nd/N\right\}.\end{aligned} \tag{104}$$

For the boundary between the Nth slab grating and region 3 ($z = d$), the boundary condition for tangential E is

$$\sum_{q'=1}^{2s} C_{q',N} w_{p',q',N} \exp\left\{\left[\lambda_{q',N} - j(\bar{\sigma}_{i,N} \cdot \hat{z})\right] d\right\} = T_i \tag{105}$$

and for tangential H is

$$\begin{aligned}\sum_{q'=1}^{2s} & C_{q',N} w_{p',q',N}\left[\lambda_{q',N} - j(\bar{\sigma}_{i,N} \cdot \hat{z})\right] \\ & \cdot \exp\left\{\left[\lambda_{q',N} - j(\bar{\sigma}_{i,N} \cdot \hat{z})\right] d\right\} \\ & = -j(\bar{k}_{3i} \cdot \hat{z}) T_i.\end{aligned} \tag{106}$$

Equations (101)–(106) represent a total of $2(N+1)s$ equations. There are s unknown values each of R_i and T_i and $2s$ unknown values of $C_{q',n}$ for each slab grating. Thus the total number of unknowns is $2(N+1)s$, the same as the number of boundary condition equations. If s values of i are retained in the analysis, then the calculations will yield s transmitted wave amplitudes (T_i) and s reflected wave amplitudes (R_i).

An efficient procedure to solve this large system of equations is to use a technique like Gauss elimination [74] applied successively to each boundary starting at the $z = 0$ input surface. By using this technique $N + 1$ times in sequence, the s values of R_i and s values of T_i may be obtained in a single pass on the last step. As depicted in Fig. 11, the boundary condition equations are written as a matrix equation. The matrix is $2(N+1)s$ by $2(N+1)s$ and consists of the coefficients of $C_{q',n}$ (for $q' = 1$ to $2s$ and $n = 1$ to N), R_i (s values), and T_i (s values). For each slab

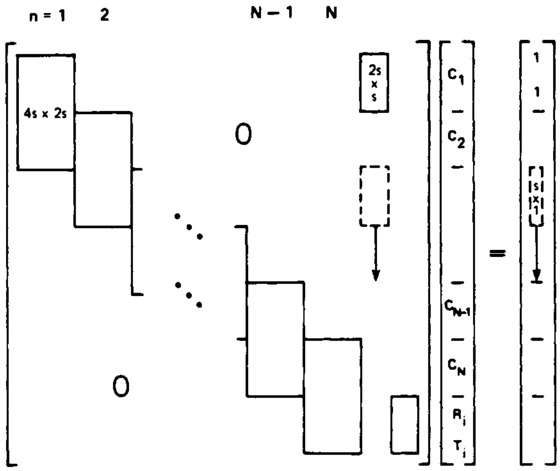

Fig. 11. Matrix-equation representation of $2(N+1)s$ boundary-condition equations, where s is the total number of diffracted waves retained in the analysis. C_1 represents the column vector $C_{q',1}$, where $q' = 1$ to $2s$ and likewise for C_2 through C_N. The reflected and transmitted amplitudes R_i and T_i are column vectors of length s. The product output vector, before manipulations, is all zeros except for the two ones that are shown. These correspond to the normalized E and H values in the input wave.

grating, the boundary condition equations for its two boundaries produces a $4s$ by $2s$ submatrix. Starting with the first ($n = 1$) slab grating (represented by upper left submatrix), a technique like Gauss elimination is applied to make all of the elements of the lower half of the submatrix equal to zero. This reduces the system to $2Ns$ equations. Repeating this procedure on the next ($n = 2$) $4s$ by $2s$ submatrix reduces the system to $2(N-1)s$ equations. This process is continued until after N steps, only $2s$ equations in the diffracted amplitudes R_i and T_i remain. These are then solved for R_i and T_i. At each step in this sequential process, a new set of coefficients of R_i are produced as shown by the dashed box in Fig. 11. After N steps, these coefficients have moved to the bottom of the matrix and the final set of $2s$ equations in R_i and T_i are formed. This sequential procedure enormously reduces the storage and computational requirements for this type of problem. At each step, only a small $4s$ by $2s$ matrix is being treated as opposed to the entire $2(N+1)s$ by $2(N+1)s$ matrix where N might typically be 50.

When the amplitude R_i and T_i are known, then the diffraction efficiencies (ratio of diffracted intensity to input intensity) may be directly determined from (61) and (62). For lossless gratings the input power is conserved and thus the sum of all of the efficiencies for the propagating waves is unity (63).

D. Example Results

Using the method of solution described in the previous section, it is possible to calculate the diffraction efficiencies of dielectric surface relief gratings to an arbitrary level of accuracy. The analysis contains no restrictions with respect to grating profile, groove depth, angle of incidence, or wavelength. Example results are presented in [73] for sinusoidal, square-wave, triangular, and sawtooth gratings. Unlike previous methods, large groove depths do not cause numerical instabilities. Results for groove depths as deep as four grating periods are presented for all of these grating profiles in [73]. For these calculations the input region has a relative permittivity of $\varepsilon_I = 1.00$ (air) and the substrate a relative permittivity of $\varepsilon_{III} = 2.50$ (refractive index of 1.59). For the cases presented, $\lambda = \Lambda$ and incidence was at the first Bragg angle ($\theta' = 30°$). With the exception of the zero-order wave, the reflected waves had diffraction efficiencies of less than 1 percent. The zero-order (specularly reflected) wave generally was found to decrease in intensity from the Fresnel reflection value with increasing groove depth producing an efficient antireflection coating effect [75]. For the sinusoidal, square-wave, and triangular grating profiles, the first-order diffraction efficiency was found to reach nearly 100 percent for the properly chosen groove depth. For the sawtooth gratings, however, the maximum first-order diffraction efficiency was only about 50 percent. A result found in this work was: Dielectric gratings with profiles that are expressable as even functions are capable of high (greater than 85-percent) diffraction efficiency. Thus if the $x = 0$ origin can be chosen so that the grating profile $F(x)$ is an even function, then large first-order diffraction efficiencies are possible. For grating profiles that cannot be expressed as an even function, such as the sawtooth profile, the maximum diffraction efficiencies are correspondingly less. Maximum diffraction efficiency results for several profiles are given in Table 2. Notice that the stairstep grating

Table 2 Maximum Transmitted First-Order ($i = +1$) Diffraction Efficiencies for Various Grating Profiles. (Incidence is at first Bragg angle, $\theta' = 30°$, $\varepsilon_I = 1.00$, and $\varepsilon_{III} = 2.50$. Diffraction efficiencies correspond to the value at the first peak of the $DE_{3,1}$ versus d/Λ curve.)

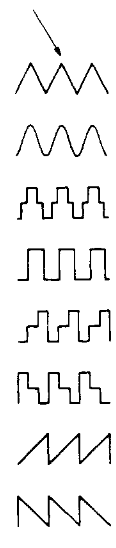

$(DE_{3,1})_{max}$	$\frac{d}{\Lambda}$
99.0	2.10
95.9	1.75
89.4	1.60
88.5	1.55
71.8	1.62
67.7	1.67
51.0	2.10
50.6	2.10

profile of even symmetry has maximum first-order diffraction efficiency of 89.4 percent. However, the same stairstep grating with steps shifted producing a profile of only odd symmetry has a maximum first-order diffraction efficiency of only 67.7 or 71.8 percent (depending on orientation of Bragg angle). The lack of even symmetry obviously produces dephasing of the fundamental first-order diffracted beam and causes the diffraction efficiency not to reach a large value. Higher maximum diffraction efficiencies are obtained with sharper, more pointed grating profiles. Thus in the sequence of square-wave, stairstep, sinusoid, and triangular grating, the maximum diffraction efficiency steadily increases (from 88.5 to 99.0 percent).

VII. Holographic Principles

A. Grating Recording

In this section the production of a grating by the recording of an interference pattern is discussed. In addition to this holographic method, gratings may also be produced by ruling [69]. Although the diffraction theory is independent of how the grating was fabricated, the recording of an interference pattern (making a hologram) leads naturally to a very large number of applications. Thus it is important to review briefly the essential features of the holographic recording of gratings.

A schematic view of a portion of two equal amplitude intersecting plane waves at an instant of time is depicted in Fig. 12. For simplicity, the polarization may be taken as being perpendicular to the page. The solid lines represent

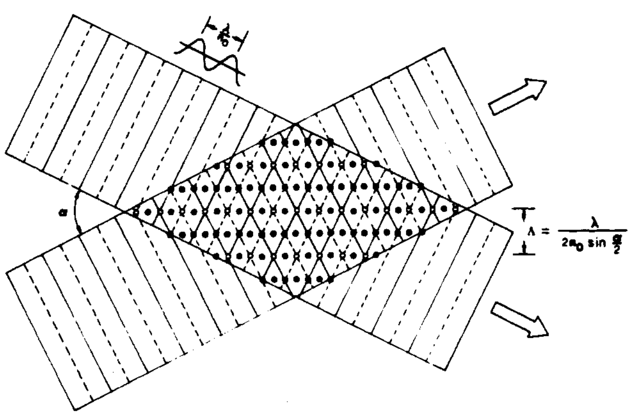

Fig. 12. Interference of portions of two plane waves at an instant of time.

phasefronts along which the electric field has a maximum magnitude and is pointing out of the page. The dashed lines represent phasefronts along which the electric field also has a maximum magnitude but is pointing into the page. The total field at this instant of time has a maximum magnitude at the locations where two solid lines or two dashed lines intersect. These points are shown by the open circles (representing "bright" spots). At the locations where a solid line and a dashed line intersect, the total electric field sums to zero and these are indicated by solid circles (representing "dark" spots). In addition, if a zero field point of one wave coincides with a zero field point of the other wave, the total field will also be zero. These points are also indicated by solid circles in Fig. 12. As time progresses, these waves move to the upper right and to the lower right as indicated by the arrows. The intersections, however, move horizontally to the right. Each horizontal row of "bright" and "dark" spots smears into a bright fringe. Likewise, each horizontal row of all "dark" spots represents a dark fringe. The light and dark fringes form parallel planes. The distance between neighboring light (or dark) fringes is the period of the interference pattern. It is given by

$$\Lambda = \lambda/2n_0 \sin(\alpha/2) \tag{107}$$

where n_0 is the average refractive index in the medium. The intensity variation in a direction perpendicular to the fringes (x) is given by

$$I(x) = I_0(1 + m\cos Kx) \tag{108}$$

where I_0 is the sum of the intensities in the two beams ($I_0 = I_1 + I_2$), m is the modulation ratio of the interference pattern given by $m = 2(I_1 I_2)^{1/2}/(I_1 + I_2)$, and K is the magnitude of the grating vector ($K = 2\pi/\Lambda$).

If a material has some photosensitive property, this periodic interference pattern can be recorded as a grating. The exposure of the material to the intensity variation could cause a change in the permittivity (or equivalently refractive index) and thus produce a phase hologram grating. The exposure might cause a change in the conductivity (or equivalently optical absorption) and produce an absorption hologram grating or it could cause a change in the surface of the material producing a surface-relief hologram or the exposure might cause a mixture of these effects in forming the grating. Fig. 13 depicts the hologram grating recording

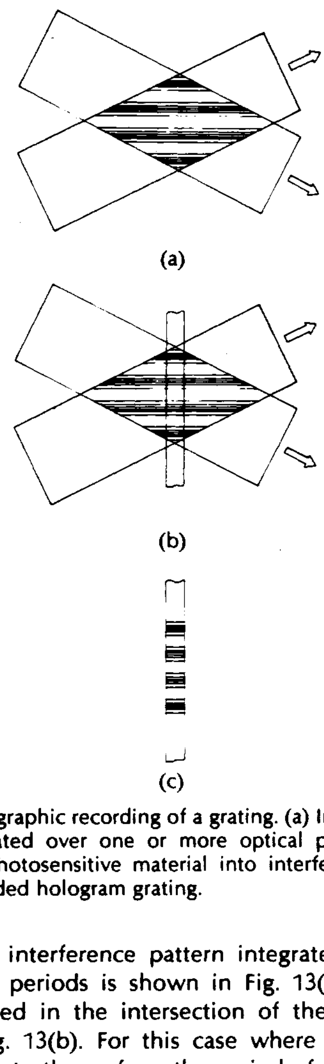

Fig. 13. Holographic recording of a grating. (a) Interference pattern integrated over one or more optical periods. (b) Insertion of photosensitive material into interference pattern. (c) Recorded hologram grating.

process. The interference pattern integrated over one or more optical periods is shown in Fig. 13(a). A recording material placed in the intersection of the two beams is shown in Fig. 13(b). For this case where the fringes are perpendicular to the surface, the period of the interference pattern is the same inside and outside the material. If the interference fringes are not normal to the surface, they will bend at the surface and the period of the grating produced will differ from the period of the interference pattern outside of the material. The recorded grating is schematically shown in Fig. 13(c).

B. Holographic Recording Materials

A wide variety of photosensitive materials exist that may be used for holographic recording of interference patterns. These materials may be organic or inorganic. The holograms produced may be phase or absorption or mixed gratings. The holograms may be planar gratings or surface-relief gratings. The diffracted power may be primarily in backward-diffracted orders (such as in metallic gratings) or primarily in forward-diffracted orders. Extensive reviews of holographic recording materials have been written [76]–[78]. A few recording materials will be mentioned here.

Silver halide photographic emulsions [79] are capable of recording interference patterns at visible wavelengths. After development, an absorption hologram is produced. Bleaching the developed silver allows these recordings to be converted to the more efficient phase holograms. Photoresists are organic materials containing photosensitizers that become soluble (positive resist) or insoluble (negative resist) upon exposure to light. Photoresist may be used in a photolithographic process to allow the "etching" of a grating into another material or it may be used directly to produce a surface-relief grating in itself [80], [81]. Dichromated gelatin [82], [83] is a type of photoresist that when hardened exhibits a refractive-index change but without requiring development. Photopolymers [84], [85] start as a monomer–catalyst mixture that polymerizes upon exposure to produce a phase hologram. A widely used photopolymer is polymethyl methacrylate (PMMA) [86]. Thermoplastic materials [87], [88] may be used together with a photoconducting layer to produce a charged surface that is a replica of the exposure pattern. Upon heating, the thermoplastic flows to produce a surface-relief hologram. Photochromic materials exhibit optically induced changes of color (absorption) upon exposure [89], [90]. These materials may be crystals, glasses, or organic substances. Photodichroic materials exhibit optically induced changes of absorption of selected polarizations of light [91]–[93]. This recording effect can be produced by the anisotropy of certain color centers that occur in alkali halide materials such as KCl. Photorefractive crystals exhibit optically induced refractive-index changes upon exposure [94]. Photorefractive recording consists of charge migration (due to a combination of bulk photovoltaic effect, drift in an applied and/or space charge field, and diffusion) followed by an electrooptic effect (either the linear Pockels effect or the quadratic Kerr effect). Electrons are photoexcited in the bright regions of the interference pattern and migrate to the darker regions producing local space-charge fields that cause the index of refraction to change via the electrooptic effect. Thus a pure phase grating is formed. Photorefractive materials include $BaTiO_3$ [95], $Bi_{12}GeO_{20}$ [96], $Bi_{12}SiO_{20}$ [96], $KNbO_3$ [97], $KTa_xNb_{1-x}O_3$ (KTN) [98], $LiNbO_3$ [99]–[101], and $LiTaO_3$ [102].

C. Wavefront Reconstruction

The two beams that interfere to produce the hologram grating may have phasefronts of arbitrary shape as opposed to the planar phasefronts of the plane waves depicted in

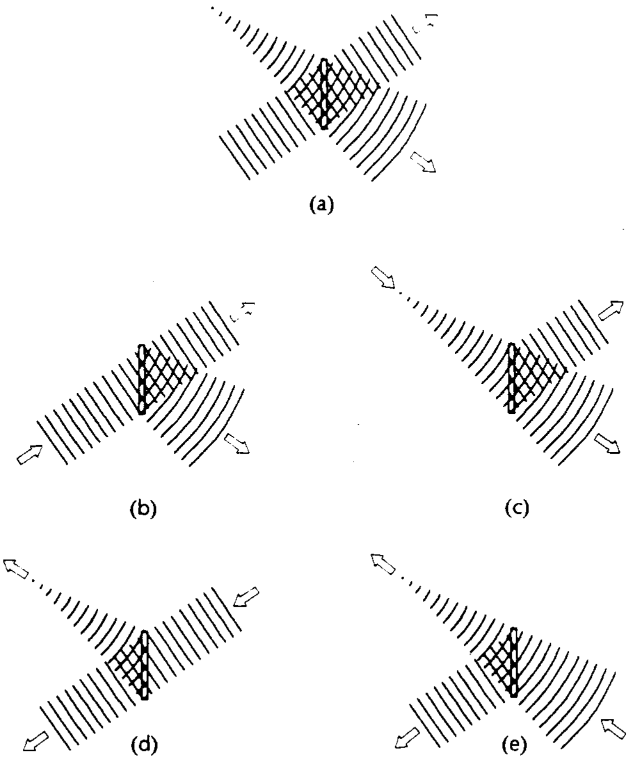

Fig. 14. Wavefront reconstruction from a holographic grating. (a) Recording a complex grating due to the interference of a plane wave (reference beam) and a spherical wave (object beam). (b) Reconstruction of the object wave by illuminating the hologram with the reference beam. (c) Reconstruction of the reference wave by illuminating the hologram with the object wave. (d) Reconstruction of the conjugate of the object wave by illuminating the hologram with the conjugate of the reference wave. (e) Reconstruction of the conjugate of the reference wave by illuminating the hologram with the conjugate of the object wave.

Figs. 12 and 13. For example, the interference of a spherical wave and a plane wave is shown in Fig. 14(a). The interference fringes formed in three-dimensional space in this case will be paraboloids of revolution rather than planes. The photosensitive material records a section through this interference pattern. For the orientation of the recording material shown, the interference fringes form ellipses at the surface of the material. It is common practice to refer to one of the waves as the object (or subject) beam and to the other as the reference beam. Either beam can be labeled either way. In this case, the plane wave might be called the reference beam.

Wavefront reconstruction is illustrated in Fig. 14(b) and (c). One of the two original waves (same wavelength and orientation) illuminates the hologram grating. This wave interacts with the grating and is partially transmitted and partially diffracted as shown. The diffracted wave reproduces or reconstructs the other beam. Illumination with the reference wave reconstructs the object wave [Fig. 14(b)]. Likewise illumination with the object wave reconstructs the reference wave [Fig. 14(c)]. This is the basic holographic playback process. Only the $i = +1$ fundamental-order diffracted wave is shown in these diagrams. Higher order forward- and backward-diffracted waves have not been included.

In Fig. 14(d) and (e), the same grating is shown illuminated by the time-reversed versions of the original waves. These waves have the same shape wavefronts but move in the opposite directions. These are commonly referred to as conjugate waves. Illumination of the grating with the conjugate of the reference beam [Fig. 14(d)] produces by diffraction, the conjugate of the object beam. Similarly, illumination with the conjugate of the object beam [Fig. 14(e)] produces the conjugate of the reference beam. This is the basis of phase conjugation and this process is central to many of the applications that will be discussed in the next section.

VIII. Grating Applications

A. Perspective on Grating Diffraction Applications

Important practical applications of grating diffraction are extremely widespread in modern optical technology. The broad areas of acoustooptics, holography, integrated optics, quantum electronics, and spectral analysis are inherently interwoven with grating diffraction. These practical applications have provided steady motivation to develop a complete rigorous understanding and description of grating diffraction. The material developed in Sections II, III, and IV of this paper is, in part, a response to this need.

In this section, a review of some representative grating diffraction applications is presented. However, it is clear that any such review cannot be totally comprehensive. In the present case, a large number of representative applications are presented in brief. The alphabetic ordering of these applications is indicative of the lack of any attempt to group these applications according to significance, chronology, or broad area of application. Likewise, the published literature that has been cited for each application is merely representative of the application and these references are not intended to be comprehensive or chosen according to significance. A previous review of grating diffraction applications appearing in the PROCEEDINGS OF THE IEEE was written by Elachi [103]. A more recent issue of the PROCEEDINGS OF THE IEEE had a special section devoted to acoustooptic devices and applications [104].

1) Acoustic Wave Generation: Acoustic waves of accurately known direction of propagation and wavelength can be used to measure crystal elastic constants, acoustic absorption spectra, photoeleastic constants, and other acoustic properties of a material. Precisely controllable ultrasonic waves can be induced in a material by the interference of two coherent laser pulses [105]–[108]. The geometry is the same as that shown in Fig. 13(a). Through absorption or stimulated Brillouin scattering (electrostriction) of the laser pulses, an ultrasonic wave is produced that has its wavelength equal to the period of the induced grating and whose direction of propagation (wavevector) is along the grating vector of the induced grating. Generally there are two counterpropagating ultrasonic waves ($\pm\bar{K}$ directions) induced. In the case of an absorbing medium, the spatially periodic intensity distribution (108) produces a periodic temperature distribution and thermal expansion launches acoustic waves. The necessary temperature modulation can be produced with short laser pulses [105] or by amplitude modulating the laser light at the sound frequency desired [107] so that the interference pattern is correspondingly modulated at this frequency. Monitoring of the sound waves may be accomplished with acoustic-wave tranducers or by optical diffraction from the acoustic-wave grating. This latter method will be discussed in "Diagnostic Techniques."

2) Ambiguity Processing: The cross-ambiguity function of two one-dimensional signals can be evaluated using acoustooptic signal processing techniques [109]–[112]. The cross-ambiguity function may be expressed as the complex correlation of one of the signals with a frequency-shifted version of the other signal. Correlation processing will be discussed in a later section. Ambiguity processing can be accomplished using three acoustooptic diffraction (grating) cells together with a series of spherical and cylindrical lenses and stops to remove unwanted diffraction orders. Two of the acoustooptic cells are driven, respectively, by the two signals and the third is driven by a sinusoidal signal that is linearly changing in frequency (chirp). The output of the system is a two-dimensional distribution which when integrated in time (such as with a television camera) and bandpass filtered gives the desired ambiguity function.

3) Analog-to-Digital Conversion: Permittivity gratings can be directly induced in electrooptic materials through the use of interdigitated electrodes on the surface of the material. Such a device is schematically shown in Fig. 15. A

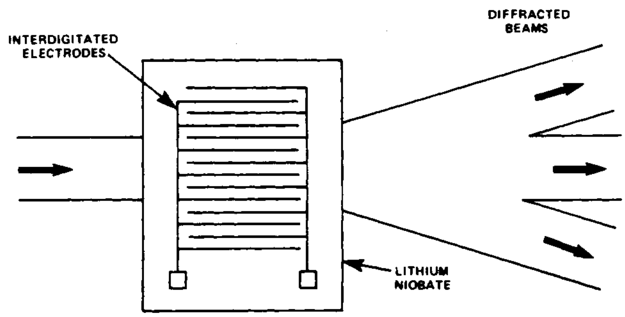

Fig. 15. Electrooptic grating modulator. Voltage applied across interdigitated electrodes induces a phase grating beneath the electrodes via the linear electrooptic effect.

voltage difference is applied between the two electrode pads. This causes each interdigitated electrode to have the opposite polarity of its neighbors. Thus a periodic electric field is produced in the material beneath the electrodes. The period of the field is equal to the spacing between adjacent electrodes of the same polarity. Through the electrooptic effect, the electric field causes a corresponding periodic change in the index of refraction and therefore a grating is produced. The diffraction efficiency associated with the various diffracted orders, of course, depends on the applied voltage. This is true independently of whether the diffraction exhibits Bragg regime behavior, Raman–Nath regime behavior, or requires a more complete theory for its description. If the crystal has $3m$ point group symmetry (such as lithium niobate) and the optic axis is parallel to the grating vector (perpendicular to the interdigitated electrode fingers), then for light with polarization parallel to the optic axis, the applied field in the optic axis direction causes a change in permittivity of

$$\Delta\varepsilon = -n_E^4 r_{33} E_c \tag{109}$$

where n_E is the principal extraordinary refractive index, r_{33}

is the linear electrooptic coefficient appropriate for this direction of propagation and for this polarization, and E_c is the component of the electric field along the optic axis. For the same geometry but with polarization perpendicular to the optic axis, the change in the permittivity is

$$\Delta\varepsilon = -n_0^4 r_{13} E_c \tag{110}$$

where n_0 is the ordinary refractive index and r_{13} is the electrooptic coefficient appropriate for this case. The amplitude of the grating permittivity modulation ε_1 is approximately equal to $\Delta\varepsilon$.

A high-speed analog-to-digital converter that uses the configuration shown in Fig. 15 has been described by Wright *et al.* [113]. This device is designed to operate in the Raman–Nath diffraction regime and so the diffraction efficiencies are given by (86). The diffracted beams illuminate photodetectors which, together with threshold detectors, give an output depending on whether the optical power is above or below the threshold setting. By applying a constant bias to the electrodes in addition to the signal to be digitized, a suitable operating point can be obtained so that output of the device is directly a 3-bit Gray code (unit-distance binary code).

4) Antennas: Gratings can be used to couple beams from air into a dielectric waveguide (e.g., slab waveguide, channel waveguide, fiber waveguide) or they can be used to couple power from the waveguide into the air. In the latter case, power in a guided mode radiates (or "leaks") into the space over the open waveguide structure and thus the grating acts as an antenna [114]–[118]. These devices are sometimes called leaky wave antennas. This same basic structure can also be an output coupler (e.g., from slab waveguide to optical fiber) in integrated optics. Input and output couplers are discussed in "Beam Coupling."

A wave in a dielectric waveguide that is incident upon a grating generally produces a beam traveling into the substrate and a beam that radiates into the region above the grating. For antenna applications, the power in the substrate is unwanted loss. For this output coupling configuration, a symmetric grating profile generally causes the incident power to divide about equally between the two beams. However, coupling into the radiated beam can be greatly increased by using asymmetric grating profiles [115], [116]. In addition, it is possible to design these high-efficiency asymmetric profiles so that they are insensitive to fabricational tolerances [118].

5) Antireflection Properties: Dielectric surface-relief gratings, as discussed in Section VI, can exhibit very low diffraction efficiency in the backward-diffracted orders [73]. Therefore these gratings can be used to give excellent antireflection properties. Enger and Case [75] have experimentally demonstrated reflectivities of about 0.035 percent across the visible spectrum for normal incidence on an etched quartz surface-relief grating. Thus these gratings may be a durable alternative to the more damage-prone multilayer antireflection coatings.

6) Associative Storage: Holography can obviously be used as a means of storing information. A page of data can be stored holographically and the data can be recalled by diffraction of the reference beam. Therefore the system is acting as a memory. Fig. 14 can be used to represent the memory capabilities of a holographic system. In Fig. 14, the spherical wave could be replaced by a more complicated wavefront representing a two-dimensional page of analog data (an image) or digital data. In Fig. 14(a), the data page is recorded. In Fig. 14(b), the wavefront corresponding to the data page is reconstructed by diffraction of the reference beam. This system operated in this manner is called a direct or location-addressable memory (addresses are the input and data are the output).

However, as previously discussed, it is possible to illuminate the hologram with the object beam and reconstruct the reference beam as shown in Fig. 14(c). For a holographic recording material that is thick in the angular selectivity sense, many holograms can be angularly multiplexed in a common volume of the material [119], [120]. Each of these holograms is recorded with the reference beam at a different angle of incidence. For reconstruction, the reference beam can be positioned at an angle corresponding to the location of the reference beam during recording of a particular hologram. Then, the wavefront from that particular hologram will be reconstructed. Likewise, as the reference beam is repositioned to a new angle corresponding to another hologram, the wavefront for that hologram will be reconstructed.

In associative storage, the holographic system operates as a content-addressable memory. The configuration is basically that shown in Fig. 14(c). The angularly multiplexed group of holograms is illuminated with a data page wavefront. If that data page wavefront matches a wavefront that was used in recording one of the holograms, then the reference wave corresponding to that hologram will be reconstructed. If the data page wavefront does not match any of those that were used during recording, then there will be diminished diffraction (because the wavefront does not satisfy the Bragg condition everywhere at the stored hologram grating). This basic procedure can be used to search the contents of the memory in parallel [121]–[126]. If a particular reference pattern (data page) occurs at one or more locations in the memory, this will be indicated by the diffracted reference beam(s) that are produced. Thus the searching is done in parallel without the need for any type of sequential scanning and the system acts as a content-addressable memory (data are the input and the addresses of those data are the output).

7) Beam-Coded Multiplex Holography: In a conceptually similar manner to the way in which holograms can be angularly multiplexed in a thick recording medium, it is also possible to phase code the reference beam to achieve multiplexing of holograms [127]–[130]. In angular multiplexing, the reference wave is a simple wave (e.g., plane wave) and its angle of incidence is changed to record different data pages. In beam-coded multiplexing, the reference wave angle of incidence does not change. Instead, a complex wavefront reference wave is used and this complex wavefront is changed to record different data pages. This can be accomplished by using a different pseudorandom phase pattern in the reference beam for each recording. Then, at playback, a particular pseudorandom phase pattern in the reference beam will cause a particular data page wavefront to be reconstructed. A major difficulty is that a given phase-coded reference beam usually reconstructs not only the correct wavefront, but also portions of the wavefronts from the other holograms thus producing undesirable crosstalk. This can be minimized by having the autocorrelation function of each phase pattern approach a delta function and each pair-wise cross-correlation function as small as possible. Binary gold codes commonly used in spread-spectrum communications have been shown to have these desirable characteristics for phase coding the reference beams [130].

8) Beam Coupling: In integrated- and guided-wave optics, it is necessary to couple light into waveguides, out of waveguides, and between waveguides. Grating couplers appear to be some of the most versatile and promising devices to accomplish this. Grating couplers have been theoretically analyzed and have been shown to be capable of high coupling efficiencies [116], [118], [131]. Diffraction gratings can be used to couple light from air into a slab waveguide [132], [133]. This is schematically shown in Fig. 16. The angle of incidence θ_a in the cover region (air) is

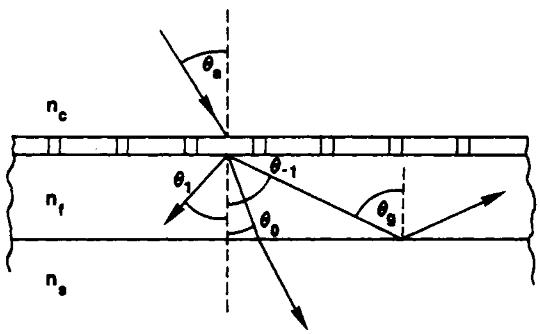

Fig. 16. Input grating coupler. Light in the cover region (air) is coupled into a guided mode of the film waveguide.

chosen so that the $i = -1$ diffracted wave from the grating is at a zig-zag angle θ_g for the guided mode of the waveguide that is to be excited. This requires that

$$n_f \sin\theta_g = \sin\theta_a - i\lambda/\Lambda \tag{111}$$

where n_f is the index of refraction of the film waveguide.

A grating coupler can also be used to couple light out of a slab waveguide into the air [115], [116], [134]. This output coupler operation is essentially the same as that of an antenna (see Section 4). An output coupler is shown in the device depicted in Fig. 17 [135]. Gratings have also been used in this device for laser feedback and beam expansion.

Grating couplers can also be used to interconnect dielectric waveguides [136], [137]. An example of a holographic grating coupler used to interconnect single-mode fibers is shown in Fig. 18 [136]. The radiation wavefront S_1 from fiber no. 1 is interfered with a plane reference wave R_1 and the interference pattern is recorded as hologram no. 1 as shown in Fig. 18(a). Similarly, a hologram grating is recorded with the radiation wavefront from fiber no. 2 and a plane wave. In coupling operation, the light from fiber no. 1 is diffracted by hologram no. 1 producing a plane wave. This wave (R_1) is the conjugate of R_2. When R_1 illuminates hologram no. 2, it produces the conjugate wavefront S_2^* which is the time-reversed version of S_2. This wave launches the reverse-traveling version of the mode that was present in fiber no. 2 during recording. Thus fiber-to-fiber coupling has been achieved. The gratings produced remain with their respective fibers. If multiple holographic recordings are made with angularly separated reference beams, it is then possible to connect one waveguide to multiple waveguides. In this case the grating acts as a branching element [138].

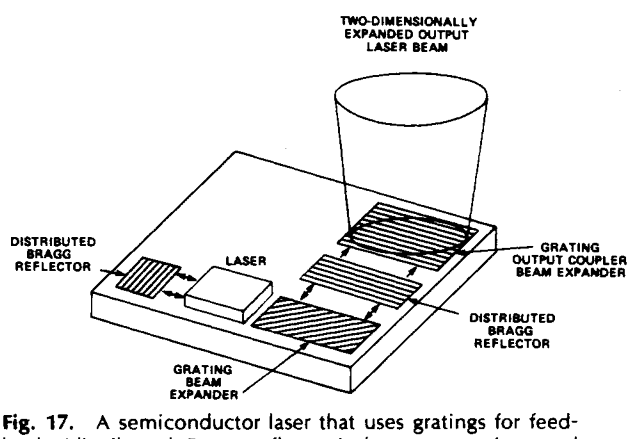

Fig. 17. A semiconductor laser that uses gratings for feedback (distributed Bragg reflectors), beam expansion, and output coupling [135].

9) Beam Deflection: Through grating diffraction a light beam can be deflected or scanned. The grating producing the diffraction can be an acoustic wave, an electrooptically induced grating, or a holographically recorded grating that is moved in the incident beam. Each of these types of deflectors has its own set of characteristics and areas of application. Reviews of laser-beam deflection techniques have previously appeared in the literature [139], [140].

Both bulk acoustic wave and surface acoustic wave (SAW) deflectors have been fabricated and extensively analyzed [141]–[150]. From the grating equation for forward-diffracted waves (43), it is clear that the diffraction angle of a particular diffracted order (usually $i = +1$) can be changed by varying the period of the grating. In the case of the acoustooptic deflector, the grating period is given by

$$\Lambda = v_s/f_s \tag{112}$$

where v_s is the velocity of the sound wave and f_s is the frequency of the sound wave. By changing the input frequency to the transducer on the acoustooptic material, the grating period is correspondingly changed and the direction of diffraction altered producing a scanning of the beam. An integrated optics version of an acoustooptic deflector is shown in Fig. 19. In this case, the material must be piezoelectric so that a voltage applied across the interdigitated electrodes will produce an acoustic wave directly. (For other materials, a piezoelectric transducer must be bonded to the material in order to launch acoustic waves from an input voltage signal.) The interdigitated transducer will function efficiently if the wavelength of the sound wave produced is equal to the distance between neighboring interdigitated fingers of like polarity. In this case, the ultrasonic wave travels a distance of one period of the interdigitated transducer in one temporal period of the voltage signal and thus there is a strong constructive addition to the amplitude of the sound wave as it propagates beneath the interdigitated electrodes. In this situation, the amplitude of the acoustic wave launched will increase rapidly with increasing number of electrode fingers used. However, the ability of the interdigitated electrodes to launch acoustic waves of wavelengths that do not match the period of the transducer fingers (and thus the signal bandwidth) diminishes with increasing number of electrode fingers. Wider bandwidths can be obtained by using multi-

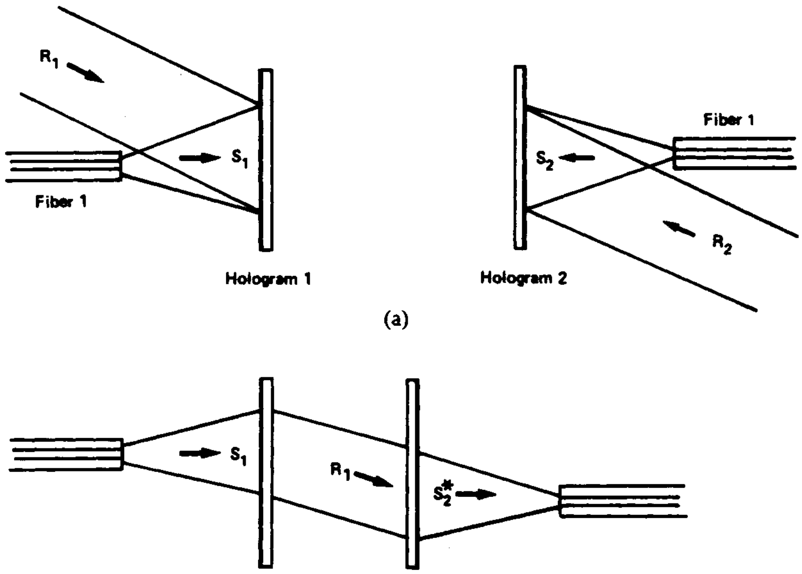

Fig. 18. Holographic grating coupler for single-mode optical fibers. (a) Recording hologram gratings. (b) Coupling of light from one fiber to the other [136].

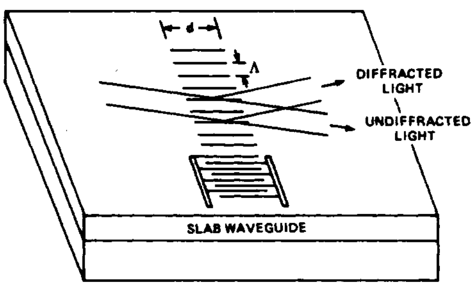

Fig. 19. Diffraction of guided optical wave by surface acoustic wave (SAW).

ple tilted surface acoustic wave interdigitated transducers. In this case, the transducers have different orientations so that the acoustic wave launched by a set of electrodes will be at its first Bragg angle ($m = 1$) with respect to the optical beam when the signal frequency produces an acoustic wavelength that is equal to the period for that particular interdigitated transducer.

Electrooptically induced refractive-index gratings can also be used to deflect a laser beam [151]–[154]. They have the advantage of higher speed than the acoustooptic devices. A configuration such as that shown in Fig. 15 is used. For this situation, the period of the grating induced is always the same as the period of the interdigitated electrodes. Thus for a fixed angle of incidence, the angle of diffraction for a given order is always the same. Thus these "digital" deflectors are not capable of scanning by themselves, but must be cascaded to produce more than two resolvable spots.

A third type of grating deflector is the holographic scanner [155]–[161]. In such a system, holographically recorded gratings are moved in an input beam. At each position the input beam is diffracted to a new location. One of the positions might appear as shown in Fig. 14(e). The input beam (plane wave) is diffracted producing a focused beam. As the holographic plate is moved in front of the input beam, a different holographic grating appears and now diffracts and focuses the light to a new location. Using a series of hologram gratings it is possible to scan the beam continuously. Applications include Universal Product Code scanners, document readers, etc.

10) Beam Expansion: Gratings can be used as expanders for laser beams [135], [162]. An example of this is illustrated in Fig. 17. A grating reflector inserted in the cavity of a semiconductor laser allows the width of the beam to be expanded. The profile of the diffracted beam depends on the geometry and diffraction efficiency of the grating.

11) Beam Sampling: Two gratings (either reflection or transmission) of the same period, oriented so that they are parallel to each other can be used as a laser-beam sampler [163]. Such two-grating rhombic beam samplers are frequently used to obtain amplitude and phase maps of high-energy laser beams. The first grating diffracts into the $i = +1$ order a sample of the beam. The second grating corrects the ellipticity in the beam profile introduced by the first grating. For nonplanar beams, the design of the grating rhomb beam sampler must be optimized to reduce aberrations in the sampled beam.

12) Beam Shaping: In the beam expansion application mentioned above, the profile of the laser beam is modified by a grating. In a conceptually similar manner, a series of gratings can be used to shape the profile of a laser beam [164] in an arbitrary way for applications where specific beam profiles are required.

13) Beam Splitting: A straightforward application of a grating is as a beam splitter. These devices are used both in bulk optics and in integrated optics applications [165]. A grating beamsplitter as it might be used in a dielectric channel waveguide is shown in Fig. 20. The incident wave ideally is divided into the $i = 0$ transmitted wave and the $i = +1$ diffracted wave. The grating might, for example, be a planar grating formed holographically through the photorefractive effect or it might be a surface-relief grating formed using photolithography.

14) Coherent Light Generation: The dispersive character

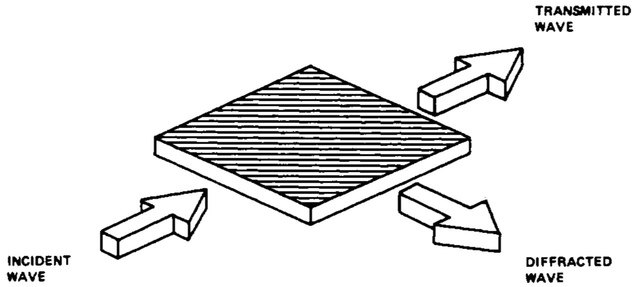

Fig. 20. Channel waveguide beam-splitting grating.

of grating diffraction is clear from the grating equations [(42) and (43)]. Both the forward- and backward-diffracted waves have directions of propagation that depend on the wavelength of the incident light. This dispersive property allows diffraction gratings to be used in laser resonators to control the oscillation frequency and to produce spectral narrowing of the output [166]–[175]. The grating can be used internally in the laser cavity to produce broad-band tuning such as with a dye laser. Alternatively, a reflection grating may be used as part of the laser cavity. In this type of open resonator it is possible to have the ith order diffracted wave to be reflected back in the direction of the incident wave along the resonator axis. The $i = 0$ wave can be reflected out of the resonator and used as the laser output.

15) Convolution Processing: The convolution of two one-dimensional signals $A(t)$ and $B(t)$ may be defined as

$$A(t) \bullet B(t) = \int_{-\infty}^{+\infty} A(\tau) B(t-\tau)\, d\tau \tag{113}$$

where τ is a dummy variable representing a time delay between one function and the time-reversed version of the other function. Acoustooptic grating devices can be constructed to perform the convolution operation [112], [176]–[178]. A basic acoustooptic convolver is shown in Fig. 21. The signals $A(t)$ and $B(t)$ are used to amplitude-modulate acoustic waves that travel in opposite directions. The acoustic waves have a radian frequency of $\omega_s = 2\pi f_s$. An optical wave of radian frequency ω_0 ($\omega_0 = 2\pi c/\lambda$) is incident upon these acoustic gratings at the first Bragg angle. The acoustic waves diffract the light and a lens at the output combines the beams as shown. The upper detector receives undiffracted light and doubly diffracted light. The undiffracted light has radian frequency ω_0. The doubly diffracted light is increased in frequency by the sound frequency at each diffraction by the Doppler effect. Thus the doubly diffracted light has a radian frequency of $\omega_0 + 2\omega_s$. The lower detector receives singly diffracted light from each grating. In one case, the optical frequency is increased because the light wave has a component opposite to the direction that the grating is moving. This wave has a radian frequency of $\omega_0 + \omega_s$. In the other case, the optical radian frequency is decreased and is $\omega_0 - \omega_s$. At either photodetector, after heterodyne detection, a signal of frequency $2\omega_s$ is present. If the duration of the input signals $A(t)$ and $B(t)$ are less than the time aperture of the interaction region and if both signals occur in the same time span and if the signals are band-limited to one octave centered at ω_s, then the convolution signal can be separated from other signals by bandpass filtering.

16) Correlation Processing: The cross correlation of two one-dimensional signals $A(t)$ and $B(t)$ may be defined as

$$A(t) \star B(t) = \int_{-\infty}^{+\infty} A(\tau) B(\tau - t)\, d\tau. \tag{114}$$

Acoustooptic devices have been constructed to operate as correlators [112], [178]–[182]. Thus the form of the correlation operation is similar to that of convolution. However, for convolution the process may be visualized as moving a time-reversed version of one function by the other function, whereas for correlation the process may be visualized as moving one function by the other function without any time reversal. Since in Fig. 21 the two acoustic waves are counter propagating, the time reversal is automatically provided and convolution is produced. The configuration of Fig. 21 can also be used to produce the cross-correlation function. If one of the signals is time reversed before applying it to the transducer, then there will be effectively two time reversals and the functions will be oriented the same way in time as they move past each other. Subject to the conditions discussed for convolution, the cross correlation of the two functions will be produced after square-law detection and bandpass filtering.

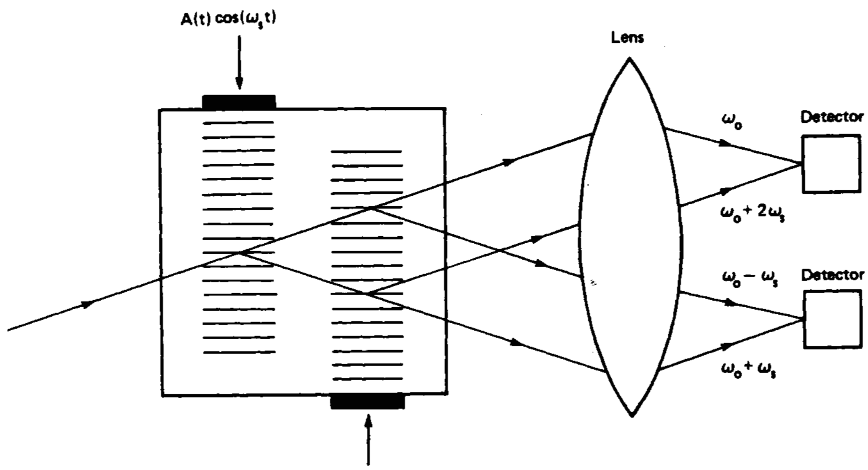

Fig. 21. Acoustooptic space-integrating convolver. If one of the amplitude-modulated sound waves is time reversed, this device becomes a correlator.

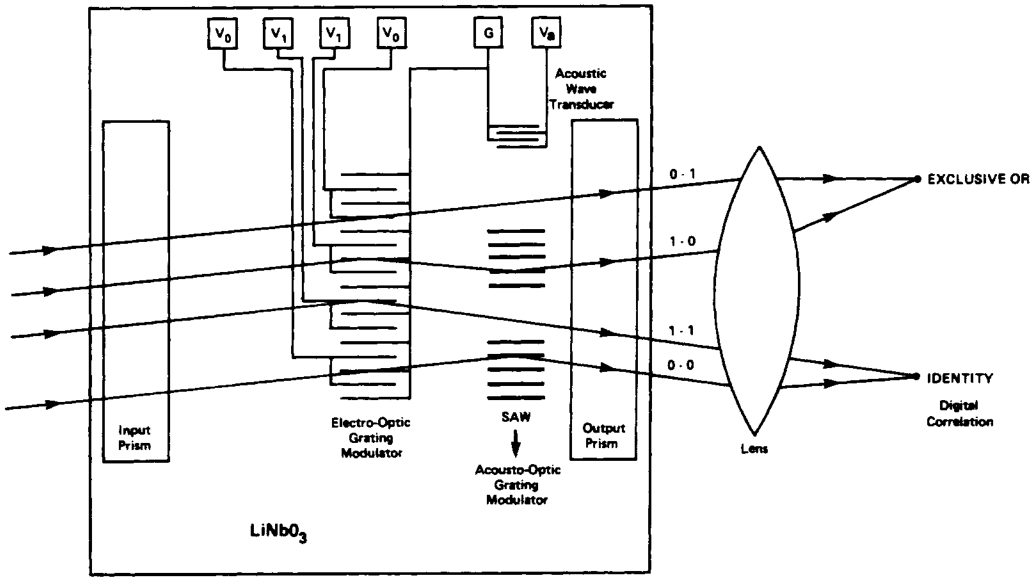

Fig. 22. Integrated optical electrooptic, acoustooptic digital correlator [183].

An integrated optical digital correlator developed at Battelle Columbus Laboratories is shown in Fig. 22. This device uses both an electrooptic and an acoustooptic interaction. Light is coupled into a slab waveguide by a prism coupler. The light wave is incident at the Bragg angle on a grating produced by a set of interdigitated electrodes. The voltage to each set of electrodes is separately controllable. For a "zero," no voltage is applied. For a "one," a voltage is applied and the electrooptically induced grating diffracts the light as shown. The second digital signal is represented by a SAW that is launched by an interdigitated transducer. For a "zero," a constant amplitude acoustic wave is produced. For a "one," no acoustic wave is produced. The light that is transmitted or diffracted by the electrooptic grating is incident at the Bragg angle of the acoustic grating. At an instant of time if the two digital functions do not match, a combination of undiffracted and doubly diffracted light is focused on the upper detector. The detector output represents the sum of the bit-by-bit Boolean logical EXCLUSIVE-OR operations. Likewise, if the two digital functions are the same, singly diffracted light is focused on the lower detector. Its output represents the sum of the bit-by-bit Boolean logical IDENTITY operations. This output as a function of time will give the digital correlation between the two functions.

17) Data Processing and Optical Logic: A wide variety of data processing applications exist that are based on grating diffraction. Many of the optical systems involved perform Boolean logical operations such as AND, OR, EXCLUSIVE-OR, and NAND. Of course, modern electronic computers use Boolean logical functions in combinations to produce calculations of arbitrary complexity. A number of researchers have used gratings to perform logical functions on parallel optical inputs [165], [184]–[189]. These logical operations may be an end in themselves in some applications. Combining the associative property of holographic storage together with the Boolean logical operation EXCLUSIVE-OR or NAND, it is possible to construct a truth-table look-up data processor. The Boolean logical functions are used to indicate the matches that occur between the input data and the holographically prestored data that represent the entries from a truth table. With this type of data processing system it is possible to perform operations like addition and multiplication on pairs of input words in parallel.

18) Data Storage: Holographic memory systems for high-speed and high-capacity data storage have been extensively studied [120], [190]–[207]. The data recording and readout are generally of the form as represented in Fig. 23(a) and (b), respectively. An expanded object beam illuminates a page composer (spatial light modulator) that contains the data to be recorded [object *A* in Fig. 23(a)]. Using a lens, the image of the data is two-dimensionally Fourier transformed at the location of the recording medium. This pattern is interfered with a reference wave and the resulting intensity distribution is recorded. Such a hologram grating is called a Fourier transform hologram. Upon illumination with the reference beam the Fourier transform of the amplitude distribution of object *A* is reconstructed. After another Fourier transforming operation, the image of object *A* (upside down and backwards) is produced at the output image plane as shown in Fig. 23(b). Thus data can be stored and read out so that the system operates as a memory. In this configuration, lateral movement of the hologram does not cause a movement of the image and so there is an important insensitivity of the position of the detectors that would be used at the output image plane. One of the features that has motivated research on this type of memory is the potentially very high data capacity associated with holographic storage [119]. Volume storage, for example, can be achieved by angularly multiplexing the holograms as previously discussed [120].

19) Diagnostic Measurements: The intersection of two time-coincident laser pulses in a material using the configuration shown in Fig. 13(b) can produce a transient grating and thus can be used to measure some of the physical properties of the solid or liquid [106]–[108], [208]–[218]. The period of the induced grating is given by (107). If the two crossed beams approximate uniform plane waves, the light intensity distribution in the sample is given by (108). This pattern, for example, could lead to a similar distribution of excited electronic states in the material which can change the optical properties of the material and thus produce a

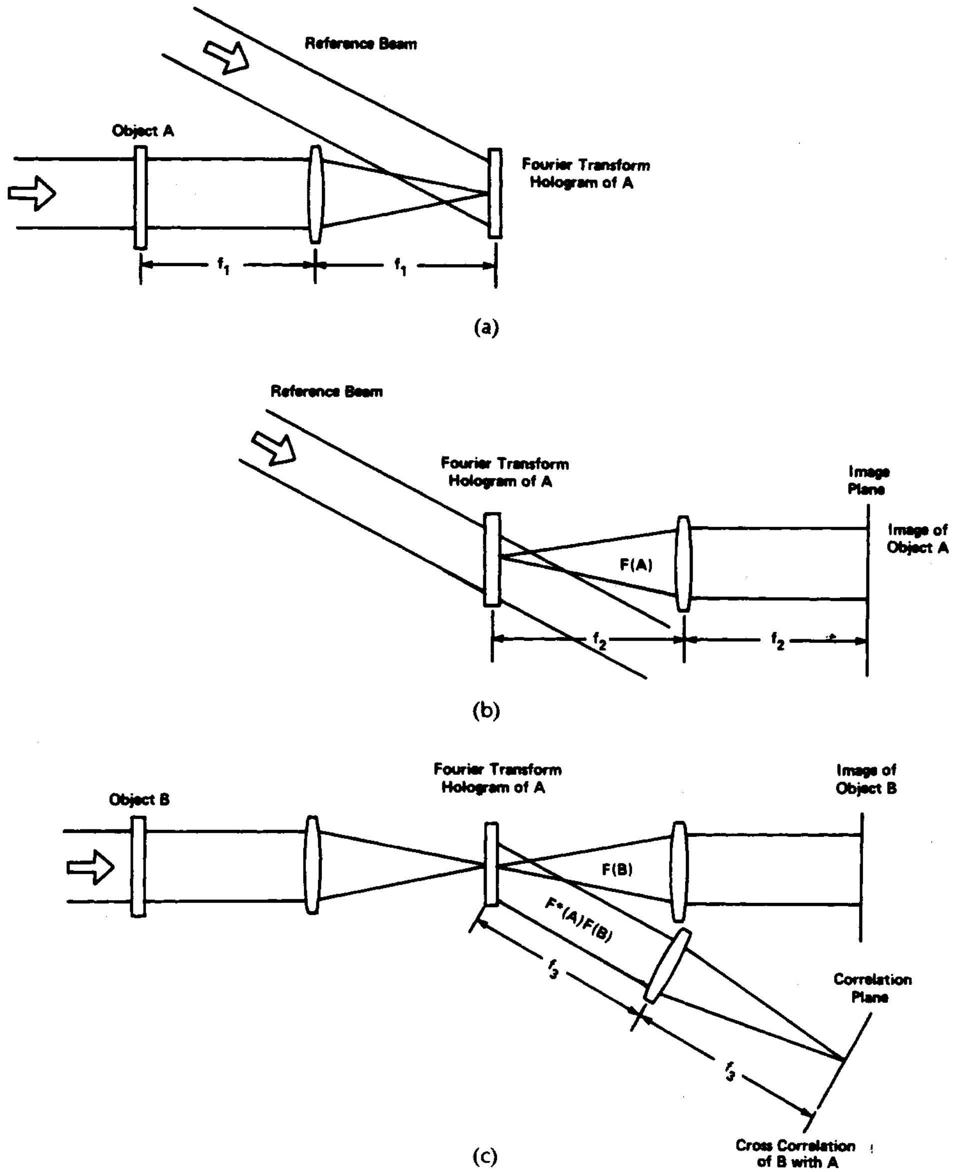

Fig. 23. Data storage and correlative pattern recognition. (a) Recording data page A as a Fourier transform hologram. (b) Playback of data page A. (c) Obtaining the cross correlation of new data page B with stored data page A.

diffraction grating. By observing the time-dependent decay of the diffraction from this grating, information about the dynamic properties of the physical system can be obtained. Transient grating experiments have been used to measure electronic excited state energy transport and momentum transport, trapping rates, hot-electron relaxation rates, fluorescence quantum yields, orientational relaxation times, thermal diffusion rates, mass diffusion rates, and coherence time of picosecond pulses. The diffraction from the induced grating may be monitored by any of several ways as shown in Fig. 24. Higher order diffraction of the two exciting beams can be measured as shown in Fig. 24(a). In this case, the detector is shown measuring a beam which is the combination of the $i = +2$ diffracted order of the exciting beam that is propagating to the lower right and the $i = -1$ order of the exciting beam that is propagating to the upper right. In Fig. 24(b), a beam of a different wavelength is shown probing the grating. This beam is aligned to its first Bragg angle and the efficiency of the $i = +1$ diffracted order is measured. For the configuration shown, the monitoring wavelength is longer than the exciting wavelength. Alternatively, the probe beam could be normally incident upon the grating as shown in Fig. 24(c). This has the disadvantage that the incident probe beam is not at a Bragg angle. However, this configuration has the advantage that the probe beam can be the same wavelength as the exciting beams. In Fig. 24(d), one of the exciting beams is reflected (or partially reflected) back into the grating and thus it serves as the probe beam. It is automatically at the Bragg angle and the diffracted power is monitored using a beam splitter to separate it from the path of the exciting beam.

20) Displays: The ability of a holographic reconstruction to give a three-dimensional view of the object is well known. The analysis and construction of three-dimensional holographic displays has received considerable attention [219]–[223]. These displays are important in those applications that require being able to see the object in three dimensions. Holographic systems, for example, have been

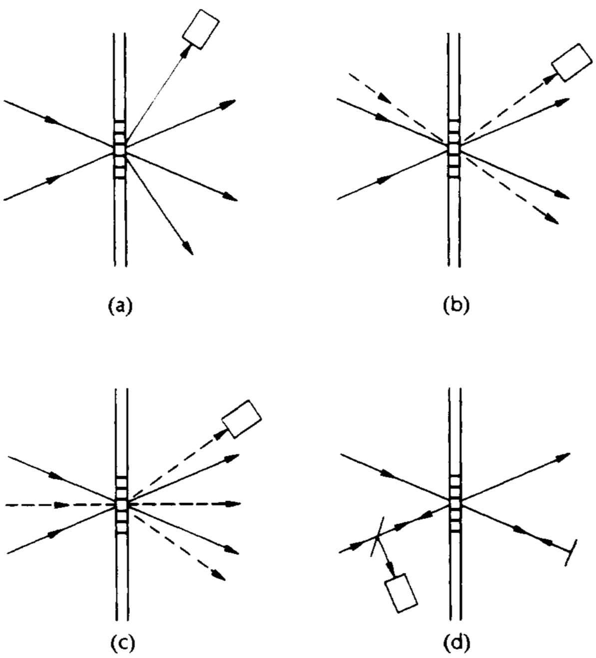

Fig. 24. Diagnostic configurations for measuring the diffraction from a grating in real time. (a) Monitoring a combination of the $i = -1$ and $i = +2$ (from the lower and upper incident waves, respectively) higher order self-diffracted waves. (b) Monitoring the diffraction from a separate beam aligned to its Bragg angle. (c) Monitoring the $i = +1$ wave from a normally incident probe beam. (d) Monitoring the diffraction of one of the writing beams reflected back into grating (four-wave mixing configuration).

implemented for displaying the core of a nuclear reactor and for making measurements in a bubble chamber.

Diffraction gratings are also used for producing and filtering colors in more conventional displays [224]–[227]. The diffraction efficiency of the $i = 0$ (transmitted) order is strongly wavelength-dependent in some surface-relief gratings. Thus these gratings can be used as color filters in on-axis projection systems that transmit only the zero-order light. Gratings that produce the three subtractive primary colors, cyan, magenta, and yellow have been produced [227].

Volume holograms have been used for spatial filtering to detect size, shape, orientation, and color for applications such as the recognition of biological cells (e.g., red blood cells) [225]. Gratings in the form of a half-tone screen have been used as overlays with gray-scale transparency imagery to disperse colors into various diffracted orders. With the appropriate spatial filtering, this produces a pseudocolor display of the gray-scale information [226].

21) Distributed Feedback: Gratings in slab waveguides have previously been discussed in connection with antennas, beam coupling, beam expansion, and beam splitting. If the slab waveguide contains an active medium capable of lasing, then a grating or gratings can be used to provide the feedback required for laser action [228]–[244]. In contrast to a discrete resonator mirror at a specific location, the gratings acts as a distributed reflector. If a single grating is used that is continuous throughout the active region, the device is called a distributed feedback (DFB) laser. If two grating reflectors are used in the slab waveguide on either side of the active region, the device is called a distributed Bragg reflector (DBR) laser, as is shown in Fig. 17. The guided wave to be reflected should be incident upon the grating at a Bragg angle. From the Bragg condition the grating period required is

$$\Lambda = m\lambda/2n_f \sin\theta_g \tag{115}$$

where θ_g is the zig-zag angle of the guided wave and n_f is the refractive index of the slab waveguide film. The Bragg condition is satisfied for the ith diffracted order where $i = m$. The directions of all the diffracted orders (if they are not evanescent) are determined from the grating equation and are

$$\theta_i = \sin^{-1}\left[(i\lambda/n_f\Lambda) - \sin\theta_g\right]. \tag{116}$$

For a fundamental or first-order Bragg reflector, $m = 1$. For GaAs ($\lambda \approx 840$ nm and $n_f \approx 3.58$) with a guided mode zig-zag angle near 90° (which is typically the case), the grating period should be $\Lambda = 117$ nm. Since this grating period is very small and difficult to fabricate, higher order ($m = 2, 3, \cdots$) grating reflectors are frequently constructed. These higher order grating reflectors, though easier to build, have smaller diffraction efficiencies. The spectral purity and the frequency stability with changing temperature of a distributed feedback thin-film laser are markedly superior to that of a cleaved-face discrete feedback semiconductor laser.

22) Filtering: Due to the wavelength selectivity of the diffraction by a grating, spectral filtering is a natural application for them. In integrated optics, surface-relief gratings are used with slab waveguides to provide filtering of the optical wave [245]–[252]. An example of this is shown in Fig. 25. The function of the grating in this case is the same as in distributed feedback. That is, a narrow band around a given wavelength is reflected with high efficiency. The wavelength reflected is the value that satisfies the Bragg condition for the grating. Gratings with linearly varying periodicity (chirped) produce reflection over a range of wavelengths and thus allow broad-band filtering [248].

In addition to waveguide grating filters there are

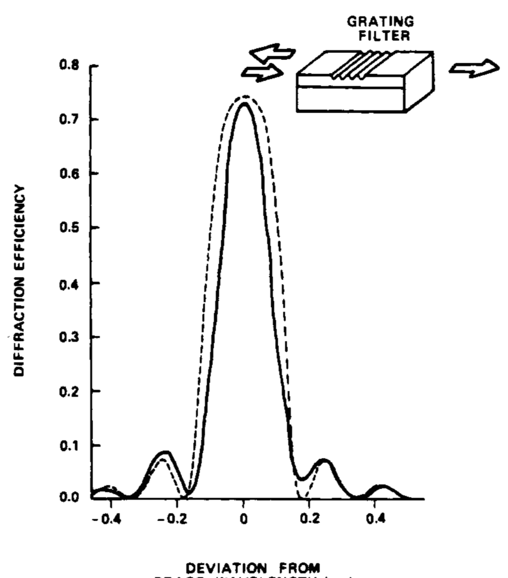

Fig. 25. Diffraction behavior of a slab waveguide surface-relief grating as a function of wavelength deviation from the Bragg wavelength [246].

acoustooptic spectral filters [253]–[259]. These filters are generally bulk acoustooptic devices rather than integrated optical devices. Acoustooptic filters have the advantage of being electronically tunable. Changing the frequency of the voltage signal applied changes the period of the acoustic grating produced as indicated by (112). If the light propagates in the same direction as the acoustic wave it is called a collinear configuration. In this case, the grating fringes are perpendicular to the direction of the light propagation and the grating behaves as a pure reflection grating. If the wavevector of the light and the acoustic wave are not parallel, it is called a noncollinear configuration. Acoustooptic filters generally utilize the anisotropic properties of crystals that cause the polarization of the diffracted light to be rotated by 90° by way of the photoelastic effect. This allows the filtered light to be separated from the remainder of the light by the use of polarizers.

23) Head-Up Displays: Another way in which the wavelength selectivity of a thick grating can be used is to combine a narrow band of wavelengths with an existing field of view. Such a device is called holographic beam combiner and can be used to construct a head-up display [260]–[262]. An example head-up display is shown in Fig. 26. The observer or pilot sees the scene in front of them. At the

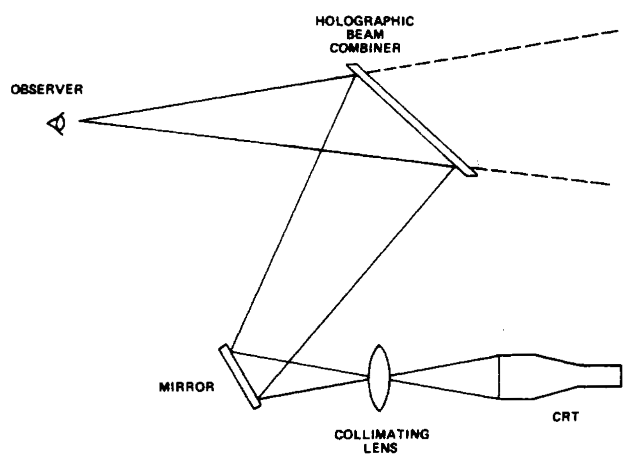

Fig. 26. Narrow spectral band holographic beam combiner used to make a head-up display.

same time, a holographic grating diffracts light of the wavelength corresponding to the color of the phosphor of the cathode-ray tube (CRT). In this manner, data displayed on the CRT can appear superposed at infinity with the scene in the field of view. Thus pilots would not have to turn their heads to read instruments and data during periods when intense concentration is essential. The holographic beam combiner will also diffract out of the scene the color corresponding to the phosphor. However, if the phosphor and the beam combiner are sufficiently narrow-band in their operation, this will not produce a noticeable effect.

24) Holographic Optical Elements: By recording the interference pattern produced by two arbitrary wavefronts, it is possible to produce a device that transforms one wavefront into another [e.g., Fig. 14(a) and (b)]. By recording the interference patterns associated with multiple wavefronts, it is possible to transform one incident wave into multiple diffracted waves. Holographic optical elements constructed in this way have been widely investigated [263]–[273]. For example, a plane wavefront might be converted to a converging spherical wavefront producing the effect of a spherical focusing lens. Similarly, a plane wave could be converted to a cylindrical wave or to an arbitrary wavefront. They can perform the functions of conventional refractive and reflective optical components. Since these holographic optical elements can be recorded on plates, they may be relatively small and lightweight. Solymar and Cooke [20] list a number of additional potential advantages of holographic optical elements: 1) An element may perform several functions simultaneously (e.g., deflection, focusing, filtering). 2) Arrays of elements can be constructed on a single plate (e.g., a lenslet array). 3) Elements can be easily stacked together owing to their planar structure. 4) Elements can be formed on curved substrates if needed. 5) Production costs could ultimately be small.

25) Image Amplification: Some holographic recording materials do not require any developing. The interference pattern is recorded directly in the material. The photorefractive materials are an important example of self-developing recording media. In these materials, such as lithium niobate, the recording in general is a dynamic process. That is, as the hologram grating is recorded it diffracts light from both of the recording beams into the incident beams. These diffracted light beams interfere with the incident beams and this interference is also recorded as part of the total hologram. Depending on the crystal and the physical configuration, it is possible for one of the recording beams to be diminished and the other one to be correspondingly amplified. This dynamic recording process has been used to produce image amplification [274]–[276]. In this case the reference beam (the pump beam) is depleted and the object beam is enhanced.

26) Image Processing:

Image Subtraction can be accomplished directly by holographic techniques [275], [277]–[281]. Two exposures are typically made in a Fourier transform configuration such as shown in Fig. 23(a). With equal amplitudes and 180° phase shift between the two recordings, it is possible to produce a point-by-point subtraction of the images in the output image plane. The two exposures can be in photographic film [277] in which the image subtraction then appears after development. The two exposures can be done in a self-developing material such as a photorefractive crystal of lithium niobate [278] in which case the image subtraction can be monitored continuously during the subtractive recording. Further, the second image to be subtracted need not be recorded into the material. The second object can be placed in the input plane and its wavefront superposed (equal in amplitude and with 180° phase shift) with the diffracted wavefront from the hologram of the first object and thus produce image subtraction without changing the stored image [279]. Alternatively, image subtraction can be implemented using the energy transfer between the two writing beams in dynamic holography [275].

Edge Enhancement in images can be achieved using nonlinear holographic recording [282], [283]. In photorefractive crystals it is possible to have the induced refractive index change proportional to the modulation ratio of the interference pattern [cf. (108)]. If the object beam is much more intense than the reference beam, then the modulation ratio will be small everywhere except where there is a transition from light to dark (an edge) in the object beam. Because the modulation ratio is near unity at these points, they are recorded with high diffraction efficiency and an edge-enhanced image is produced.

Image Deblurring can be accomplished with the use of various types of gratings [284]–[288]. If the image moved linearly with respect to the recording device it is possible to restore the original image by a number of techniques. Deconvolution of the image and the linear blurring function can be achieved using various grating filters placed in the back focal plane of a lens that performs the Fourier transform of the coherently illuminated blurred image. Depending on the configuration used, the deblurring mask might be a holographically recorded complex grating or a simple square-wave (Ronchi ruling) grating. Linear motion deblurring can also be accomplished by using angularly multiplexed volume holograms. In this approach, an appropriate set of gratings with different slant angles (ϕ) but with the same period along the surface ($\Lambda/\sin\phi$) are recorded. From the grating equation for forward-diffracted waves, (43), it is observed that for a given diffracted order, all of the gratings diffract the incident wave in the same direction. The diffraction efficiency of each grating depends on the amount of dephasing that exists from the Bragg condition. The object produces an entire angular spectrum of plane waves. Each component of this spectrum is modified (weighted) by the set of multiplexed gratings. By selecting the appropriate set of volume gratings it is possible to accomplish image deblurring directly. In this technique there are no auxiliary components such as Fourier transform lenses. The filter is simply placed adjacent to the coherently illuminated blurred image (with fringes perpendicular to linear blur) and the resulting diffracted wave represents the deblurred image.

27) Incoherent-to-Coherent Converter: Many optical signal and data processing systems require coherent images for their operation. However, many times the imagery only exists in incoherent form (e.g., from a CRT). The use of the photorefractive material bismuth silicon oxide to make a two-dimensional incoherent-to-coherent converter has been recently demonstrated [289]. In this device, the interference of two coherent plane waves [cf. (108)] is recorded as a planar fringe phase grating. Before, during, or after this exposure, an incoherent image can be focused onto the crystal. In the region where the incoherent image is bright, the charge carriers are photoexcited and redistributed within that bright region. Thus the overall grating is locally erased in bright regions of the image. When coherent light is diffracted from the resultant grating, the efficiency of the diffraction varies inversely with the intensity of the incoherent image. A negative coherent replica of the input incoherent image is produced in the diffracted beam. Therefore the device functions as an incoherent-to-coherent converter.

28) Interferometry: Nondestructive testing using holographic interferometry [290]–[295] has already achieved a high degree of commercial success. Turbine blades, helicopter blades, and automobiles are being vibration tested in this manner. A double-exposure hologram grating of the object is recorded with the same reference beam and played back. The result of deformation between the two exposures appears as fringes on the reconstruction of the object. Interpretation of the fringe pattern allows the locations and amounts of deformation to be determined. The holographic gratings can be recorded on film emulsions when there is appreciable time between the exposures or they can be recorded on a real-time basis (millisecond time scale) in high-sensitivity photorefractive materials such as bismuth silicon oxide and bismuth germanium oxide.

29) Lenses: Gratings to focus light can be recorded holographically or the location of the grating fringes can be calculated from a knowledge of the incident and the desired focused wave. Grating lenses have been investigated for bulk optics (two-dimensional wavefronts) [296]–[301] and for integrated optics [302]–[312]. A schematic illustration of a grating waveguide lens for integrated optics is shown in Fig. 27. The angular field of view over which

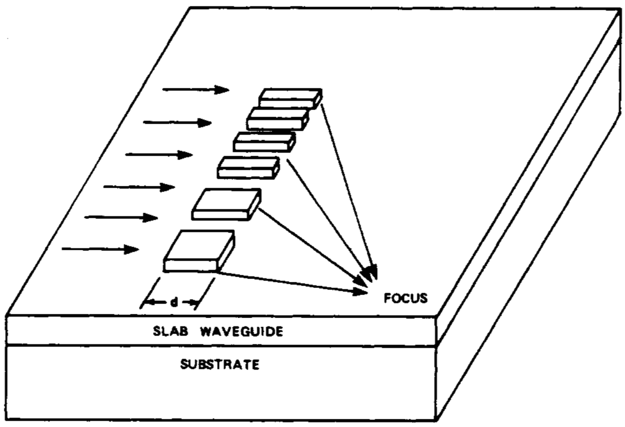

Fig. 27. Slab waveguide chirped grating lens [309].

grating lenses will operate is determined by the angular selectivity of the grating. The field of view can be made large by decreasing the thickness of the grating, but this decreases the diffraction efficiency. Waveguide grating lenses with nearly diffraction-limited performance have been constructed with 90 percent diffraction efficiency and 3° field of view.

30) Mode Conversion: In bulk optics or in integrated optics, if the polarization of the light is rotated, then mode conversion is said to have occurred. In a bulk acoustooptic device such as a tunable filter, the polarization of the light can be rotated by the nature of the photoelastic effect that describes the change of refractive index that is produced by the acoustic strain wave. For guided modes in a dielectric waveguide, TE_n and TM_n ($n = 0,1,2,\cdots$) guided modes may exist. Mode conversion, in general, describes all of the possible transformations $TE_n \rightarrow TE_m$, $TE_n \rightarrow TM_m$, $TM_n \rightarrow TM_m$, and $TM_n \rightarrow TE_m$. When the total field of a particular waveguide mode is decomposed into two zig-zag plane waves it is clear that the waveguide grating vector does not lie in the plane of incidence for either of the component plane waves. As discussed in Section II-E, this situation requires a three-dimensional vector diffraction analysis [29] and coupling between the polarization component perpendicular to the plane of incidence and the component lying in the plane of incidence is inherent. Mode conversion has been extensively studied for the acoustooptic grating case [313], [314] and for the waveguide grating case [315]–[317].

31) Modulation: High-speed electrooptic grating modulators can be constructed using interdigitated electrodes on a substrate [152], [318]–[322]. If the electrode period is large, the modulator will operate in the Raman–Nath regime such as indicated in Fig. 15 where the incident beam is shown normally incident upon the grating. If the interdigitated electrode period is sufficiently small, the modulator will operate in the more efficient Bragg regime such as indicated in Fig. 22 where the beam is shown incident at the first Bragg angle. These devices can be operated in a digital ("on" or "off") or analog manner. Usually the $i = +1$ diffracted beam is used as the output of the device, though the other orders are also modulated.

Acoustooptic grating modulators are inherently not as fast as electrooptic devices, but acoustooptic modulators can be configured in more versatile ways [150], [178], [323]–[327]. A basic acoustooptic waveguide modulator is shown in Fig. 19. The period of the acoustic grating produced is inversely proportional to the input frequency as given by (112). Because of the wide range of possible input frequencies, the resulting grating diffraction can change from Raman–Nath regime behavior (at low frequencies) to Bragg regime behavior (at high frequencies). An amplitude-modulated sound wave (such as depicted in Fig. 21) will produce amplitude modulation of the $i = 0$ transmitted wave. For small amplitude acoustic waves, the depth of modulation of the amplitude-modulated light wave is proportional to the acoustic power rather than the acoustic amplitude which might be a more desirable situation. This applies for both the Raman–Nath and Bragg regimes. Multiple tilted surface acoustic wave transducers (sets of interdigitated electrodes) can be used to extend greatly the bandwidth of these devices. At its design frequency, each set of electrodes produces an acoustic wave grating that is oriented at its first Bragg angle with respect to the guided light beam. The transducers, connected in parallel, each diffract out of the light beam a different range of frequencies present in the input signal. The $i = 0$ transmitted wave is amplitude modulated by all of the SAW transducers and the signal bandwidth is greatly increased. Frequency modulation can also be produced by an acoustooptic modulator. From the phase-matching requirement, it follows that the frequency of the diffracted orders are given by

$$f_i = f_o \pm i f_s \tag{117}$$

where f_o is the incident optical frequency. The + or − is determined by the Doppler effect and depends on which direction the sound grating is moving. Therefore, the $i = 0$ transmitted beam is not frequency-modulated. However, the other orders are frequency-modulated.

32) Monochromator: The wavelength dispersion of a given diffracted order of a grating can be determined from the grating equations [(42) and (43)]. This property is widely used to select a narrow band of wavelengths from a broad-band optical source such as an arc lamp. The source illuminates the grating and an exit slit placed in one of the diffracted orders selects a range of wavelengths that is passed to the output of the monochromator. Either transmission or reflection gratings can be used in various configurations so that as the grating is rotated to change the wavelength selected, the output light always has the same direction. By electrically controlling the rotation of the grating it is possible to change the center wavelength of the output linearly in time so that the absorption or reflection spectra (or other property) of a sample can be plotted. Possible configurations for an ultraviolet monochromator based on a transmission grating, for example, are given in [328].

33) Multiport Storage: Electronic semiconductor memories can only be read by one user at any given time. Frequently, however, there are many users that need the stored data and so each must wait in a queue to gain access to it. Holographic systems for data storage, associative recall, and data processing have been discussed in previous sections. Another capability of holographic systems is multiport access [329], [330]. This would circumvent the queuing problem of ordinary (single-port) memories and would allow simultaneous access by multiple users to the same data or to other data in the memory. Optical memory systems based on angular multiplexing of thick holograms can have multiport access to the stored data by having multiple simultaneous reference beams. These beams can be arrayed angularly above and below the plane of incidence that was used for recording those data. The well-known angular selectivity characteristics of thick hologram gratings occur for angular changes of the reference beam *in* the plane of incidence. However, angular changes of the reference beam *perpendicular* to the plane of incidence produce very little dephasing from the vector form of the Bragg condition and thus allow additional simultaneous positions for other reference beams to read out data [330]. Because of the angular separation of the beams, the data page images produced will be spatially separated and can be read with different detector arrays.

34) Multiple Beam Generation: Diffraction by a grating produces multiple beams as pictured in Fig. 4 and whose directions are given by the grating equations [(42) and (43)]. Tailoring the number and intensities of the diffracted beams by adjusting the period and the profile of the grating is of great interest for a variety of applications [331]. An important example of this type of application is a grating to produce three beams for reading video disks. A reading beam to detect the pits and two tracking beams (one on each side of the row of pits) are needed in this case. Gratings can be synthesized so that most of the power is in the $i = -1$, 0, and +1 orders for this application.

35) Multiplexing, Demultiplexing: Wavelength division multiplexing and demultiplexing can be used to increase the channel capacity of a communications system. The wavelength dispersion characteristics of diffraction gratings allow them to be used directly as multiplexers and demultiplexers [332]–[339]. The grating can be an acoustic wave, an etched surface-relief grating, a hologram grating, etc. In addition, it is possible to use a chirped grating period to give broader band multiplexing and demultiplexing.

36) Optical Testing: Gratings are widely used in optical system testing. Applications include measurement of the refractive index of a lens [340], laser damage testing [341], modulation transfer function (MTF) measurement [342], and many more. For example, the measurement of the MTF of a lens can be accomplished by using diffraction-shearing interferometry. This may be implemented by two diffraction gratings, in contact and rotatable with respect to each other. This replaces a rotating-parallel-plate shearing interferometer MTF measurement system in which large plate thicknesses are required.

37) Pattern Recognition: Optical devices to perform the cross correlation between two one-dimensional signals have been discussed in the section "Correlation Processing." Optical systems using hologram gratings can also be used to obtain the cross correlation between two-dimensional signals (images). This type of system was first developed by Vander Lugt [343] and has been studied in various forms since then [344]–[346]. To accomplish pattern recognition, the system is normally used as a matched filter. That is, when a signal (image) appears that matches the recorded image, the autocorrelation that is produced is threshold detected since its amplitude will be larger than that for any cross correlation that may occur when the signal does not match the recorded pattern. An optical configuration for producing the two-dimensional cross correlation is shown in Fig. 23. The Fourier transform hologram of an image A is recorded as shown in Fig. 23(a). If a new image (B) is placed in the input plane and similarly coherently illuminated, the light diffracted in the direction of the original reference beam will be the product of the complex conjugate of the Fourier transform of A and the Fourier transform of B. Upon Fourier transformation with a lens, this product becomes the cross correlation of A and B. If B matches A, then the intensity of the light in the correlation plane exceeds the threshold level of the detector and the presence of the autocorrelation (match) is registered. Further, the location of the match in the correlation plane corresponds to the location of the match in the stored image A.

38) Phase Conjugation: The diffraction grating geometry for the production of a conjugate wavefront was shown in Fig. 14. If the recording material is a self-developing material of high sensitivity such as photorefractive bismuth silicon oxide, it is possible to produce the conjugate wave in real time. This process is called phase conjugation [347]–[355] and is depicted in Fig. 28. An incoming wave is shown distorted as a result of passing through an aberrating medium. The interference pattern between the distorted wavefront and a plane reference wave is recorded as a grating in the photorefractive crystal. The conjugate reference wave (which could be produced by a plane mirror reflecting the reference wave in this case) then illuminates the recorded hologram grating. The $i = +1$ diffracted wave from the conjugate reference wave is the conjugate of the incoming wave. This predistorted wave upon passing back through the aberrating medium will approximately reproduce the conjugate of the wave that was incident upon the aberrating medium. Thus by predistorting the return wave, a process of wavefront correction in the return signal has been implemented. If the recording material is sufficiently sensitive, the aberrating medium can change in real time and new gratings will be recorded that will provide wavefront correction by predistorting the return wave to compensate for the changed aberrating medium. Since there are four waves present in the recording material (the reference wave and its conjugate, the incoming and the outgoing waves), the process is frequently called "four-wave mixing."

Phase conjugation can be used to provide feedback in a laser cavity [356]–[360]. The phase conjugation system in this case acts as a reflector that always returns the conjugate of the wave received. Therefore, changes causing wavefront distortion can occur within the laser cavity which are corrected in real time by the phase conjugate mirror. The four-wave mixing geometry is the same as that shown in Fig. 24(d) in the section on "Diagnostic Measurements."

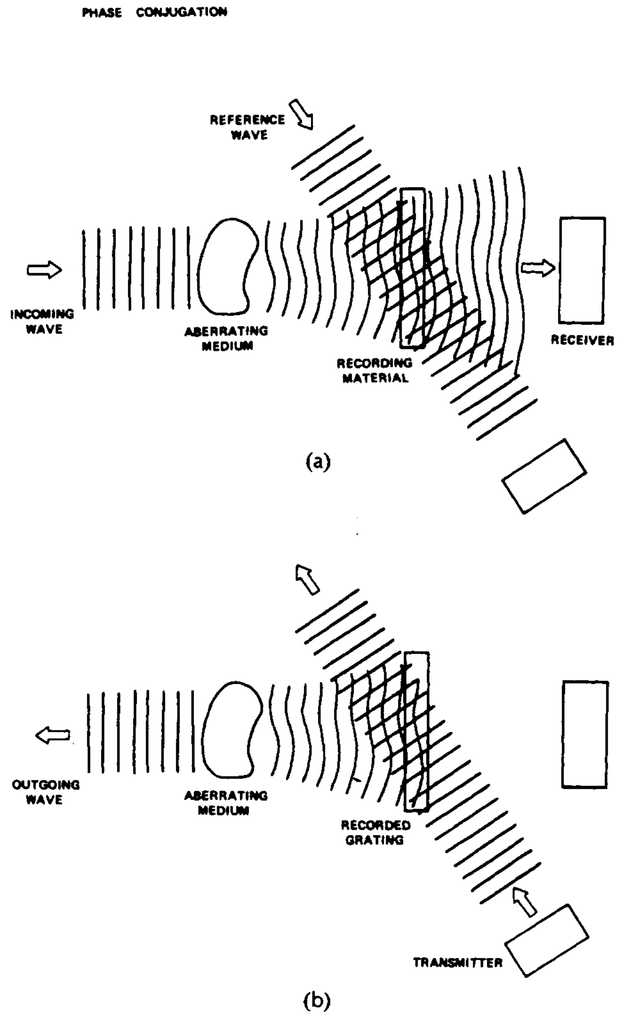

Fig. 28. Phase conjugation configuration. (a) Recording the interference pattern produced by distorted wavefront and reference wavefront. (b) Production of conjugate of incoming wave by illuminating grating with the conjugate of the reference wave. This predistorts the return wave so that its wavefront is corrected traveling back through the aberrating medium.

Thus the equivalence of phase conjugation and real-time holography is apparent [361]–[363].

39) Pulse Shaping and Compression:

Electronic Pulse Compression can be achieved by chirping the pulse, launching it as an acoustic wave, and diffracting light from the resulting acoustic grating [178], [364]–[365]. This is shown schematically in Fig. 29. The linearly swept frequency pulse is converted to an acoustic wave. From the grating equation (43), the $i = +1$ forward-diffracted waves will have differing directions over the variable-period grating. This results in a focusing of the light to a focal length of $F = v_s^2 \Delta T / \lambda \Delta f$ where ΔT is the time duration of the pulse and Δf is the range of frequencies in the pulse. Diffraction-limited focusing is possible in these devices. The focused spot moves at the speed of sound v_s. A detector at the focal plane will detect a new pulse that has been compressed by a factor of $\Delta T \cdot \Delta f$. Compression ratios of 500 are possible with these devices.

Passive Optical Pulse Shaping is possible using a pair of reflection gratings oriented parallel and facing each other

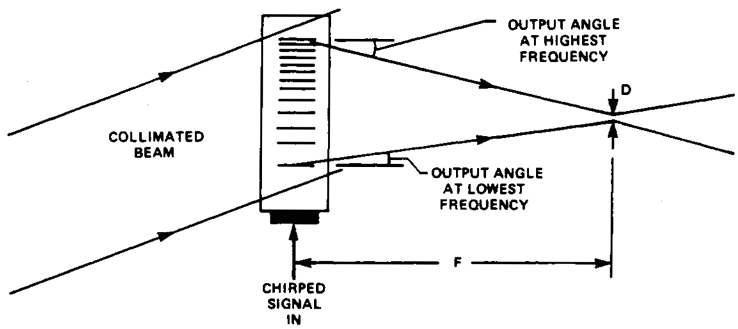

Fig. 29. Acoustooptic pulse compressor. Chirped electronic pulse is received and compressed by detection of the focused light by a detector in the focal plane [365].

[366], [367]. The incident light is reflected from one grating to the other and exits the second grating traveling parallel to its original direction. The grating pair used together with an appropriate filter mask is capable of producing short pulses (nanosecond to picosecond) of arbitrary pulse shapes. Properly tailored temporal intensity profiles are essential in applications such as laser fusion.

Active Optical Pulse Compression down to femtosecond time scales can be achieved using a grating pair together with a spectrally chirped optical pulse [368]–[371]. The parallel gratings have the property of producing a time delay in the output light that increases with wavelength. If the input pulse is frequency swept in time, this chirped pulse will have its envelope compressed in time when it passes through the grating pair which acts as a dispersive delay line. The frequency chirp can be produced by self-phase modulation which can be imposed on the incident pulse by passing it through an optical Kerr-effect liquid or a length of optical fiber.

40) Q-Switching, Mode Locking, Cavity Dumping:

Q-Switching of a laser cavity to produce a high-power output pulse can be accomplished with an acoustooptic grating inside the cavity [372]. When the acoustic grating is aligned to the first Bragg angle and the acoustic grating is "on," the Q factor for the resonator is very low and the lasing action is quenched. With further pumping of the active medium, the gain of the laser increases. When the acoustic wave is switched "off," the Q of the cavity is restored and an intense pulse is emitted.

Mode Locking of a laser to obtain a train of very short pulses can also be done by using an acoustooptic modulator in the laser cavity [372]–[376]. A configuration similar to that described for Q-switching can be used except that the loss introduced into the cavity must occur at a repetition rate equal to the frequency spacing between longitudinal modes of the laser cavity. This produces a train of intense pulses that are emitted at the modulation rate.

Cavity Dumping to obtain a single high-intensity pulse can be achieved using an acoustooptic device in the laser cavity [374]–[377]. In this case, the laser resonator mirrors are designed to be totally reflecting rather than allowing some of the light to be transmitted out of the cavity. In the absence of the acoustic grating, energy builds up in the highly reflective cavity. Then an acoustic pulse propagates into the beam and diffracts energy out of the cavity producing a high-power pulse of light.

41) Solar Concentration: The efficient use of photovoltaic cells requires that a large amount of solar energy be concentrated on each cell. Since large-size refractive optical elements are prohibitively expensive, it has been proposed that holographic optical elements be used for solar concentration [378]–[380]. These concentrators can be lightweight and, because of generally relaxed tolerances, they can be replicated easily.

42) Spectral Analysis:

Microwave Spectral Analysis can be performed using acoustooptic devices. The microwave signal is launched as an acoustic wave and a collimated light wave is diffracted from the acoustic grating. For a given diffracted order, the grating equation (43) indicates that a particular grating period (inversely proportional to microwave frequency) will diffract light at a specific angle. Collimated light at a given angle with respect to a lens axis will be focused by the lens to a spot with a corresponding displacement from the axis in the focal plane. Thus the lens performs an angle-to-displacement conversion. A lens is used in a microwave spectrum analyzer in this way. At microwave frequencies, the acoustic grating periods produced are large compared to the wavelength of light and thus the grating equation shows that the angles of diffraction will be small. For small angles, the displacement of the focused spot from the axis is directly proportional to the microwave frequency. Thus a linear array of detectors can be used in the back focal plane of the lens and the received frequency will increase linearly with detector number. The frequency range covered at each detector will be the same. The fundamental $i = +1$ diffracted order is used in practice. From the grating equation, it can be shown that one octave of frequencies can be covered by the spectrum analyzer without any higher order diffracted waves being focused onto the detector array. At the low-frequency limit of an octave bandwidth spectrum analyzer, the $i = +1$ diffracted order is at its smallest angle of diffraction and the $i = +2$ diffracted order is focused adjacent to the high-frequency end of the detector array. Acoustooptic spectrum analyzers have been implemented in bulk optical form [381]–[384] and in integrated optical form using surface acoustic waves [178], [385]–[391].

Optical Spectral Analysis can be accomplished directly using the wavelength dispersive property of a diffraction grating. The spectrum contained in the incoming light is angularly dispersed by the grating. Spectroscopy may be the oldest and most widely used application of gratings [69]. Applications in the visible region of the spectrum date back to the nineteenth century. In addition to the visible, there is current work on ultraviolet region gratings [392], [393] and X-ray region gratings [394], [395].

43) Switching: Switching of light can be achieved using an acoustooptic or electrooptic grating [396]–[400]. An integrated optics electrooptic Bragg switch is pictured in Fig. 30. A set of interdigitated electrodes at the intersection of two multimode channel waveguides is aligned so that the

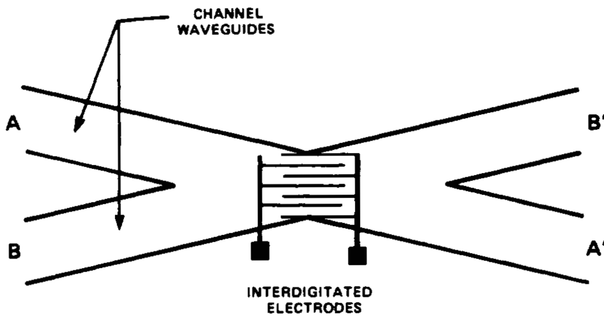

Fig. 30. Channel waveguide electrooptic switch [398].

electrooptically induced permittivity grating is at the first Bragg angle. Without a voltage applied to the interdigitated electrodes, there is no grating and light propagates $A \rightarrow A'$ and $B \rightarrow B'$. If a voltage is applied, the induced grating diffracts the light so that it propagates $A \rightarrow B'$ and $B \rightarrow A'$ thus producing switching action as might be used in a communication bus between processors in a computer.

B. Other Applications

Numerous applications of grating diffraction have been presented in this section. While the applications of the gratings are distinct, the use of the basic diffraction characteristics are common among them. Some applications are really combinations of others. Many other important applications have not been discussed due to space limitations. These include Bragg diffraction imaging [401], a raster-scan TV display system [402], a multichannel digital processor [403], and others.

IX. Summary

A rigorous electromagnetic analysis of diffraction by dielectric slab gratings and surface-relief gratings has been reviewed. Numerous alternative representations of the total field inside the grating have been shown to be equivalent. By selecting the appropriate coupled-wave expansion, the amplitudes of the space-harmonic components of the field have been shown to be directly obtainable using a state-variables approach from linear systems theory. The amplitudes of the evanescent and propagating orders outside of the grating can then be calculated using electromagnetic boundary conditions. Using a series of fundamental assumptions, rigorous coupled-wave theory is shown to reduce to the various existing approximate theories in the appropriate limits. The effects of the fundamental assumptions in the approximate theories have been quantified and discussed.

A wide variety of applications of grating diffraction in the broad areas of acoustooptics, holography, integrated optics, quantum electronics, and spectral analysis have been discussed. The use of gratings is very widespread in modern optical technology and directly affects many areas of electrical engineering. Grating structures are even appearing in the everyday lives of lay people. There have, for example, been 10.5 million copies distributed of the "eagle" hologram grating that appears on a cover of the *National Geographic* [404]. Indeed, it appears that grating diffraction will be even more pervasive and important in the future.

References

[1] R. R. Aggarwal, "Diffraction of light by ultrasonic waves," *Proc. Ind. Acad. Sci. A*, vol. 31, pp. 417–426, June 1950.

[2] P. Phariseau, "On the diffraction of light by progressive supersonic waves," *Proc. Ind. Acad. Sci. A*, vol. 44, pp. 165–170, Oct. 1956.

[3] W. R. Klein and B. D. Cook, "Unified approach to ultrasonic light diffraction," *IEEE Trans. Sonics Ultrason.*, vol. SU-14, pp. 123–134, July 1967.

[4] H. Kogelnik, "Coupled wave theory for thick hologram gratings," *Bell Syst. Tech. J.*, vol. 48, pp. 2909–2947, Nov. 1969.

[5] G. L. Fillmore and R. F. Tynan, "Sensitometric characteristics of hardened dichromated-gelatin films," *J. Opt. Soc. Amer.*, vol. 61, pp. 199–203, Feb. 1971.

[6] J. A. Kong, "Second-order coupled-mode equations for spatially periodic media," *J. Opt. Soc. Amer.*, vol. 67, pp. 825–829, June 1977.

[7] R. Magnusson and T. K. Gaylord, "Analysis of multiwave diffraction of thick gratings," *J. Opt. Soc. Amer.*, vol. 67, pp. 1165–1170, Sept. 1977.

[8] M. G. Moharam and T. K. Gaylord, "Rigorous coupled-wave analysis of planar-grating diffraction," *J. Opt. Soc. Amer.*, vol. 71, pp. 811–818, July 1981.

[9] M. G. Moharam and T. K. Gaylord, "Three-dimensional vector coupled-wave analysis of planar-grating diffraction," *J. Opt. Soc. Amer.*, vol. 73, pp. 1105–1112, Sept. 1983.

[10] T. Tamir, H. C. Wang, and A. A. Oliner, "Wave propagation in sinusoidally stratified dielectric media," *IEEE Trans. Microwave Theory Tech.*, vol. MTT-12, pp. 323–335, May 1964.

[11] T. Tamir and H. C. Wang, "Scattering of electromagnetic waves by a sinusoidal stratified half-space, I," *Can. J. Phys.*, vol. 44, pp. 2073–2094, Sept. 1966.

[12] T. Tamir, "Scattering of electromagnetic waves by a sinusoidal stratified half-space, II," *Can. J. Phys.*, vol. 44, pp. 2461–2494, Oct. 1966.

[13] C. B. Burckhardt, "Diffraction of a plane wave at a sinusoidally stratified dielectric grating," *J. Opt. Soc. Amer.*, vol. 56, pp. 1502–1509, Nov. 1966.

[14] L. Bergstein and D. Kermisch, "Image storage and reconstruction in volume holography," in *Proc. Symp. on Modern Optics*, MRI ser., vol. 17. Brooklyn, NY: Polytechnic Press, 1967, pp. 655–680.

[15] R. S. Chu and T. Tamir, "Guided-wave theory of light diffraction by acoustic microwaves," *IEEE Trans. Microwave Theory Tech.*, vol. MTT-18, pp. 486–504, Aug. 1970.

[16] ——, "Wave propagation and dispersion in space-time periodic media," *Proc. Inst. Elec. Eng.*, vol. 119, pp. 797–806, July 1972.

[17] F. G. Kaspar, "Diffraction by thick, periodically stratified gratings with complex dielectric constant," *J. Opt. Soc. Amer.*, vol. 63, pp. 37–45, Jan. 1973.

[18] S. T. Peng, T. Tamir, and H. L. Bertoni, "Theory of periodic dielectric waveguides," *IEEE Trans. Microwave Theory Tech.*, vol. MTT-23, pp. 123–133, Jan. 1975.

[19] R. S. Chu and J. A. Kong, "Modal theory of spatially periodic media," *IEEE Trans. Microwave Theory Tech.*, vol. MTT-25, pp. 18–24, Jan. 1977.

[20] L. Solymar and D. J. Cooke, *Volume Holography and Volume Gratings*. London, England: Academic Press, 1981.

[21] P. St. J. Russell, "Optical volume holography," *Phys. Rep.*, vol. 71, pp. 209–312, May 1981.

[22] T. K. Gaylord and M. G. Moharam, "Planar dielectric grating diffraction theories," *Appl. Phys. B*, vol. 28, pp. 1–14, May 1982.

[23] R. Magnusson and T. K. Gaylord, "Equivalence of multiwave coupled-wave theory and modal theory for periodic-media diffraction," *J. Opt. Soc. Amer.*, vol. 68, pp. 1777–1779, Dec.

1978.
[24] See, e.g., L. Brillouin, *Wave Propagation in Periodic Structures.* New York: Dover, 1953 (reprint).
[25] See, e.g., C. L. Liu and J. W. S. Liu, *Linear Systems Analysis.* New York: McGraw-Hill, 1975.
[26] N. Uchida, "Calculation of diffraction efficiency in hologram gratings attenuated along the direction perpendicular to the grating vector," *J. Opt. Soc. Amer.*, vol. 63, pp. 280–287, Mar. 1973.
[27] R. R. A. Syms and L. Solymar, "Planar volume phase holograms formed in bleached photographic emulsions," *Appl. Opt.*, vol. 22, pp. 1479–1496, May 15, 1983.
[28] W. E. Baird, M. G. Moharam, and T. K. Gaylord, "Diffraction characteristics of planar absorption gratings," *Appl. Phys. B*, vol. 32, pp. 15–20, Sept. 1983.
[29] M. G. Moharam and T. K. Gaylord, "Rigorous coupled-wave analysis of grating diffraction--E mode polarization and losses," *J. Opt. Soc. Amer.*, vol. 73, pp. 451–455, Apr. 1983.
[30] ——, "Coupled-wave analysis of reflection gratings," *Appl. Opt.*, vol. 20, pp. 240–244, Jan. 15, 1981.
[31] ——, "Chain-matrix analysis of arbitrary-thickness dielectric reflection gratings," *J. Opt. Soc. Amer.*, vol. 72, pp. 187–190, Feb. 1982.
[32] For example, Program EIGRF from the International Mathematics and Statistics Library (IMSL), Houston, TX.
[33] For example, B. Carnahan, H. A. Luther, and J. O. Wilkes, *Applied Numerical Methods.* New York: Wiley, 1969.
[34] P. St. J. Russell, "Power conservation and field structures in uniform dielectric gratings," *J. Opt. Soc. Amer. A*, vol. 1, pp. 293–299, Mar. 1984.
[35] F. Lederer and U. Langbein, "Modal theory for thick holographic gratings with sharp boundaries. II. Unslanted transmission and reflection gratings," *Opt. Acta*, vol. 27, pp. 183–200, Feb. 1980.
[36] S. Kessler and R. Kowarschik, "Diffraction efficiency of volume holograms. Part I: Transmission holograms," *Opt. Quant. Electron.*, vol. 7, pp. 1–4, Jan. 1975.
[37] R. Kowarschik and S. Kessler, "Zum Beugungswirkungsgrad von Volumenhologrammen. Teil II. Reflexionshologramme," *Opt. Quant. Electron.*, vol. 7, pp. 399–411, Sept. 1975.
[38] R. Kowarschik, "Diffraction efficiency of attenuated sinusoidally modulated gratings in volume holograms," *Opt. Acta*, vol. 23, pp. 1039–1051, Dec. 1976.
[39] T. Jaaskelainen, O. Salminen, R. M. K. Hamalainen, "Effect of 2nd order derivatives in the coupled wave analysis of volume holograms," *Acta Polytech. Appl. Phys.*, vol. 126, pp. 3–12, 1979.
[40] C. V. Raman and N. S. N. Nath, "The diffraction of light by high frequency sound waves: Part IV," *Proc. Ind. Acad. Sci. A*, vol. 3, pp. 119–125, Feb. 1936.
[41] ——, "The diffraction of light by high frequency sound waves: Part I," *Proc. Ind. Acad. Sci. A*, vol. 2, pp. 406–412, Oct. 1935.
[42] ——, "The diffraction of light by sound waves of high frequency: Part II," *Proc. Ind. Acad. Sci. A*, vol. 2, pp. 413–420, Oct. 1935.
[43] ——, "The diffraction of light by high frequency sound waves: Part III," *Proc. Ind. Acad. Sci. A*, vol. 3, pp. 75–84, Jan. 1936.
[44] ——, "The diffraction of light by high frequency sound waves: Part V," *Proc. Ind. Acad. Sci. A*, vol. 3, pp. 459–465, May 1936.
[45] N. S. N. Nath, "The diffraction of light by supersonic waves," *Proc. Ind. Acad. Sci. A*, vol. 8, pp. 499–503, Nov. 1938.
[46] ——, "The diffraction of light by high frequency sound waves: Generalized theory," *Proc. Ind. Acad. Sci. A*, vol. 4, 222–242, Aug. 1936.
[47] M. V. Berry, *The Diffraction of Light by Ultrasound.* London: Academic Press, 1966.
[48] P. St. J. Russell, L. Solymar, and M. P. Jordan, "Borrman-like effects in volume holography," in *Proc. ICO-11 Conf.*, pp. 635–638, 1978.
[49] M. G. Moharam, T. K. Gaylord, and R. Magnusson, "Bragg diffraction of finite beams by thick gratings," *J. Opt. Soc. Amer.*, vol. 70, pp. 300–304, Mar. 1980.
[50] L. Solymar and M. P. Jordan, "Finite beams in large volume holograms," *Microwaves Opt. Acoust.*, vol. 1, pp. 89–92, Apr. 1977.
[51] R. P. Kenan, "Theory of crossed-beam diffraction gratings," *IEEE J. Quantum Electron.*, vol. QE-14, pp. 924–930, Dec. 1978.
[52] M. G. Moharam, T. K. Gaylord, and R. Magnusson, "Diffraction characteristics of three-dimensional crossed-beam volume gratings," *J. Opt. Soc. Amer.*, vol. 70, pp. 437–442, Apr. 1980.
[53] N. Uchida, "Calculation of diffraction efficiency in hologram gratings attenuated along the direction perpendicular to the grating vector," *J. Opt. Soc. Amer.*, vol. 63, pp. 280–287, Mar. 1973.
[54] U. Killat, "Coupled wave theory of hologram gratings with arbitrary attenuation," *Opt. Commun.*, vol. 21, pp. 110–111, Apr. 1977.
[55] M. P. Owen and L. Solymar, "Efficiency of volume phase reflection holograms recorded in an attenuating medium," *Opt. Commun.*, vol. 34, pp. 321–326, Sept. 1980.
[56] M. G. Moharam, T. K. Gaylord, and R. Magnusson, "Criteria for Bragg regime diffraction by phase gratings," *Opt. Commun.*, vol. 32, pp. 14–18, Jan. 1980.
[57] T. K. Gaylord and M. G. Moharam, "Thin and thick gratings: Terminology clarification," *Appl. Opt.*, vol. 20, pp. 3271–3273, Oct. 1981.
[58] R. R. A. Syms and L. Solymar, "A comparison of the optical path and differential equation methods for optically thin phase gratings," *Opt. Quant. Electron.*, vol. 12, pp. 383–391, Sept. 1980.
[59] F. H. Sanders, "Intensity measurements in the diffraction of light by ultrasonic waves," *Can. J. Phys.*, vol. 14, pp. 158–171, 1936.
[60] M. G. Moharam, T. K. Gaylord, and R. Magnusson, "Criteria for Raman-Nath regime diffraction by phase gratings," *Opt. Commun.*, vol. 32, pp. 19–23, Jan. 1980.
[61] K. L. Zankel and E. A. Hiedemann, "Diffraction of light by ultrasonic waves progressing with finite but moderate amplitudes in liquids," *J. Acoust. Soc. Amer.*, vol. 31, pp. 44–54, Jan. 1959.
[62] R. Magnusson and T. K. Gaylord, "Diffraction efficiencies of thin phase gratings with grating shape," *J. Opt. Soc. Amer.*, vol. 68, pp. 806–809, June 1978.
[63] ——, "Solutions of the thin phase grating equation," *Opt. Commun.*, vol. 25, pp. 129–132, May 1978.
[64] J. W. Goodman, *Introduction to Fourier Optics.* New York: McGraw-Hill, 1968.
[65] W. T. Cathey, *Optical Information Processing and Holography.* New York: Wiley, 1974.
[66] H. M. Smith, *Principles of Holography.* New York: Wiley, 1969.
[67] R. J. Collier, C. B. Burckhardt, and L. H. Lin, *Optical Holography.* New York: Academic Press, 1971.
[68] R. Magnusson and T. K. Gaylord, "Diffraction efficiencies of thin absorption and transmittance gratings," *Opt. Commun.*, vol. 28, pp. 1–3, Jan. 1979.
[69] For example, M. C. Hutley, *Diffraction Gratings.* London: Academic Press, 1982.
[70] R. Extermann and G. Wannier, "Theorie de la diffraction de la lumiere par les ultrasons," *Helv. Phys. Acta*, vol. 9, no. 7, pp. 520–532, 1936.
[71] G. W. Willard, "Criteria for normal and abnormal ultrasonic light diffraction effects," *J. Acoust. Soc. Amer.*, vol. 21, pp. 101–108, Mar. 1949.
[72] B. Benlarbi, D. J. Cooke, and L. Solymar, "Higher-order modes in thick phase gratings," *Opt. Acta*, vol. 27, pp. 885–895, July 1980.
[73] M. G. Moharam and T. K. Gaylord, "Diffraction analysis of dielectric surface-relief gratings," *J. Opt. Soc. Amer.*, vol. 72, pp. 1385–1392, Oct. 1982.
[74] For example, B. Carnahan, H. A. Luther, and J. O. Wilkes, *Applied Numerical Methods.* New York: Wiley, 1969.
[75] R. C. Enger and S. K. Case, "Optical elements with ultrahigh spatial-frequency surface corrugations," *Appl. Opt.*, vol. 22, pp. 3220–3228, Oct. 15, 1983.
[76] H. M. Smith, Ed., *Holographic Recording Materials* (*Topics in Applied Physics*, vol. 20). New York: Springer-Verlag, 1977.
[77] P. Hariharan, "Holographic recording materials: Recent

developments," *Opt. Eng.*, vol. 19, pp. 636–641, Sept./Oct. 1980.
[78] J. W. Gladden and R. D. Leighty, "Recording media," in *Handbook of Optical Holography*, H. J. Caulfield, Ed. New York: Academic Press, 1979.
[79] For example, "Kodak Plates and Films for Science and Industry," Eastman Kodak Co., Rochester, NY, 1967.
[80] M. J. Beesley and J. G. Castledine, "The use of photoresist as a holographic recording medium," *Appl. Opt.*, vol. 9, pp. 2720–2724, Dec. 1970.
[81] M. G. Moharam, T. K. Gaylord, G. T. Sincerbox, H. Werlich, and B. Yung, "Diffraction characteristics of photoresist surface-relief gratings," *Appl. Opt.*, vol. 23, pp. 3214–3220, Oct. 1, 1984.
[82] T. A. Shankoff, "Phase holograms in dichromated gelatin," *Appl. Opt.*, vol. 7, pp. 2101–2105, Oct. 1968.
[83] T. Kubota, T. Ose, M. Sasaki, and K. Honda, "Hologram formation with red light in methylene blue sensitized dichromated gelatin," *Appl. Opt.*, vol. 15, pp. 556–558, Feb. 1976.
[84] B. L. Booth, "Photopolymer material for holography," *Appl. Opt.*, vol. 14, pp. 593–601, Mar. 1975.
[85] W. J. Tomlinson, E. A. Chandross, H. P. Weber, and G. D. Aumiller, "Multicomponent photopolymer systems for volume phase holograms and grating devices," *Appl. Opt.*, vol. 15, pp. 534–541, Feb. 1976.
[86] J. M. Moran and I. P. Kaminow, "Properties of holographic gratings photo-induced in polymethyl methacrylate," *Appl. Opt.*, vol. 12, pp. 1964–1970, Aug. 1973.
[87] J. W. Lin and T. C. Lee, "Diffraction efficiency of the thermoplastic-photoconductor device for holographic recording," *Photog. Sci. Eng.*, vol. 23, pp. 213–215, July/Aug. 1979.
[88] B. Ineichen, C. Liegeois, and P. Meyrueis, "Thermoplastic film camera for holographic recording of extended objects in industrial applications," *Appl. Opt.*, pp. 2209–2214, June 15, 1982.
[89] W. J. Tomlinson, "Volume holograms in photochromic materials," *Appl. Opt.*, vol. 14, pp. 2456–2467, Oct. 1975.
[90] I. Schneider and M. E. Gingerich, "Diffraction by M Centers in KCl," *Appl. Opt.*, vol. 15, pp. 2428–2431, Oct. 1976.
[91] D. Casasent and F. Caimi, "Photodichroic recording and storage material," *Appl. Opt.*, vol. 15, pp. 815–820, Mar. 1976.
[92] L. Nikolova and T. Todorov, "Volume amplitude holograms in photodichroic materials," *Opt. Acta*, vol. 24, pp. 1179–1192, Dec. 1977.
[93] L. Nikolova, T. Todorov, D. Popov, and K. Tersiiski, "Laser induced fast reversible processes in additively coloured KCl containing F_A centres," *Phys. Status Solidi*, vol. 55A, pp. 333–337, Sept. 1979.
[94] A. M. Glass, "The photorefractive effect," *Opt. Eng.*, vol. 17, pp. 470–479, Sept./Oct. 1978.
[95] E. Kratzig, F. Welz, R. Orlowski, V. Doormann, and M. Rosenkra, "Holographic storage properties of $BaTiO_3$," *Solid State Commun.*, vol. 34, pp. 817–819, June 1980.
[96] M. Peltier and F. Micheron, "Volume hologram recording and charge transfer process in $Bi_{12}SiO_{20}$ and $Bi_{12}GeO_{20}$," *J. Appl. Phys.*, vol. 48, pp. 3683–3690, Sept. 1977.
[97] A. Krumins and P. Gunter, "Diffraction efficiency and energy transfer during hologram formation in reduced $KNbO_3$," *Appl. Phys.*, vol. 19, pp. 153–163, June 1979.
[98] L. A. Boatner, E. Kratzig, and R. Orlowski, "KTN as a holographic storage material," *Ferroelectr.*, vol. 27, pp. 247–250, Jan. 1980.
[99] D. L. Staebler and W. Phillips, "Fe-doped $LiNbO_3$ for read-write applications," *Appl. Opt.* vol. 13, pp. 788–794, Apr. 1974.
[100] J. P. Huignard, J. P. Herriau, and F. Micheron, "Optical storage in $LiNbO_3$:Fe with selective erasure capability," *Rev. Phys. Appl.*, vol. 18, pp. 417–423, Nov. 1975.
[101] H. Kurz, "Photorefractive recording of volume holograms in doped $LiNbO_3$," *Ferroelectr.*, vol. 13, pp. 291–294, Sept. 1976.
[102] E. Kratzig and R. Orlowski, "$LiTaO_3$ as holographic storage materials," *Appl. Phys.*, vol. 15, pp. 133–139, Feb. 1978.
[103] C. Elachi, "Waves in active and passive periodic structures: A review," *Proc. IEEE*, vol. 64, pp. 1666–1698, Dec. 1976.
[104] *Proc. IEEE* (Special Section on Acousto-Optic Signal Processing), vol. 69, pp. 48–118, Jan. 1981.
[105] D. C. Auth, "New high power source of coherent microwave phonons," *Appl. Phys. Lett.*, vol. 16, pp. 521–523, June 15, 1970.
[106] R. H. Enns and S. S. Rangnekar, "Diffraction by a laser induced thermal phase grating. I," *Can. J. Phys.*, vol. 52, pp. 99–109, Jan. 15, 1974.
[107] H. J. Eichler, "Laser-induced grating phenomena," *Opt. Acta*, vol. 24, pp. 631–642, June 1977.
[108] K. A. Nelson, R. Casalegno, R. J. D. Miller, and M. D. Fayer, "Laser-induced excited state and ultrasonic wave gratings: Amplitude and phase grating contribution to diffraction," *J. Chem. Phys.*, vol. 77, pp. 1144–1152, Aug. 1, 1982.
[109] T. M. Turpin, "Time integrating optical processors," *Proc. SPIE*, vol. 154, pp. 196–203, 1978.
[110] R. A. K. Said and D. C. Cooper, "Crosspath real-time optical correlator and ambiguity function processor," *Proc. Inst. Elec. Eng.*, vol. 120, pp. 423–428, Apr. 1973.
[111] J. D. Cohen, "Ambiguity processor architectures using one-dimensional acousto-optical transducers," *Proc. SPIE*, vol. 180, pp. 134–142, 1979.
[112] W. T. Rhodes, "Acousto-optic signal processing: Convolution and correlation," *Proc. IEEE*, vol. 69, pp. 65–79, Jan. 1981.
[113] S. Wright, I. M. Mason, and M. G. F. Wilson, "High-speed electro-optic analogue-digital conversion," *Electron. Lett.*, vol. 10, pp. 508–509, Nov. 28, 1974.
[114] L. R. Lewis and A. Hessel, "Propagation characteristics of periodic arrays of dielectric slabs," *IEEE Trans. Microwave Theory Tech.*, vol. MTT-19, pp. 276–286, Mar. 1971.
[115] W. Streifer, D. R. Scifres, and R. D. Burnham, "Analysis of grating-coupled radiation in GaAs: GaAlAs lasers and waveguides," *IEEE J. Quantum Electron.*, vol. QE-12, pp. 422–428, July 1976.
[116] T. Tamir and S. T. Peng, "Analysis and design of grating couplers," *Appl. Phys.*, vol. 14, pp. 235–254, Nov. 1977.
[117] S. V. Zaitsev, A. S. Kuzali, and A. V. Chekan, "Controlled correction of phase distribution of the field along a thin-film optical waveguide with a diffraction grating," *Opt. Spectrosc.*, vol. 45, pp. 791–792, Nov. 1978.
[118] T. Tamir, "Microwave modeling of optical periodic waveguides," *IEEE Trans. Microwave Theory Tech.*, vol. MTT-29, pp. 979–983, Sept. 1981.
[119] P. J. van Heerden, "Theory of optical information storage in solids," *Appl. Opt.*, vol. 2, pp. 393–400, Apr. 1963.
[120] L. D'Auria, J. P. Huignard, C. Slezak, and E. Spitz, "Experimental holographic read-write memory using 3-D storage," *Appl. Opt.*, vol. 13, pp. 808–818, Apr. 1974.
[121] H. Akahori and K. Sakurai, "Information search using holography," *Appl. Opt.*, vol. 11, pp. 413–415, Feb. 1972.
[122] G. R. Knight, "Page-oriented associative holographic memory," *Appl. Opt.*, vol. 13, pp. 904–912, Apr. 1974.
[123] ——, "Holographic associative memory and processor," *Appl. Opt.*, vol. 17, pp. 1088–1092, May 1975.
[124] A. A. Vasilev, I. N. Kompanets, S. P. Kotova, and V. N. Morozov, "Associative access to data in holographic memories with controlled transparencies," *Sov. J. Quantum Electron.*, vol. 8, pp. 740–743, June 1978.
[125] P. E. Tverdokhleb, "Optical memory system with content access," in *Optical Information Processing*, vol. 2, E. S. Barrekette, G. W. Stroke, Y. E. Nesterikhin, and W. E. Kock, Eds. New York: Plenum, 1978, pp. 283–304.
[126] A. A. Verbovetskii and V. B. Fyodorov, "Optical memory systems with associative-addressed access," *Sov. J. Quantum Electron.*, vol. 10, pp. 1020–1024, Aug. 1980.
[127] N. Nishida, M. Sakaguchi, and F. Saito, "Holographic coding plate: A new application of holographic memory," *Appl. Opt.*, vol. 12, pp. 1663–1674, July 1973.
[128] V. N. Morozov, "Theory of holograms formed using a coded reference beam," *Sov. J. Quantum Electron.*, vol. 7, pp. 961–964, Aug. 1977.
[129] A. E. Krasnov, "Thick-film phase holograms recorded by means of coded reference waves," *Sov. J. Quantum Electron.*, vol. 7, pp. 1147–1148, Sept. 1977.
[130] T. F. Krile, M. O. Hagler, W. D. Redus, and J. F. Walkup, "Multiplex holography with chirp-modulated binary phase-

coded reference-beam masks," *Appl. Opt.*, vol. 18, pp. 52–56, Jan. 1, 1979.

[131] A. Gruss, K. T. Tam, and T. Tamir, "Blazed dielectric gratings with high beam-coupling efficiencies," *Appl. Phys. Lett.*, vol. 36, pp. 523–525, Apr. 1, 1980.

[132] M. L. Dakss, L. Kuhn, P. F. Heidrich, and B. A. Scott, "Grating coupler for efficient excitation of optical guided waves in thin films," *Appl. Phys. Lett.*, vol. 16, pp. 523–525, June 15, 1970.

[133] Y. A. Bykovskii, A. V. Makovkin, and V. L. Smirnov, "Excitation of thin film waveguides by a holographic method," *Opt. Spectrosc.*, vol. 37, pp. 579–580, Nov. 1974.

[134] W. Streifer, D. R. Scifres, R. D. Burnham, and R. I. MacDonald, "On grating-coupled radiation from waveguides," *IEEE J. Quantum Electron.*, vol. QE-13, pp. 67–68, Feb. 1977.

[135] G. Evans, J. Leary, and J. Wilcox, "Applications of semiconductor lasers in space communications," *Opt. Eng.*, vol. 22, pp. 247–255, Mar./Apr. 1983.

[136] A. M. P. P. Leite, O. D. D. Soares, and E. A. Ash, "Optical-fibre-bundle holographic coupler," *Microwaves Opt. Acoust.*, vol. 2, pp. 45–54, Mar. 1978.

[137] C. H. Bulmer and M. G. F. Wilson, "Single mode grating coupling between thin-film and fiber optical waveguides," *IEEE J. Quantum Electron.*, vol. QE-14, pp. 741–749, Oct. 1978.

[138] G. Goldmann and H. H. Witte, "Holograms as optical branching elements," *Opt. Quant. Electron.*, vol. 9, pp. 75–78, Jan. 1977.

[139] V. J. Fowler and J. Schlafer, "A survey of laser beam deflection techniques," *Proc. IEEE*, vol. 54, pp. 1437–1444, Oct. 1966.

[140] J. D. Zook, "Light beam deflector performance: A comparative analysis," *Appl. Opt.*, vol. 13, pp. 875–887, Apr. 1974.

[141] L. Kuhn, M. L. Dakss, P. F. Heidrich, and B. A. Scott, "Deflection of an optical guided wave by a surface acoustic wave," *Appl. Phys. Lett.*, vol. 17, pp. 265–267, Sept. 15, 1970.

[142] D. A. Pinnow, "Acousto-optic light deflection: Design consideration for first order beam steering transducers," *IEEE Trans. Sonics Ultrason.*, vol. SU-18, pp. 209–214, Oct. 1971.

[143] N. Uchida and N. Niizeki, "Acoustooptic deflection materials and techniques," *Proc. IEEE*, vol. 61, pp. 1073–1092, Aug. 1973.

[144] G. A. Alphonse, "Broadband acoustooptic deflectors: New results," *Appl. Opt.*, vol. 14, pp. 201–207, Jan. 1975.

[145] I. C. Chang and D. L. Hecht, "Doubling acousto-optic deflector resolution utilizing second-order birefringent diffraction," *Appl. Phys. Lett.*, vol. 27, pp. 517–518, Nov. 15, 1975.

[146] Y. Nomura, M. Nunoshita, and T. Nakayama, "Efficiency of thin-film acoustooptic light deflectors for a Gaussian guided optical beam," *Appl. Opt.*, vol. 16, pp. 2729–2731, Oct. 1977.

[147] E. G. Lean and W. H. Chen, "Large-angle acoustic-beam steering in acoustically anisotropic crystal," *Appl. Phys. Lett.*, vol. 35, pp. 101–103, July 15, 1979.

[148] J. B. Merry and L. Bademian, "Acousto-optic laser scanning," *Proc. SPIE*, vol. 169, pp. 56–59, 1979.

[149] F. W. Freyre, "Zero frequency shift Bragg cell beam deflection and translation," *Appl. Opt.*, vol. 20, pp. 3896–3900, Nov. 15, 1981.

[150] C. S. Tsai, M. A. Alhaider, L. T. Nguyen, and B. Kim, "Wide-band guided-wave acoustooptic Bragg diffraction and devices using multiple tilted surface acoustic waves," *Proc. IEEE*, vol. 64, pp. 318–328, Mar. 1976.

[151] M. G. Cohen and E. I. Gordon, "Electro-optic $[KTa_xNb_{1-x}O_3(KTN)]$ gratings for light beam modulation and deflection," *Appl. Phys. Lett.*, vol. 5, 181–182, Nov. 1, 1964.

[152] J. M. Hammer, "Digital electro-optic grating deflector and modulator," *Appl. Phys. Lett.*, vol. 18, pp. 147–149, Feb. 15, 1971.

[153] J. M. Hammer, D. J. Channin, and M. T. Duffy, "Fast electro-optic waveguide deflector modulator," *Appl. Phys. Lett.*, vol. 23, pp. 176–177, Aug. 15, 1973.

[154] S. Wright and M. G. F. Wilson, "New form of electrooptic deflector," *Electron. Lett.*, vol. 9, pp. 169–170, May 3, 1973.

[155] J. C. Wyant, "Rotating diffraction grating laser beam scanner," *Appl. Opt.*, vol. 14, pp. 1057–1058, May 1975.

[156] O. Bryngdahl and W. Lee, "Laser beam scanning using computer-generated holograms," *Appl. Opt.*, vol. 15, pp. 183–194, Jan. 1976.

[157] R. V. Pole, H. W. Werlich, and R. J. Krusche, "Holographic light deflection," *Appl. Opt.*, vol. 17, pp. 3294–3297, Oct. 15, 1978.

[158] S. K. Case and V. Gerbig, "Laser beam scanners constructed from volume holograms," *Opt. Eng.*, vol. 19, pp. 711–717, Sept./Oct. 1980.

[159] ——, "Efficient and flexible laser-beam scanners constructed from volume holograms," *Opt. Commun.*, vol. 36, pp. 94–100, Jan. 15, 1981.

[160] Y. Ishii, "Reflection volume holographic scanners with field-curvature corrections," *Appl. Opt.*, vol. 22, pp. 3491–3499, Nov. 15, 1983.

[161] C. J. Kramer, "Hologon laser scanners for nonimpact printing," *Proc. SPIE*, vol. 390, pp. 165–173, Jan. 1983.

[162] I. Shoshan and U. P. Oppenheim, "The use of a diffraction grating as a beam expander in a dye laser cavity," *Opt. Commun.*, vol. 25, pp. 375–378, June 1978.

[163] M. F. Becker, "Correcting inherent aberrations in the grating rhomb beam sampler," *Appl. Opt.*, vol. 18, pp. 4178–4181, Dec. 15, 1979.

[164] W. B. Veldkamp, "Laser beam profile shaping with interlaced binary diffraction gratings," *Appl. Opt.*, vol. 21, pp. 3209–3212, Sept. 1, 1982.

[165] D. W. Vahey, C. M. Verber, and R. P. Kenan, "Development of an integrated-optics multichannel data processor," *Proc. SPIE*, vol. 139, pp. 151–158, 1978.

[166] B. H. Soffer and B. B. McFarland, "Continuously tunable narrow band organic dye lasers," *Appl. Phys. Lett.*, vol. 10, pp. 266–267, May 15, 1967.

[167] T. Itoh and R. Mittra, "An analytical study of the echelette grating with applications to open resonators," *IEEE Trans. Microwave Theory Tech.*, vol. MTT-17, pp. 319–327, June 1969.

[168] T. J. Manuccia and G. J. Wolga, "The properties and application of diffraction gratings in frequency-selective laser resonators," *IEEE J. Quantum Electron.*, vol. QE-6, p. 185, Mar. 1970.

[169] I. P. Kaminow, H. P. Weber, and E. A. Chandross, "Poly (methyl methacrylate) dye laser with internal diffraction grating resonator," *Appl. Phys. Lett.*, vol. 18, pp. 497–499, June 1, 1971.

[170] A. Hardy and D. Treves, "Modes of a diffraction grating optical resonator," *Appl. Opt.*, vol. 14, pp. 589–592, Mar. 1975.

[171] K. R. German, "Diffraction grating tuners for CW lasers," *Appl. Opt.*, vol. 18, pp. 2348–2349, July 15, 1979.

[172] O. Nilsson, S. Saito, and Y. Yamamoto, "Oscillation frequency, linewidth reduction and frequency modulation characteristics for a diode laser with external grating feedback," *Electron. Lett.*, vol. 17, pp. 589, 591, Aug. 1981.

[173] E. Armandillo and G. Giuliani, "Estimation of the minimum laser linewidth achievable with a grazing-grating configuration," *Opt. Lett.*, vol. 8, pp. 274–276, May 1983.

[174] S. Saito, O. Nilsson, and Y. Yamamoto, "Oscillation center frequency tuning, quantum FM noise, and direct frequency modulation characteristics in external grating loaded semiconductor lasers," *IEEE J. Quantum Electron.*, vol. QE-18, pp. 961–970, June 1982.

[175] Z. Bor, B. Racz, and A. Muller, "Generation of 6-psec pulses with nitrogen-laser-pumped distributed feedback dye laser," *Appl. Opt.*, vol. 22, pp. 3327–3330, Nov. 1983.

[176] W. S. C. Chang, C. S. Tasi, R. A. Becker, and I. W. Yao, "Convolution using guided acousto optical interaction in thin-film waveguides," *IEEE J. Quantum Electron.*, vol. QE-13, pp. 208–215, Apr. 1977.

[177] J. N. Lee, B. J. Udelson, and N. J. Berg, "Acousto-optic signal processing for radar applications," *Proc. SPIE*, vol. 128, pp. 192–201, 1977.

[178] C. S. Tsai, "Guided-wave acoustooptic Bragg modulators for wide-band integrated optics communications and signal processing," *IEEE Trans. Circuits Syst.*, vol. CAS-26, pp. 1972–1098, Dec. 1979.

[179] R. A. Spraque, "A review of acousto-optic signal correlators, *Opt. Eng.*, vol. 16, pp. 467–474, Sept./Oct. 1977.

[180] N. J. Berg, B. J. Udelson, and J. N. Lee, "A new acousto-optic memory correlator," *IEEE Trans. Electron Devices*, vol. ED-24, pp. 1191–1192, Sept. 1977.

[181] N. J. Berg, B. J. Udelson, J. N. Lee, and E. Katzen, "An acousto-optic real-time 'two-crystal' correlator," *Appl. Phys. Lett.*, vol. 32, pp. 85–87, Jan. 15, 1978.

[182] M. W. Casseday, N. J. Berg, I. J. Abramovitz, and J. N. Lee, "Wide-band signal processing using the two-beam surface acoustic wave acoustooptic time integrating correlator," *IEEE Trans. Microwave Theory Tech.*, vol. MTT-29, pp. 483–490, May 1981.

[183] C. M. Verber, R. P. Kenan, and J. R. Busch, "Correlator based on an integrated optical spatial light modulator," *Appl. Opt.*, vol. 20, pp. 1626–1629, May 1, 1981.

[184] K. Preston, *Coherent Optical Computers.* New York: McGraw-Hill, 1972.

[185] P. Chavel, A. A. Sawchuk, T. C. Strand, A. R. Tanguay, and B. H. Soffer, "Optical logic with variable-grating-mode liquid-crystal devices," *Opt. Lett.*, vol. 5, pp. 398–400, Sept. 1980.

[186] A. R. Tanguay, C. S. Wu, P. Chavel, T. C. Strand, A. A. Sawchuk, and B. H. Soffer, "Physical characterization of the variable grating mode liquid crystal device," *Opt. Eng.*, vol. 22, pp. 687–694, Nov./Dec. 1983.

[187] T. K. Gaylord, R. Magnusson, and J. E. Weaver, "Digital processing capabilities using holographically recorded data pages in electro-optic crystals," *Opt. Commun.*, vol. 20, pp. 365–366, Mar. 1977.

[188] C. C. Guest and T. K. Gaylord, "Truth-table look-up processors using binary and residue arithmetic," *Appl. Opt.*, vol. 19, pp. 1201–1207, Apr. 1, 1980.

[189] M. M. Mirsalehi, C. C. Guest, and T. K. Gaylord, "Residue number system holographic truth-table look-up processing: Detector threshold setting and probability of error due to amplitude and phase variations," *Appl. Opt.*, vol. 22, pp. 3583–3592, Nov. 15, 1983.

[190] J. A. Rajchman, "An optical read-write mass memory," *Appl. Opt.*. vol. 9, pp. 2269–2271, Oct. 1970.

[191] W. C. Stewart, R. S. Mezrich, L. S. Cosentino, E. M. Nagle, F. S. Wendt, and R. D. Lohman, "An experimental read-write holographic memory," *RCA Rev.*, vol. 34, pp. 3–44, Mar. 1973.

[192] A. Vander Lugt, "Design relationships for holographic memories," *Appl. Opt.*, vol. 12, pp. 1675–1685, July 1973.

[193] A. Bardos, "Wideband holographic recorder," *Appl. Opt.*, vol. 13, no. 4, pp. 832–840, Apr. 1974.

[194] H. Kiemle, "Considerations on holographic memories in the gigabyte region," *Appl. Opt.*, vol. 13, pp. 803–807, Apr. 1974.

[195] R. H. Nelson, A. Vander Lugt, and R. G. Zech, "Holographic data storage and retrieval," *Opt. Eng.*, vol. 13, pp. 429–434, Sept./Oct. 1974.

[196] H. N. Roberts, J. W. Watkins, and R. H. Johnson, "High speed holographic digital recorder," *Appl. Opt.*, vol. 13, pp. 841–856, Apr. 1974.

[197] K. K. Sutherlin, J. P. Lauer, and R. W. Olenick, "Holoscan: A commercial holographic ROM," *Appl. Opt.*, vol. 13, pp. 1345–1354, June 1974.

[198] A. Akaev and S. A. Maiorov, "Optimal relationship between geometric parameters of a high-capacity holographic digital memory," *Sov. J. Quantum Electron.*, vol. 5, pp. 384–388, Oct. 1975.

[199] A. Vander Lugt, "Packing density in holographic systems," *Appl. Opt.*, vol. 14, pp. 1081–1087, May 1975.

[200] G. A. Alphonse and W. Phillips, "Read-write holographic memory with iron-doped lithium niobate," *Ferroelectr.*, vol. 11, pp. 397–401, June 1976.

[201] J. P. Huignard, F. Micheron, and E. Spitz, "Optical systems and photosensitive materials for information storage," in *Optical Properties of Solids New Developments*, B. O. Seraphin, Ed. New York: North-Holland, American Elsevier, 1976.

[202] V. N. Morozov and Y. M. Popov, "High-capacity holographic memories with synthesized aperture," *Sov. J. Quantum Electron.*, vol. 6, pp. 1265–1271, Nov. 1976.

[203] A. L. Mikaeliane, "Holographic bulk memories using lithium niobate crystals for data recording," in *Optical Information Processing*, vol. 2, E. S. Barrekette, G. W. Stroke, Y. E. Nesterikhin, and W. E. Kock, Eds. New York: Plenum, 1978, pp. 217–233.

[204] R. Csomor, "Alignment and design conditions for optical memory systems using Fourier transform holograms," *Opt. Acta*, vol. 25, pp. 107–112, Feb. 1978.

[205] S. I. Soskin and S. A. Shoidin, "Design of the optical arrangement of a holographic memory," *Opt. Spectrosc.*, vol. 44, pp. 327–331, Mar. 1978.

[206] K. Chalasinsha-Macukow and T. Szoplik, "Simple holographic permanent memory system," *Appl. Opt.*, vol. 17, pp. 3722–3726, Dec. 1, 1978.

[207] T. Sugaya, M. Ishikawa, I. Hoshino, and A. Iwamoto, "Holographic system for filing and retrieving patents," *Appl. Opt.*, vol. 20, pp. 3104–3108, Sept. 15, 1981.

[208] H. Eichler, G. Salje, and H. Stahl, "Thermal diffusion measurements using spatially periodic temperature distributions induced by laser light," *J. Appl. Phys.*, vol. 44, pp. 5383–5388, Dec. 1973.

[209] T. A. Wiggins and A. Salik, "Temporary gratings in germanium," *Appl. Phys. Lett.*, vol. 25, pp. 438–439, Oct. 15, 1974.

[210] D. W. Phillion, D. J. Kuizenga, and A. E. Siegman, "Subnanosecond relaxation time measurements using a transient induced grating method," *Appl. Phys. Lett.*, vol. 27, pp. 85–87, July 15, 1975.

[211] A. E. Siegman, "Proposed measurement of subpicosecond excited-state dynamics using tunable-laser-induced grating," *Appl. Phys. Lett.*, vol. 30, pp. 21–23, Jan. 15, 1977.

[212] K. Jarasiunas and H. J. Gerritsen, "Ambipolar diffusion measurements in semiconductors using transient gratings," *J. Opt. Soc. Amer.*, vol. 68, pp. 679–680, May 1978.

[213] J. R. Salcedo and A. E. Siegman, "Laser induced photoacoustic grating effects in molecular crystals," *IEEE J. Quantum Electron.*, vol. QE-15, pp. 250–256, Apr. 1979.

[214] A. von Jena and H. E. Lessing, "Theory of laser-induced amplitude and phase gratings including photoselection, orientational relaxation, and population kinetics," *Opt. Quant. Electron.*, vol. 11, pp. 419–439, Sept. 1979.

[215] H. J. Eichler, U. Klein, and D. Langhaus, "Coherence time measurement of picosecond pulses by a light-induced grating method," *Appl. Phys.*, vol. 21, pp. 215–219, Mar. 1980.

[216] D. R. Lutz, K. A. Nelson, C. R. Gochanour, and M. D. Fayer, "Electronic excited state energy transfer, trapping by dimers and fluorescence quenching in concentrated dye solutions: Picosecond transient grating experiments," *Chem. Phys.*, vol. 58, pp. 325–334, July 1, 1981.

[217] A. L. Smirl, T. F. Boggess, B. S. Wherrett, G. P. Perryman, and A. Miller, "Picosecond transient orientational and concentration gratings in germanium," *IEEE J. Quantum Electron.*, vol. QE-19, pp. 690–700, Apr. 1983.

[218] A. M. Weiner and E. P. Ippen, "Novel transient scattering technique for femtosecond dephasing measurements," *Appl. Opt.*, vol. 9, pp. 53–55, Feb. 1984.

[219] E. N. Leith, D. B. Brumm, and S. S. H. Hsiao, "Holographic cinematography," *Appl. Opt.*, vol. 11, pp. 2016–2023, Sept. 1972.

[220] B. R. Clay and D. A. Gore, "Holographic moving map display," *Proc. SPIE*, vol. 45, pp. 149–155, Mar. 1974.

[221] J. Upatnieks, "360 degrees hologram displays for educational uses," *J. Opt. Soc. Amer.*, vol. 64, p. 1396, Oct. 1974.

[222] S. A. Benton, "Holographic displays—A review," *Opt. Eng.*, vol. 14, pp. 402–407, Sept./Oct. 1975.

[223] O. D. D. Soares and J. C. A. Fernandes, "Cylindrical hologram of 360° field of view," *Appl. Opt.*, vol. 21, pp. 3194–3196, Sept. 1, 1982.

[224] H. Dammann, "Color separation gratings," *Appl. Opt.*, vol. 17, pp. 2273–2279, Aug. 1, 1978.

[225] N. K. Shi and A. L. DeSouza, "Application of volume holograms as color-sensitive spatial filters," *J. Opt. Soc. Amer.*, vol. 68, p. 1415, Oct. 1978.

[226] A. Tai, F. T. S. Yu, and H. Chen, "White-light pseudo-color encoder," *Opt. Lett.*, vol. 3, pp. 190–192, Nov. 1978.

[227] K. Knop, "Diffraction gratings for color filtering in the zero diffraction order," *Appl. Opt.*, vol. 17, pp. 3598–3603, Nov. 15, 1978.

[228] H. Kogelnik and C. V. Shank, "Stimulated emission in a periodic structure," *Appl. Phys. Lett.*, vol. 18, pp. 152–154,

Feb. 15, 1971.
[229] C. V. Shank, J. E. Bjorkholm, and H. Kogelnik, "Tunable distributed feedback dye laser," *Appl. Phys. Lett.*, vol. 18, pp. 395–396, May 1, 1971.
[230] J. E. Bjorkholm and C. V. Shank, "Higher-order distributed feedback oscillators," *Appl. Phys. Lett.*, vol. 20, pp. 306–308, Apr. 15, 1972.
[231] D. B. Anderson, P. R. August, and J. E. Coker, "Distributed-feedback double-heterostructure GaAs injection laser with fundamental grating," *Appl. Opt.*, vol. 13, pp. 2742–2744, Dec. 1974.
[232] M. Nakamura, K. Aiki, J. I. Umeda, A. Yariv, H. W. Yen, and T. Morikawa, "GaAs-$Ga_{1-x}Al_xAs$ double-heterostructure distributed-feedback diode lasers," *Appl. Phys. Lett.*, vol. 25, pp. 487–488, Nov. 1, 1974.
[233] S. Wang, "Principles of distributed feedback and distributed Bragg-reflector lasers," *IEEE J. Quantum Electron.*, vol. QE-10, pp. 413–427, Apr. 1974.
[234] D. R. Scifres, R. D. Burnham, and W. Streiffer, "Output coupling and distributed feedback utilizing substrate corrugations in double-heterostructure GaAs lasers," *Appl. Phys. Lett.*, vol. 27, pp. 295–297, Sept. 1, 1975.
[235] K. Aiki, M. Nakamura, J. Umeda, A. Yariv, A. Katzir, and H. W. Yen, "GaAs-GaAlAs distributed-feedback diode lasers with separate optical and carrier confinement," *Appl. Phys. Lett.*, vol. 27, pp. 145–146, Aug. 1, 1975.
[236] H. C. Casey, Jr., S. Somekh, and M. Ilegems, "Room-temperature operation of low-threshold separate-confinement heterostructure injection laser with distributed feedback," *Appl. Phys. Lett.*, vol. 27, pp. 142–144, Aug. 1, 1975.
[237] W. Ng, H. W. Yen, A. Katzir, I. Samid, and A. Yariv, "Room-temperature operation of GaAs Bragg-mirror lasers," *Appl. Phys. Lett.*, vol. 29, pp. 684–686, Nov. 15, 1976.
[238] N. Namizaki, M. K. Shams, and S. Wang, "Large-optical-cavity GaAs-(GaAl)As injection laser with low-loss distributed Bragg reflectors," *Appl. Phys. Lett.*, vol. 31, pp. 122–124, July 15, 1977.
[239] M. A. DiForte, M. Papuchon, C. Puech, P. Allemand, and D. B. Ostrowsky, "Tunable optically pumped GaAs-GaAs-GaAlAs distributed-feedback lasers," *IEEE J. Quantum Electron.*, vol. QE-14, pp. 560–562, Aug. 1978.
[240] A. Doi, T. Fukuzawa, M. Nakamura, R. Ito, and K. Aiki, "GaAsP/InP distributed-feedback injection lasers fabricated by one-step liquid phase epitaxy," *Appl. Phys. Lett.*, vol. 35, pp. 441–443, Sept. 15, 1979.
[241] H. Kawanishi, Y. Suematsu, K. Utaka, Y. Itaya, and S. Arai, "$Ga_xIn_{1-x}As_yP_{1-y}$/InP injection laser partially loaded with first-order distributed Bragg reflector," *IEEE J. Quantum Electron.*, vol. QE-15, pp. 701–706, Aug. 1979.
[242] F. K. Reinhart, R. A. Logan, and C. V. Shank, "GaAs-$Al_xGa_{1-x}As$ injection lasers with distributed Bragg reflectors," *Appl. Phys. Lett.*, vol. 27, pp. 45–48, July 1, 1979.
[243] K. Sakai, K. Utaka, S. Akiba, and Y. Matsushima, "1.5 μm range InGaAsP/InP distributed feedback lasers," *IEEE J. Quantum Electron.*, vol. QE-18, pp. 1272–1278, Aug. 1982.
[244] T. Kurobori and N. Takeuchi, "A novel distributed feedback colour center laser," *Opt. Acta*, vol. 30, pp. 1363–1365, Oct. 1983.
[245] D. C. Flanders, H. Kogelnik, R. V. Schmidt, and C. V. Shank, "Grating filters for thin film optical waveguides," *Appl. Phys. Lett.*, vol. 24, pp. 194–196, Feb. 15, 1974.
[246] R. V. Schmidt, D. C. Flanders, C. V. Shank, and R. D. Standley, "Narrowband grating filters for thin-film optical waveguides," *Appl. Phys. Lett.*, vol. 25, pp. 651–652, Dec. 1, 1974.
[247] P. S. Cross and H. Kogelnik, "Sidelobe suppression in corrugated waveguide filters," *Opt. Lett.*, vol. 1, pp. 43–45 July 1977.
[248] A. Katzir and A. Livanos, "Chirped gratings and their applications in integrated optics," *J. Opt. Soc. Amer.*, vol. 68, p. 1364, Oct. 1978.
[249] A. Basu and J. M. Ballantyne, "Second- and higher-order waveguide grating filters. 1: Theory," *Appl. Opt.*, vol. 18, pp. 3620–3626, Nov. 1, 1979.
[250] ____, "Second- and higher-order waveguide grating filters. 2: Experiment," *Appl. Opt.*, vol. 18, pp. 3627–3632, Nov. 1, 1979.
[251] S. H. Kim and C. G. Fonstad, "Tunable narrow-band thin-film waveguide grating filters," *IEEE J. Quantum Electron.*, vol. QE-15, pp. 1405–1408, Dec. 1979.
[252] Z. Y. Yin, P. E. Jessop, and B. K. Garside, "Photoinduced grating filters in GeO_2 thin-film waveguides," *Appl. Opt.*, vol. 22, pp. 4088–4098, Dec. 15, 1983.
[253] S. E. Harris, S. T. K. Nieh, and D. K. Winslow, "Electronically tunable acousto-optic filter," *Appl. Phys. Lett.*, vol. 15, pp. 325–326, Nov. 15, 1969.
[254] R. W. Dixon, "Acoustic diffraction of light in anisotropic media," *IEEE J. Quantum Electron.*, vol. QE-3, pp. 85–93, Feb. 1967.
[255] S. E. Harris and R. W. Wallace, "Acousto-optic tunable filter," *J. Opt. Soc. Amer.*, vol. 59, pp. 744–747, June 1969.
[256] D. J. Taylor, S. E. Harris, S. T. K. Nieh, and T. W. Hansch, "Electronic tuning of a dye laser using the acousto-optic filter," *Appl. Phys. Lett.*, vol. 19, pp. 269–271, Oct. 15, 1971.
[257] T. Yano and A. Watanabe, "Acousto-optic TeO_2 tunable filter using far-off-axis anisotropic Bragg diffraction," *Appl. Opt.*, vol. 15, pp. 2250–2258, Sept. 1976.
[258] B. Kim and C. S. Tsai, "Thin film tunable optical filtering using anisotropic and noncollinear acoustooptic interaction in $LiNbO_3$ waveguides," *IEEE J. Quantum Electron.*, vol. QE-15, pp. 642–647, July 1979.
[259] I. C. Chang, "Acousto-optic tunable filters," *Opt. Eng.*, vol. 20, pp. 824–829, Nov./Dec. 1981.
[260] J. F. Coonrod and M. N. Ernstoff, "Advanced head-up display technology—The integrated HUD," in *Naecon 77 Rec.*, pp. 981–990, 1977.
[261] R. J. Withrington, L. G. Cook, and H. H. Jones, "Holographic head-up displays," U.S. Patent 4 218 111 assigned to Hughes Aircraft Company, Aug. 19, 1980.
[262] H. J. Caulfield,, "Holography: A reassessment," *IEEE Spectrum*, vol. 19, pp. 39–45, Aug. 1982.
[263] D. G. McCauley, C. E. Simpson, and W. J. Murbach, "Holographic optical elements for visual display applications," *Appl. Opt.*, vol. 12, pp. 232–242, Feb. 1973.
[264] S. J. Bennett, "Achromatic combinations of hologram optical elements," *Appl. Opt.*, vol. 15, pp. 542–545, Feb. 1976.
[265] W. C. Sweatt, "Describing holographic optical elements as lenses," *J. Opt. Soc. Amer.*, vol. 67, pp. 803–808, June 1977.
[266] ____, "Designing and constructing thick holographic optical elements," *Appl. Opt.*, vol. 17, pp. 1220–1227, Apr. 15, 1978.
[267] R. Ferrante, M. P. Owen, and L. Solymar, "Conjugate diffraction order in a volume holographic off-axis lens," *J. Opt. Soc. Amer.*, vol. 71, pp. 1385–1389, Nov. 1981.
[268] S. K. Case, P. R. Haugen, and O. J. Lokberg, "Multifacet holographic optical elements for wavefront transformations," *Appl. Opt.*, vol. 20, pp. 2670–2675, Aug. 1981.
[269] R. Silvennoinen and T. Jaaskelainen, "Design procedures using coupled multiwave efficiency analysis for wavelength shifted holographic optical elements," *Opt. Commun.*, vol. 39, pp. 123–126, Oct. 1981.
[270] D. Courjon and C. Bainier, "Holographic optical elements used as stereoscopic screens,," *Appl. Opt.*, vol. 21, pp. 3804–3805, Nov. 1, 1982.
[271] R. C. Fairchild and J. R. Fienup, "Computer-oriented aspheric holographic optical elements," *Opt. Eng.*, vol. 21, pp. 133–140, Jan./Feb. 1982.
[272] T. Stone and N. George, "Bandwidth of holographic optical elements," *Opt. Lett.*, vol. 7, pp. 445–447, Sept. 1982.
[273] K. A. Winick and J. R. Fienup, "Optimum holographic elements recorded with nonspherical wave fronts," *J. Opt. Soc. Amer.*, vol. 73, pp. 208–217, Feb. 1983.
[274] V. L. Vinetskii and N. V. Kukhtarev, "Geometric factors in the dynamic holographic conversion of light beams," *Sov. J. Quantum Electron.*, vol. 8, pp. 231–235, Feb. 1978.
[275] V. Markov, S. Odulov, and M. Soskin, "Dynamic holography and optical image processing," *Opt. Laser Tech.*, vol. 11, pp. 95–99, Apr. 1979.
[276] N. V. Kukhtarev, V. B. Markov, S. G. Odulov, M. S. Soskin, and V. L. Vinetskii, "Holographic storage in electro-optic crystals. II. Beam coupling—Light amplification," *Ferroelectr.*, vol. 22, pp. 961–964, July 1979.
[277] D. Gabor, G. W. Stroke, R. Restrick, A. Funkhouser, and D. Brum, "Optical image synthesis (complex amplitude ad-

dition and subtraction) by holographic Fourier transformation," *Phys. Lett.*, vol. 18, pp. 116–118, Aug. 15, 1965.
[278] J. P. Huignard, J. P. Herriau, and F. Micheron, "Coherent selective erasure of superimposed volume holograms in $LiNbO_3$," *Appl. Phys. Lett.*, vol. 26, pp. 256–258, Mar. 1, 1975.
[279] C. C. Guest, M. M. Mirsalehi, and T. K. Gaylord, "EXCLUSIVE OR processing (binary image subtraction) using thick Fourier holograms," *Appl. Opt.*, vol. 23, pp. 3444–3454, Oct. 1, 1984.
[280] I. Schneider, W. C. Collins, M. J. Marrone, and M. E. Gingerich, "Holographic subtraction using anisotropic centers in alkali halide crystals," *Appl. Phys. Lett.*, vol. 27, pp. 348–350, Sept. 15, 1975.
[281] E. Marom and N. Konforti, "Subtraction via processing simultaneously recorded holographic images," *Opt. Commun.*, vol. 21, pp. 63–66, Apr. 1977.
[282] J. P. Huignard and J. P. Herriau, "Real-time coherent object edge reconstruction with $Bi_{12}SiO_{20}$ crystals," *Appl. Opt.*, vol. 17, pp. 2671–2672, Sept. 1, 1978.
[283] J. Feinberg, "Real-time edge enhancement using the photorefractive effect," *Opt. Lett.*, vol. 5, pp. 330–332, Aug. 1980.
[284] E. N. Leith, "Complex spatial filters for image deconvolution," *Proc. IEEE*, vol. 65, pp. 18–28, Jan. 1977.
[285] D. Peri and A. A. Friesem, "Image restoration using volume diffraction gratings," *Opt. Lett.*, vol. 3, pp. 124–126, Oct. 1978.
[286] ——, "Volume holograms for image restoration," *J. Opt. Soc. Amer.*, vol. 70, pp. 515–522, May 1980.
[287] E. N. Leith, "Image deblurring using diffraction gratings," *Opt. Lett.*, vol. 5, pp. 70–72, Feb. 1980.
[288] R. M. Vasu and G. L. Rogers, "Construction of a phase-inverting grating and its use in a deblurring filter," *Appl. Opt.*, vol. 19, pp. 469–473, Feb. 1, 1980.
[289] Y. Shi, D. Psaltis, A. Marrakchi, and A. R. Tanguay, "Photorefractive incoherent-to-coherent optical converter," *Appl. Opt.*, vol. 22, pp. 3665–3667, Dec. 1, 1983.
[290] J. P. Huignard and J. P. Herriau, "Real-time double-exposure interferometry with $Bi_{12}SiO_{20}$ crystals in transverse electro optic configuration," *Appl. Opt.*, vol. 16, pp. 1807–1809, July 1977.
[291] J. P. Huignard, J. P. Herriau, and T. Valentin, "Time average holographic interferometry with photoconductive electro-optic $Bi_{12}SiO_{20}$ crystals," *Appl. Opt.*, vol. 16, pp. 2796–2798, Nov. 1977.
[292] K. N. Petrov and Y. P. Presnyakov, "Holographic interferometry of the corrosion process," *Opt. Spectrosc.*, vol. 44, pp. 179–181, Feb. 1978.
[293] D. M. Rowley, "Interferometry with miniature format volume reflection holograms," *Opt. Acta*, vol. 28, pp. 907–915, July 1981.
[294] F. M. Kuchel and H. J. Tiziani, "Real-time contour holography using BSO crystals," *Opt. Commun.*, vol. 38, pp. 17–20, July 1, 1981.
[295] A. M. Tai and K. A. Winick, "Effects of the emulsion refractive index on achromatic grating interferometer applications," *Appl. Opt.*, vol. 20, pp. 3478–3480, Oct. 15, 1981.
[296] J. N. Latta and R. C. Fairchild, "Two-element hologram telescope lens," *J. Opt. Soc. Amer.*, vol. 63, p. 487, Apr. 1973.
[297] A. K. Richter and F. P. Carlson, "Holographically generated lens," *Appl. Opt.*, vol. 13, pp. 2924–2930, Dec. 1974.
[298] M. R. Latta and R. V. Pole, "Design techniques for forming 488nm holographic lenses with reconstruction at 633 nm," *Appl. Opt.*, vol. 18, pp. 2418–2421, July 15, 1979.
[299] K. Winick, "Designing efficient aberration-free holographic lenses in the presence of a construction-reconstruction wavelength shift," *J. Opt. Soc. Amer.*, vol. 72, pp. 143–148, Jan. 1982.
[300] R. R. A. Syms and L. Solymar, "Analysis of volume holographic cylindrical lenses," *J. Opt. Soc. Amer.*, vol. 72, pp. 179–186, Feb. 1982.
[301] ——, "Higher diffraction orders in on-axis holographic lenses," *Appl. Opt.*, vol. 12, pp. 3263–3268, Sept. 15, 1982.
[302] R. Shubert and J. H. Harris, "Optical guided-wave focusing and diffraction," *J. Opt. Soc. Amer.*, vol. 61, pp. 154–161, Feb. 1971.
[303] G. I. Hatakoshi and S. I. Tanaka, "Grating lenses for integrated optics," *Opt. Lett.*, vol. 2, pp. 142–144, June 1978.
[304] P. R. Ashley and W. S. C. Chang, "Fresnel lens in a thin-film waveguide," *Appl. Phys. Lett.*, vol. 33, pp. 490–492, Sept. 15, 1978.
[305] S. K. Yao and D. E. Thompson, "Chirp-grating lens for guided wave optics," *Appl. Phys. Lett.*, vol. 33, pp. 635–637, Oct. 1, 1978.
[306] G. Hatakoshi, H. Inoue, K. Naito, S. Umegaki, and S. Tanaka, "Optical waveguide lenses," *Opt. Acta*, vol. 26, pp. 961–968, Aug. 1979.
[307] W. S. C. Chang and P. R. Ashley, "Fresnel lenses in optical waveguides," *IEEE J. Quantum Electron.*, vol. QE-16, pp. 744–754, July 1980.
[308] G. Hatakoshi and S. Tanaka, "Coupling of two cylindrical guided waves in optical waveguide Bragg grating lenses," *J. Opt. Soc. Amer.*, vol. 71, pp. 121–123, Jan. 1981.
[309] C. Warren, S. Forouhar, W. S. C. Chang, and S. K. Yao, "Double ion exchanged chirp grating lens in lithium niobate waveguides," *Appl. Phys. Lett.*, vol. 43, pp. 424–426, Sept. 1, 1983.
[310] S. Forouhar, R. X. Lu, W. S. C. Chang, R. L. Davis, and S. K. Yao, "Chirped grating lenses on Nb_2O_5 transition waveguides, *Appl. Opt.*, vol. 22, pp. 3128–3132, Oct. 1, 1983.
[311] S. Forouhar, W. S. C. Chang and S. K. Yao, "Performance and limitations of chirped grating lenses of Ti-indiffused $LiNbO_3$ planar waveguides," *IEEE J. Lightwave Technol.*, vol. LT-2, pp. 503–512, Aug. 1984.
[312] G. Hatakoshi, H. Fujima, and K. Goto, "Waveguide grating lenses for optical couplers," *Appl. Opt.*, vol. 23, pp. 1749–1753, June 1, 1984.
[313] Y. Ohmachi and J. Noda, "$LiNbO_3$ TE-TM converter using collinear acoustooptic interaction," *IEEE J. Quantum Electron.*, vol. QE-13, pp. 43–46, Feb. 1977.
[314] L. N. Binh, J. Livingstone, and D. H. Steven, "Tunable acousto-optic TE-TM mode converter on a diffused optical waveguide," *Opt. Lett.*, vol. 5, pp. 83–84, Mar. 1980.
[315] K. Wagatsuma, H. Sakaki, and S. Saito, "Mode conversion and optical filtering of obliquely incident waves in corrugated waveguide filters," *IEEE J. Quantum Electron.*, vol. QE-15, 632–637, July 1979.
[316] S. R. Seshadri, "TE-TE" coupling at oblique incidence in a periodic dielectric waveguide," *Appl. Phys.*, vol. 25, pp. 211–220, Aug. 1981.
[317] G. I. Stegeman, D. Sarid, J. J. Burke, and D. G. Hall, "Scattering of guided waves by surface periodic gratings for arbitrary angles of incidence: Perturbation field theory and implications to normal-mode analysis," *J. Opt. Soc. Amer.*, vol. 71, pp. 1497–1507, Dec. 1981.
[318] M. A. R. P. de Barros and M. G. F. Wilson, "Nanosecond baseband optical-diffraction modulator," *Electron. Lett.*, vol. 7, pp. 267–269, May 20, 1971.
[319] J. M. Hammer, D. J. Chanin, M. T. Duffy, and C. C. Neil, "High-speed electro optic waveguide grating modulator using epitaxial ZnO," *IEEE J. Quantum Electron.*, vol. QE-11, pp. 138–148, Apr. 1975.
[320] J. M. Hammer and W. Phillips, "Low-loss single-mode optical waveguides and efficient high-speed modulators of $LiNb_xTa_{1-x}O_3$ on $LiTaO_3$," *Appl. Phys. Lett.*, vol. 24, pp. 545–547, June 1, 1974.
[321] J. C. An, Y. Cho, and Y. Matsuo, "Electro-optic distributed Bragg-reflection modulators or integrated optics," *IEEE J. Quantum Electron.*, vol. QE-13, pp. 206–208, Apr. 1977.
[322] R. P. Bocker, G. M. Meana, M. A. Monahan, G. C. Mooradian, W. E. Richards, and H. F. Taylor, "A large-aperture electro-optic diffraction modulator," *J. Appl. Phys.*, vol. 50, pp. 6691–6693, Nov. 1979.
[323] D. Maydan, "Acousto-optical pulse modulators," *IEEE J. Quantum Electron.*, vol. QE-6, pp. 15–25, Jan. 1970.
[324] R. V. Johnson, "Temporal responses of the acoustooptic modulator: Geometrical optics model in the low scattering efficiency limit," *Appl. Opt.*, vol. 16, pp. 507–514, Feb. 1977.
[325] L. T. Nguyen and C. S. Tsai, "Efficient wideband guided-wave acoustooptic Bragg diffraction using phased surface acoustic wave array in $LiNbO_3$ waveguides," *Appl. Opt.*, vol. 16, pp. 1297–1304, May 1977.
[326] S. K. Yao and C. S. Tsai, "Acoustooptic Bragg-diffraction with application to ultrahigh data rate laser communication systems. 1: Theoretical consideration of the standing wave ultrasonic Bragg cell," *Appl. Opt.*, vol. 16, pp. 3032–3043,

Nov. 1977.
[327] R. V. Johnson, "Temporal response of the acoustooptic modulator: Physical optics model in the low scattering efficiency limit," *Appl. Opt.*, vol. 17, pp. 1507–1518, May 15, 1978.
[328] S. A. Flodstrom and R. Z. Bachrach, "Simple far uv transmission grating monochromator for use with resonance radiation lamps," *Rev. Sci. Instrum.*, vol. 47, pp. 1464–1468, Dec. 1976.
[329] C. O. Alford and T. K. Gaylord, "The potential of multi-port optical memories in digital computing," in *Dig. 1975 Int. Optical Computing Conf.*, pp. 121–123, Apr. 25, 1975.
[330] H. J. Gallagher, T. K. Gaylord, M. G. Moharam, and C. C. Guest, "Reconstruction of binary data-page thick holograms for an arbitrarily oriented reference beam," *Appl. Opt.*, vol. 20, pp. 300–306, Jan. 15, 1981.
[331] W. H. Lee, "High efficiency multiple beam gratings," *Appl. Opt.*, vol. 18, pp. 2152–2158, July 1, 1979.
[332] C. S. Tsai and S. K. Yao, "Bragg diffraction by standing ultrasonic waves with application to optical demultiplexing," *J. Appl. Phys.*, vol. 43, pp. 5081–5084, Dec. 1972.
[333] A. C. Livanos, A. Katzir, A. Yariv, and C. S. Hong, "Chirped-grating demultiplexers in dielectric waveguides," *Appl. Phys. Lett.*, vol. 30, pp. 519–521, May 15, 1977.
[334] W. J. Tomlinson, "Wavelength multiplexing in multimode optical fibers," *Appl. Opt.*, vol. 16, pp. 2180–2194, Aug. 1977.
[335] K. I. Aoyama and J. I. Minowa, "Low-loss optical demultiplexer for WDM systems in the 0.8-μm wavelength region," *Appl. Opt.*, vol. 18, pp. 2834–2836, Aug. 15, 1979.
[336] J. L. Horner and J. E. Ludman, "Single holographic element wavelength demultiplexer," *Appl. Opt.*, vol. 20, pp. 1845–1847, May 15, 1981.
[337] T. Suhara, J. Viljanen, and M. Leppihalme, "Integrated-optic wavelength multi- and demultiplexers using a chirped grating and an ion-exchanged waveguide," *Appl. Opt.*, vol. 21, pp. 2195–2198, June 15, 1982.
[338] Y. Fujii and J. Minowa, "Optical demultiplexer using a silicon concave diffraction grating," *Appl. Opt.*, vol. 22, pp. 974–978, Apr. 1, 1983.
[339] T. Kita and T. Harada, "Use of aberration-corrected concave gratings in optical demultiplexers," *Appl. Opt.*, vol. 22, pp. 819–825, Mar. 15, 1983.
[340] R. S. Kasana, S. Boseck, and K. J. Rosenbruch, "Use of a grating in a coherent optical-processing configuration for evaluating the refractive index of a lens," *Appl. Opt.*, vol. 23, pp. 757–761, Mar. 1, 1984.
[341] T. A. Wiggins, T. T. Saito, and R. M. Herman, "Hole gratings for laser damage testing," *Appl. Opt.*, vol. 22, pp. 3388–3396, Nov. 1, 1983.
[342] P. Hariharan, W. H. Steel, and J. C. Wyant, "Double grating interferometer with variable lateral shear," *Opt. Commun.*, vol. 11, pp. 317–320, 1974.
[343] A. Vander Lugt, "Signal detection by complex spatial filtering," *IEEE Trans. Inform. Theory*, vol. IT-10, pp. 139–145, Apr. 1964.
[344] N. Brousseau and H. H. Arsenault, "Emulsion thickness and space variance: Combined effects in Vander Lugt optical correlators," *Appl. Opt.*, vol. 14, pp. 1679–1682, July 1975.
[345] S. S. Hsiao, "Nonlinearly recorded matched filter: a technique to reduce the false alarm rate," *Appl. Opt.*, vol. 16, pp. 1166–1171, May 1977.
[346] D. Casasent, G. Silbershatz, and B. V. K. V. Kumar, "Acoustooptic matched filter correlator," *Appl. Opt.*, vol. 21, pp. 2356–2364, July 1, 1982.
[347] A. Yariv and D. M. Pepper, "Amplified reflection, phase conjugation, and oscillation in degenerate four-wave mixing," *Opt. Lett.*, vol. 1, pp. 16–18, July 1977.
[348] R. L. Abrams and R. C. Lind, "Degenerate four-wave mixing in absorbing media," *Opt. Lett.*, vol. 2, pp. 94–96, Apr. 1978.
[349] R. W. Hellwarth, "Theory of phase-conjugation by four-wave mixing in a waveguide," *IEEE J. Quantum Electron.*, vol. QE-15, pp. 101–109, Feb. 1979.
[350] J. P. Huignard, J. P. Herriau, and G. Rivet, "Phase-conjugation and spatial-frequency dependence of wavefront reflectivity in $Bi_{12}SiO_{20}$ crystals," *Opt. Lett.*, vol. 5, pp. 102–104, Mar. 1980.
[351] J. P. Hermann, J. P. Herriau, and J. P. Huignard, "Nanosecond four-wave mixing and holography in BSO crystals," *Appl. Opt.*, vol. 20, pp. 2173–2175, July 1, 1981.
[352] T. Wilson and L. Solymar, "Two-dimensional coupled differential equations for degenerate four-wave mixing," *Appl. Phys. Lett.*, vol. 38, pp. 669–670, May 1, 1981.
[353] P. N. Gunter, "Electric-field dependence of phase-conjugate wave-front reflectivity in reduced $KNbO_3$ and $Bi_{12}GeO_{20}$," *Opt. Lett.*, vol. 7, pp. 10–12, Jan. 1982.
[354] M. Cronin-Golomb, J. O. White, B. Fischer, and A. Yariv, "Exact solution of a nonlinear model of four-wave mixing and phase conjugation," *Opt. Lett.*, vol. 7, pp. 313–315, July 1982.
[355] J. Falk, "Test of fidelity of phase conjugation," *Opt. Lett.*, vol. 7, pp. 620–622, Dec. 1982.
[356] P. A. Belanger, A. Hardy, and A. E. Siegman, "Resonant modes of optical cavities with phase-conjugate mirrors," *Appl. Opt.*, vol. 19, pp. 602–609, Feb. 15, 1980.
[357] R. K. Jain and G. J. Dunning, "Spatial and temporal properties of a continuous-wave phase-conjugate resonator based on the photorefractive crystal $BaTiO_3$," *Opt. Lett.*, vol. 7, pp. 420–422, Sept. 1982.
[358] L. K. Lam, T. Y. Chang, J. Feinberg, and R. W. Hellwarth, "Photorefractive-index gratings formed by nanosecond optical pulses in $BaTiO_3$," *Opt. Lett.*, vol. 6, pp. 475–477, Oct. 1981.
[359] R. A. McFarlane and D. G. Steel, "Laser oscillator using resonator with self-pumped phase-conjugate mirror," *Opt. Lett.*, vol. 8, pp. 208–210, Apr. 1983.
[360] W. B. Whitten and J. M. Ramsey, "Self-scanning of a dye laser due to feedback from a $BaTiO_3$ phase-conjugate reflector," *Opt. Lett.*, vol. 9, pp. 44–46, Feb. 1984.
[361] A. Yariv, "Four wave nonlinear optical mixing as real time holography," *Opt. Commun.*, vol. 25, pp. 23–25, Apr. 1978.
[362] J. P. Huignard, J. P. Herriau, P. Aubourg, and E. Spitz, "Phase-conjugate wavefront generation via real-time holography in $Bi_{12}SiO_{20}$ crystals," *Opt. Lett.*, vol. 4, pp. 21–23, Jan. 1979.
[363] A. Marrakchi, J. P. Huignard, and J. P. Herriau, "Application of phase conjugation in $Bi_{12}SiO_{20}$ crystals to mode pattern visualization of diffuse vibrating structures," *Opt. Commun.*, vol. 34, pp. 15–18, July 1980.
[364] M. B. Schulz, M. G. Holland, and L. Davis, Jr., "Optical pulse compression using Bragg scattering by ultrasonic waves," *Appl. Phys. Lett.*, vol. 11, pp. 237–240, Oct. 1, 1967.
[365] J. H. Collins, E. G. H. Lean, and H. J. Shaw, "Pulse compression by Bragg diffraction of light with microwave sound," *Appl. Phys. Lett.*, vol. 11, pp. 240–242, Oct. 1, 1967.
[366] J. Debois, F. Gires, and P. Tournois, "A new approach to picosecond laser pulse analysis, shaping, and coding," *IEEE J. Quantum Electron.*, vol. QE-9, pp. 213–218, Feb. 1973.
[367] J. Agostinelli, G. Harvey, T. Stone, and C. Gabel, "Optical pulse shaping with a grating pair," *Appl. Opt.*, vol. 18, pp. 2500–2504, July 15, 1979.
[368] E. B. Treacy, "Compression of picosecond light pulses," *Phys. Lett.*, vol. 28A, pp. 34–35, Oct. 1968.
[369] R. A. Fisher, P. L. Kelley, and T. K. Gustafson, "Subpicosecond pulse generation using the optical Kerr effect," *Appl. Phys. Lett.*, vol. 14, pp. 140–143, Feb. 15, 1969.
[370] E. Treacy, "Optical pulse compression with diffraction gratings," *IEEE J. Quantum Electron.*, vol. QE-5, pp. 454–458, Sept. 1969.
[371] C. V. Shank, R. L. Fork, R. Yen, R. H. Stolen, and W. J. Tomlinson, "Compression of femtosecond optical pulses," *Appl. Phys. Lett.*, vol. 40, pp. 761–763, May 1, 1982.
[372] R. B. Chesler, M. A. Karr, and J. E. Geusic, "An experimental and theoretical study of high repetition rate Q-switched Nd:YAG lasers," *Proc. IEEE*, vol. 58, pp. 1899–1914, Dec. 1970.
[373] O. R. Wood, R. L. Abrams, and T. J. Bridges, "Mode locking of a transversely excited atmospheric pressure CO_2 laser," *Appl. Phys. Lett.*, vol. 17, p. 376–378, Nov. 1, 1970.
[374] R. H. Johnson, "Characteristics of acousto-optic cavity dumping in a mode-locked laser," *IEEE J. Quantum Electron.*, vol. QE-19, pp. 255–257, Feb. 1973.

[375] D. J. Kuizenga, D. W. Phillion, T. Lund, and A. E. Siegman, "Simultaneous Q-switching and mode-locking in the CW Nd:YAG laser," *Opt. Commun.*, vol. 9, pp. 221–226, Nov. 1973.
[376] C. Loth and D. Bruneau, "Single-frequency active-passive mode-locked Nd:YLF oscillator at 1.053 μm," *Appl. Opt.*, vol. 21, pp. 2091–2092, June 15, 1982.
[377] D. Maydan, "Fast modulator for extraction of internal laser power," *J. Appl. Phys.*, vol. 41, pp. 1552–1559, March 15, 1970.
[378] J. E. Ludman, "Holographic solar concentrator," *Appl. Opt.*, vol. 21, pp. 3057–3058, Sept. 1, 1982.
[379] K. T. K. Cheng, "Energy takes on a low-cost solution: Holography," *Photonics Spectra*, vol. 16, pp. 32–38, June 1982.
[380] W. H. Bloss, M. Griesinger, and E. R. Reinhardt, "Dispersive concentrating systems based on transmission phase holograms for solar applications," *Appl. Opt.*, vol. 21, pp. 3739–3742, Oct. 15, 1982.
[381] D. L. Hecht, "Spectrum analysis using acousto-optic devices," *Opt. Eng.*, vol. 16, pp. 461–466, Sept./Oct. 1977.
[382] T. W. Cole, R. T. Stewart, and D. K. Milne, "An acousto-optical solar radio spectrograph," *Astron. Astrophys.*, vol. 67, pp. 277–279, June 1978.
[383] G. Chin, D. Buhl, and J. M. Florez, "Acousto-optic spectrometer for radio astronomy," *Proc. SPIE*, vol. 231, pp. 30–37, 1980.
[384] N. A. Espkina, B. A. Kotov, and Y. A. Kotov, "Acousto-optic spectrograph for the RATAN-600 radio telescope," *Sov. Phys. —Tech. Lett.*, vol. 5, pp. 236–240, May 1980.
[385] M. C. Hamilton, D. A. Wille, and W. J. Miceli, "An integrated optical RF spectrum analyzer," *Opt. Eng.*, vol. 16, pp. 475–478, Sept./Oct. 1977.
[386] D. B. Anderson, "Integrated optical spectrum analyzer: An imminent 'chip'," *IEEE Spectrum*, vol. 15, pp. 22–29, Dec. 1978.
[387] J. T. Boyd, "Integrated optoelectronic silicon devices for optical signal processing and communications," *Opt. Eng.*, vol. 18, pp. 14–19, Jan./Feb. 1979.
[388] B. Chen and M. K. Barnoski, "Integrated optic (Bragg) spectrum analyzer," *Proc. SPIE*, vol. 176, pp. 56–61, 1979.
[389] D. Mergerian and E. C. Malarkey, "Integrated optical RF spectrum analyzer," *Microwave J.*, vol. 23, pp. 37–48, Sept. 1980.
[390] D. Mergerian, E. C. Malarkey, R. P. Pautienus, J. C. Bradley, and A. L. Kellner, "Advances in integrated optical spectrum analyzers," *Proc. SPIE*, vol. 269, pp. 129–135, 1981.
[391] T. Suhara, H. Nishihara, and J. Koyama, "A folded-type integrated-optic spectrum analyzer using butt-coupled chirped grating lenses," *IEEE J. Quantum Electron.*, vol. QE-18, pp. 1057–1059, July 1982.
[392] D. Maystre and R. Petit, "Some recent theoretical results for gratings; application to their use in the very far ultraviolet region," *Nouv. Rev. Optique*, vol. 7, pp. 165–180, May/June 1976.
[393] J. M. Lerner, J. Flamand, A. Thevenon, and M. Neviere, "Discussion of the relative efficiency in the vacuum ultraviolet of diffraction gratings with laminar, sinusoidal, and triangular grooves," *Opt. Eng.*, vol. 22, pp. 220–223, Mar./Apr. 1983.
[394] M. Neviere, P. Vincent, and D. Maystre, "X-ray efficiencies of gratings," *Appl. Opt.*, vol. 17, pp. 843–845, March 15, 1978.
[395] N. M. Ceglio, A. M. Hawryluk, and R. H. Price, "Space and time resolved soft X-ray spectra using X-ray transmission gratings," *Opt. Eng.*, vol. 22, pp. 241–246, Mar./Apr. 1983.
[396] C. M. Verber, V. E. Wood, R. P. Kenan, and N. F. Hartman, "Large-angle optical switching in waveguides in $LiNbO_3$," *Ferroelectr.*, vol. 10, pp. 253–256, may 1976.
[397] B. Chen and C. M. Meijer, "Bragg switch for optical channel waveguides," *Appl. Phys. Lett.*, vol. 33, pp. 33–35, July 1, 1978.
[398] R. A. Becker and W. S. C. Chang, "Electro optical switching in thin film waveguides for a computer communication bus," *Appl. Opt.*, vol. 18, pp. 3296–3300, Oct. 1, 1979.
[399] P. D. Bloch and L. Solymar, "Analysis of a 4-port Bragg device," *Proc. Inst. Elec. Eng.*, vol. 127, pp. 133–137, June 1980.
[400] E. M. Philipp-Rutz, R. Linares, and M. Fakuda, "Electrooptic Bragg diffraction switches in low cross-talk integrated-optics switching matrix," *Appl. Opt.*, vol. 21, pp. 2189–2194, June 15, 1982.
[401] G. Wade, "Bragg diffraction imaging," in *Acoustic Imaging*, G. Wade, Ed. New York: Plenum, 1976, pp. 189–228.
[402] A. Korpel, R. Adler, P. Desmares, and W. Watson, "A television display using acoustic deflection and modulation of coherent light," *Appl. Opt.*, vol. 5, pp. 1667–1675, Oct. 1966.
[403] D. W. Vahey, C. M. Verber, and R. P. Kenan, "Development of an integrated-optics multichannel data processor," *Proc. SPIE*, vol. 139, pp. 151–158, 1978.
[404] *National Geographic*, vol. 165, front cover, Mar. 1984.